



# Application and Design of Acrylic Microfluidic Chips

---

A Major Qualifying Project Report:

Submitted to the Faculty

of the

WORCESTER POLYTECHNIC INSTITUTE

in partial fulfillment of the requirements for the

Degree of Bachelor of Science

In Mechanical Engineering

by

---

Katherine Comeford

---

Susan Elliott

---

Storie Nivers

---

Emma Ryan

Approved:

---

Professor Yuxiang Liu, *MQP Advisor*

November 2, 2017

## Abstract

Microfluidics is the field of study which utilizes the manipulation of small amounts of fluids to perform a certain function. The convenience and small sample size required for microfluidics has led to its growth in popularity, but many of the chips still require off chip lab equipment that can be bulky and expensive. In particular, many of these systems require a mechanical pump to force the sample to flow through the chip. Most of the current microfluidic devices are fabricated on PDMS, which requires access to a clean room and expensive equipment such as a mask aligner and a plasma cleaner. This project seeks to address these problems by attempting to create a pump that can be used for spherical droplet generation using cross flow on an acrylic microfluidic platform. Our team used laser ablation to fabricate chips to test to determine the optimal parameters that allow for spherical droplet formation. We also worked to develop a handheld pump that could produce the flow rates necessary for spherical droplet generation.

## Acknowledgements

Our team would like to thank the following people for their time, effort, help, and guidance during the completion of this project:

Professor Yuxiang Liu  
Yundong Ren  
Subhrodeep Ray  
Yao Shen  
Professor Sakthikumar Ambady  
Paula Moravek  
Lisa Wall  
Professor Robert Daniello  
Professor Christopher Brown  
Olivia Steen  
Ava Karet  
Alex Lemmon  
Barbara Furhman  
Payton Wilkins  
Everyone in Washburn Shops

## Contents

Abstract.....	2
Acknowledgements.....	3
List of Figures.....	7
List of Tables.....	10
List of Equations.....	11
Chapter 1: Introduction.....	12
Chapter 2: Background.....	14
2.1 Material Selection.....	14
2.1.1 Material Properties.....	14
2.1.2 Fabrication Methods.....	14
2.2 Microfluidic Components: Pumps.....	17
2.2.1 Importance of Steady Flow Rate Pumps.....	17
2.2.2 Types of Pumps.....	17
2.2.3 Limitations of Pumps with Current Lab on a Chip Devices.....	24
2.3 Droplet Formation.....	24
Chapter 3: Fabrication Methods and Parameters.....	27
3.1 Laser Cutter Parametric Study.....	28
3.1.1 Vector Cutting Parametric Study Results.....	29
3.1.2 Vector Engraving Parametric Study Results.....	31
3.1.3 Rastering Parametric Study Results.....	33
3.1.4 Laser Cutter Parametric Study Conclusions.....	34
3.2 Surface Roughness Study.....	35
Chapter 4: Droplet Generation: Design and Optimization.....	37
4.1 Droplet Generation.....	37
4.2 Initial Droplet Chip Design and Fabrication.....	37
4.3 Initial Droplet Testing.....	38
4.4 Revised Material and Fabrication Technique.....	38
4.5 Initial Fabrication and Testing for Droplet Angle Optimization.....	39
4.6 Scaling Down Channel Size.....	40
4.7 Continuing Issues with Inlet and Outlet Leakage.....	40
4.8 Angle Optimization for Unglued and Glued Chips.....	41
4.9 Flow Rate Optimization for Glued and Unglued Chips.....	43

4.10 Considerations for Integration with the On-Chip Pump .....	46
4.11 Optimized Droplet Generation .....	46
4.12 Blood Testing .....	48
Chapter 5: On Chip Pump Design, Prototyping, and Characterization.....	51
5.1 Paper Based Pumps .....	51
5.1.1 Paper Based Pump 1.0.....	51
5.1.2 Paper Based Pump 2.0.....	52
5.1.3 Pump 2.1.....	53
5.1.4 Pump 2.2- 2.4.....	54
5.1.5 Pump 2.5.....	55
5.1.6 Pump 2.6- Pump 2.9.....	55
5.1.7 Pumps 2.10- 2.17 .....	56
5.1.8 Pumps 2.18- 2.21 .....	57
5.1.9 Pumps 2.24 .....	61
5.1.10 Pump 2.25.....	61
5.1.11 Pump 2.26.....	62
5.1.12 Pump 2.27.....	63
5.2 Gravity Driven Pumps .....	65
5.2.1 Material Selection .....	66
5.2.2 Fabrication Process .....	67
5.2.3 Calculations for Pump Height .....	67
5.2.4 Pump Testing .....	69
5.3 Weight Driven Syringe Pump.....	71
Chapter 6: Final Results Summary and Recommendations.....	77
6.1 Droplet Results .....	77
6.1.1 Measurement and Leakage Issues.....	77
6.1.2 Angle Results.....	77
6.1.3 Flow Speed Results.....	78
6.1.4 Optimized Droplets .....	79
6.1.5 Blood Separation Testing.....	79
6.1.6 Recommendations for Future Work: .....	80
6.2 Pump Results .....	81
6.2.1 Paper Pump Results .....	81

6.2.2 Gravity Driven Pump Results .....	83
6.2.3 Weight Driven Syringe Pump Results.....	84
6.3 Combined Droplet Optimization and Handheld Pump Testing.....	85
6.3.1 Future Recommendations for Weight Driven Pumps .....	86
Chapter 7: Conclusion and Outlook.....	87
References .....	90
Appendices.....	94
Appendix A: Surface Roughness Study Confocal Microscope Images.....	94
Appendix B: Surface Roughness Study Ra Values .....	96
Appendix C: Capillary Number Calculations.....	97
Appendix D: Paper Pump Design Pictures and Settings .....	101
Appendix E: ARcare® 92892 and 92734 Material Safety Data Sheets.....	148
Appendix F: Gravity Pump Chip Assembly.....	150
Appendix G: Gravity Pump Calculations .....	151
Appendix H: Theoretical vs. Analytic Flow Rates for Olive Oil.....	154
Appendix I: Gravity Pump Pressure Equalization Calculations.....	156
Appendix J: Weight Driven Pumps Calculations.....	159
Appendix K: Weight Driven Pump Flow Rate Calculations .....	162

## List of Figures

Figure 1 a (left) Photograph of PDMS [5]. 1 b (right) Photograph of Acrylic.....	14
Figure 2: The fabrication of micropatterned slabs of PDMS. a–b   Photoresist is spincoated on a silicon wafer. c   A mask is placed in contact with the layer of photoresist. d   The photoresist is illuminated with ultraviolet (UV) light through the mask. An organic solvent dissolves and removes photoresist that is not crosslinked. The master consists of a silicon wafer with features of photoresist in bas-relief. An expanded view of one of the microfabricated structures with its characteristic critical dimensions is shown. e   PDMS is poured on the master, cured thermally and peeled away. f   The resulting layer of PDMS has microstructures embossed in its surface. PDMS, poly(dimethylsiloxane)[17].....	16
Figure 3: Membrane Driven Pump [18].....	17
Figure 4: Paper Driven SIMPLE Pump [21].....	18
Figure 5: Basic Paper Driven Pump [22] .....	19
Figure 6: Flow Rate vs. Central Paper Angle [22] .....	20
Figure 7: Gravity Driven Pump Based on Reservoir Height Difference [24] .....	20
Figure 8: Comparison of Gravity Driven Pump Flow Rates [24].....	21
Figure 9: Spring Driven Syringe Pump Diagram .....	23
Figure 10: Diagram of Cross Flow, Co-Flow, and Flow Focusing [30].....	24
Figure 11: Photographs of Droplets in the Squeezing, Dripping, and Jetting Regimes [30].....	25
Figure 12: Microfluidic Chip Channel AutoCAD Design .....	27
Figure 13: Vector Cutting Power vs. Channel Dimensions.....	29
Figure 14: Increasing Vector Cutting Power .....	30
Figure 15: Vector Cutting Speed vs. Channel Dimensions.....	30
Figure 16: Vector Cutting Increasing Speed.....	30
Figure 17: Vector Engraving Power vs. Channel Dimensions.....	31
Figure 18: Vector Engraving Increasing Power .....	31
Figure 19: Vector Engraving Speed vs. Channel Dimensions.....	31
Figure 20: Vector Engraving Increasing Speed.....	32
Figure 21: Vector Engraving Number of Passes vs. Channel Dimensions.....	32
Figure 22: Vector Engraving Increasing Number of Passes .....	32
Figure 23: Rastering Power vs. Channel Dimensions .....	33
Figure 24: Rastering Increasing Power .....	33
Figure 25: Rastering Speed vs. Channel Dimensions.....	33
Figure 26: Rastering Increasing Speed.....	34
Figure 27: Rastering Number of Passes vs. Channel Dimensions .....	34
Figure 28: Rastering Increasing Number of Passes .....	34
Figure 29: Microfluidic Chip.....	37
Figure 30: Channel Cross Section .....	38
Figure 31: Droplets formed at 15, 30,45,60,75 and 90 degrees (left to right) .....	39
Figure 32: Graph Showing Average l/w ratio versus degrees (Oil speed 5 $\mu$ L/min-water speed 4 $\mu$ L/min) .....	39
Figure 33: Incorrectly Rastered Channel .....	40
Figure 34: Droplet with measures labeled.....	42
Figure 35: Graph Depicting Length to Width Ratio in comparison to angle (Oil flow rate 5 $\mu$ L/min-Water 4 $\mu$ L/min) .....	42

Figure 36: Graph showing area versus degree for glued and unglued chips (Oil flow rate 5 $\mu$ L/min-Water 4 $\mu$ L/min) .....	43
Figure 37: Graph showing Average L/W Ratio vs. Water Speed, Oil Speed constant at 7.2 $\mu$ L/min .....	44
Figure 38: Graphs showing Average l/w and Area vs. Water Speed, Oil Speed constant at 7.2 $\mu$ L/min for glued chip.....	45
Figure 39: Graph showing l/w and area vs water flow speed, Oil speed constant at 7.2 $\mu$ L/min for glued chip .....	47
Figure 40: Graph Showing l/w and area vs. oil flow speed water held constant at 2.5 $\mu$ L/min .....	48
Figure 41: Droplets captured in outlet tubing .....	49
Figure 42: Droplet seen under a microscope. Arrows show examples of individual blood cells.....	50
Figure 43: Paper Based Pump 1.0 AutoCAD Drawing.....	51
Figure 44: Paper Based Pump 1.0 Tapered Working Channel .....	51
Figure 45: Photograph of Paper Based Pump 1.0The chip size is about 57x38x3 mm.....	52
Figure 46: Wetting Radius Depiction.....	52
Figure 47: Photograph of Paper Based Pump 2.0 with Leakage.....	52
Figure 48 : Paper Based Pump 2.0 AutoCAD Design .....	53
Figure 49 : Paper Based Pump 2.1 AutoCAD Design .....	53
Figure 50: Photograph of Paper Based Pump 2.1 Sealed with Scotch Tape.....	53
Figure 51 : Paper Based Pump 2.2 AutoCAD Design .....	54
Figure 52: Photograph of Paper Based Pump 2.2 during Testing .....	54
Figure 53 : Paper Based Pump 2.3 AutoCAD Design .....	54
Figure 54 : Paper Based Pump 2.4 AutoCAD Design .....	54
Figure 55: Photograph of Paper Based Pump 2.5 during Testing .....	55
Figure 56 : Paper Based Pump 2.5 AutoCAD Design .....	55
Figure 57 : Paper Based Pump 2.10 AutoCAD Design .....	56
Figure 58 : Paper Based Pump 2.16 AutoCAD Design .....	57
Figure 59: Photograph of Paper Based Pump 2.16 during Testing .....	57
Figure 60 : Paper Based Pump 2.18 AutoCAD Design .....	58
Figure 61: Paper Based Pump 2.18 during Testing.....	58
Figure 62 : Paper Based Pump 2.19 AutoCAD Design .....	58
Figure 63: Paper Based Pump 2.19 during Testing- Bonded with Double Sided Tape.....	59
Figure 64: Paper Based Pump during Testing 2.20- Bonded with Acetone .....	59
Figure 65: Paper Based Pump 2.22 during Testing.....	60
Figure 66 : Paper Based Pump 2.22 AutoCAD Design .....	60
Figure 67 : Paper Based Pump 2.24 AutoCAD Design .....	61
Figure 68: Paper Based Pump 2.24 during Testing.....	61
Figure 69 : Paper Based Pump 2.25 AutoCAD Design .....	61
Figure 70: Paper Based Pump 2.25 during Testing.....	62
Figure 71 : Paper Based Pump 2.26 AutoCAD Design .....	62
Figure 72: Paper Based Pump 2.26 during Testing.....	62
Figure 73: Paper Based Pump 2.27 during Testing.....	63
Figure 74: Photograph of Paper Based Pump 2.30 .....	64
Figure 75: Paper Based Pump 2.27 during Testing- Syringe Inlet and Top Acrylic Chip Sealed with Water .....	65

Figure 76: Paper Based Pump 2.27 during Testing- Syringe Inlet and Top Acrylic Chip Sealed with Packing Tape .....	65
Figure 77: Photograph of Gravity Driven Pump 5.3 with Borosilicate Tube Attached Via UV Hardened Glue .....	66
Figure 78: Force Diagram of Weight Driven Syringe Pump .....	72
Figure 79: Setup of Experiment to Measure Frictional Force in a Syringe .....	72
Figure 80: Water Volumetric Flow Rate in Gravity Driven Pump Trial with 250g Weight.....	73
Figure 81: Oil Volumetric Flow Rate in Gravity Driven Pump Trial with 450g Weight .....	74
Figure 82: Theoretical vs. Experimental Volumetric Flow Rates of Gravity Pump Trials .....	74
Figure 83: Length to Width Ratio for Droplets at different Olive Oil Weights.....	76
Figure 84: Length/Width Ratios of Glued and Unglued Chips by T-junction Degree.....	78
Figure 85: Length/Width Ratios for Glued and Unglued Chips for Various Flow Rates .....	78
Figure 86: Length/Width Ratios and Top View Areas for Various Flow rates.....	79
Figure 87: Paper Based Pump with Leakage .....	81
Figure 88: Paper Based Pump Design with Area Where Vacuum Formed Circled in Red .....	82
Figure 89: Photograph of Paper Based Pump with Gap between Working Fluid and Paper Filter Circled in Red.....	82
Figure 90: Example of Fabricated Gravity Pump.....	83
Figure 91: Weight Driven Pump Setup .....	85
Figure 92: Droplets Formed in Tube from Weight Driven Pump Experiment .....	85
Figure 93: Sphericity of Droplets Produced by Weight Driven Pump at Given Weights .....	85

## List of Tables

Table 1: Laser Cutter Parametric Study Design of Experiment.....	28
Table 2: Laser Cutter Machine Defaults .....	29
Table 3: Surface Roughness Study Results.....	35
Table 4: Length/Width Ratios and Standard deviation comparison between glued and unglued chip.....	41
Table 5: Length, width, l/w, and area of blood droplets .....	49
Table 6: Comparison of Analytic and Experimental Volumetric Flow Rates of Different Fluids.....	68
Table 7: Comparison of Analytic and Experimental Volumetric Flow Rates of Different Tube Diameters	69
Table 8: Blood Droplet Length, Width, Length to Width Ratio, Top View Area, and Cells per Droplet .....	80
Table 9: Experimental Frictions of Syringe Piston for Water and Olive Oil .....	84
Table 10: Theoretical and Analytic Volumetric Flow Rates for Water and Olive Oil.....	85

## List of Equations

Equation 1: Flow Rate within porous paper .....	19
Equation 2: Bernoulli's Equation .....	20
Equation 3: Pressure Loss due to Friction.....	21
Equation 4: Hooke's Law .....	22

## Chapter 1: Introduction

The field of microfluidics refers to systems that use small amounts of fluids for analysis. These systems are characterized by their small sample sizes (ranging from  $10^{-9}$  to  $10^{-18}$  L) which are formed by precisely cut channels only micrometers in width [1].

Whitesides [1] identifies the origins of microfluidics as emerging from four fields of study: molecular analysis, molecular biology, biodefense, and microelectronics. Each of these fields contributed advances in microfluidic technology or increased interest in microfluidics thus allowing it to grow into what it is today. Analytical chemistry provided capillary chromatography, which allows researchers to separate and identify compounds from a small sample with high resolution. Similarly, molecular biology's growing interest in DNA and genomes required an increase in sensitivity and resolution tests thus propelling that field to use microfluidic systems. Biodefense was also influential in the growth of microfluidics as the US government searched for ways to test for biological and chemical threats. This growing fear led the government to support more academic research programs looking to use microfluidics to detect these threats. Finally, microelectronics contributed a technology that would be vital to the growth of microfluidics- photolithography. In microelectronics, photolithography is used to fabricate parts on glass and silicon. Plastic based microfluidic systems use photolithography to fabricate chips although advancements in modern materials mean that glass and silicon are no longer commonly used [1].

Microfluidics continues to be relevant today due to its many advantages. One of the benefits of microfluidics is that it requires a very small amount of fluid, thus allowing more tests to be completed with a smaller sample size. Another advantage of microfluidics is the small size of the chip. This allows the chip to act as a portable lab in some applications, leading to microfluidics sometimes being referred to as lab on a chip technology or point-of-care diagnostics. The ability of microfluidic chips to function as a lab also means the samples can be analyzed quickly to receive results [2]. Just a few of the many applications of microfluidics include the analysis of glucose in urine, detection of heavy metal ions like lead and zinc, and the sorting of blood cells [3, 4]. Although microfluidic technology has many possible applications, it also has restrictions like samples needing to be treated before testing. Restrictions like this mean the chips

do not operate completely independent of a lab, demonstrating that microfluidics has not yet reached its full potential and is a field that has room for growth [2].

Our group saw this need for microfluidic devices that could operate independently of bulky lab equipment and determined that we wanted to create a device that could function independently. From our literature review, the details of which are in the section below, we identified that many chips in the literature could not be run without a mechanical pump. The need for a mechanical pump prevents completely on chip diagnostics. Due to this need, our group decided we wanted to create a handheld pump that would utilize passive droplet formation to create spherical droplets that would be useful in biological applications.

## Chapter 2: Background

### 2.1 Material Selection

#### 2.1.1 Material Properties

Microfluidic chips can be manufactured from a variety of materials including glass, silicone, paper, and several kinds of polymers. The two most commonly used polymers for plastic based microfluidic chips are Polydimethylsiloxane (PDMS) and Polymethylmethacrylate (PMMA). This project focused on creating a novel chip design from PMMA, otherwise known as acrylic, instead of PDMS because of acrylic's high elastic modulus, transparent optical properties, low cost, and ease of manufacturability.



*Figure 1 a (left) Photograph of PDMS [5]. 1 b (right) Photograph of Acrylic*

It is important for polymer based microfluidic chips to have a high elastic modulus as it ensures channel integrity during usage. This is crucial because channel structure must stay constant under varying pressures in order to provide consistent volumetric flow rate. Due to the rigidity of acrylic (with an elastic modulus ranging from 1.70 to 3.30 GPa), the channel shape of an acrylic chip is not affected by the pressures produced by microflows [7, 8].

#### 2.1.2 Fabrication Methods

##### 2.1.2.1 Acrylic

The process of creating a microfluidic chip from acrylic is simple and fast. Acrylic chips can be rapidly prototyped through laser ablation or micromilling. For laser ablation, or laser

cutting, the desired chip is designed in AutoCAD or another digital design software and exported to the pre-included software that comes with laser cutters. From there, the laser settings can be varied to meet the requirements of the design and to test channel parameters. Laser cutters can perform three kinds of laser cutting- vector cutting, vector engraving, and rastering. With vector cutting and vector engraving, the laser cutter treats the lines in a CAD drawing as full lines and does not let up on the power while cutting a line. When using rastering, the laser cutter treats shapes made in AutoCAD as individual points and cuts at each point.

On top of being able to choose what kind of cutting is performed, it is also possible to control both the speed and power of a laser cutter as well as varying number of passes. Increasing speed decreases depth of cut while increasing power increases depth of cut. Although slowing speed can increase the depth of a channel during fabrication, it can also lead to deformation and defects in the acrylic. When doing multiple passes with a laser cutter, the depth increases linearly while the width increases a small amount but after several passes remains constant [9].

Once the design is loaded and the laser settings are selected, the laser passes over the surface of the acrylic melting and ablating the material in the specified pattern. The acrylic can then be turned over and ablated on the other side or removed from the laser cutter with three sides of the microfluidic channel fabricated. In order to create the fourth channel wall, another piece of acrylic or other material, such as tape, can be reversibly or irreversibly bonded using thermal techniques or adhesives [10].

This process, taking as little as a few minutes, results in decreased manufacturing time and simple fabrication allowing the chip to be inexpensive and mass produced. This is beneficial both in industry, where a low cost will allow the chip to be widely used, and in research where design changes happen rapidly necessitating new chips. Even though the initial machine investment for this process is high, once the laser cutter is purchased, the acrylic material is far less expensive than PDMS [11]. In addition to high startup costs, the surface finish of a laser cut chip can be rougher than that of chips created through other processes [12]. This roughness can be somewhat reduced by adjusting the laser cutting parameters such as speed to increase or reduce the amount of material ablated in a given period of time. If an even smoother surface finish is desired, it can be obtained through a chemical bath following the chip being cut [13].

### 2.1.2.2 PDMS

PDMS is produced through lithography, a process shown in Figure 2. The soft lithography process used to create PDMS chips requires several extra steps and can take up to several weeks to produce [14]. In order to produce a PDMS chip, a photomask must be ordered with a desired pattern- this process typically takes one to two weeks. A silicon wafer is then coated with a layer of photoresist, a light sensitive material. The photomask is placed on top of the photoresist and exposed to ultraviolet light, leaving dissolved photoresist in a desired pattern on the wafer. Once complete, liquid PDMS is mixed with a bonding agent, poured over the wafer, and left to cure for several days [15]. In Alfayez et al, it was shown that photomasks could be printed faster at a lower resolution using a home printer and transparency sheets and the curing process could be reduced to several hours with the introduction of a heated curing process [16]. Even with this expedited process, it takes hours to manufacture a PDMS chip from a new design. This can be shortened to under a minute with the use of laser cut acrylic.

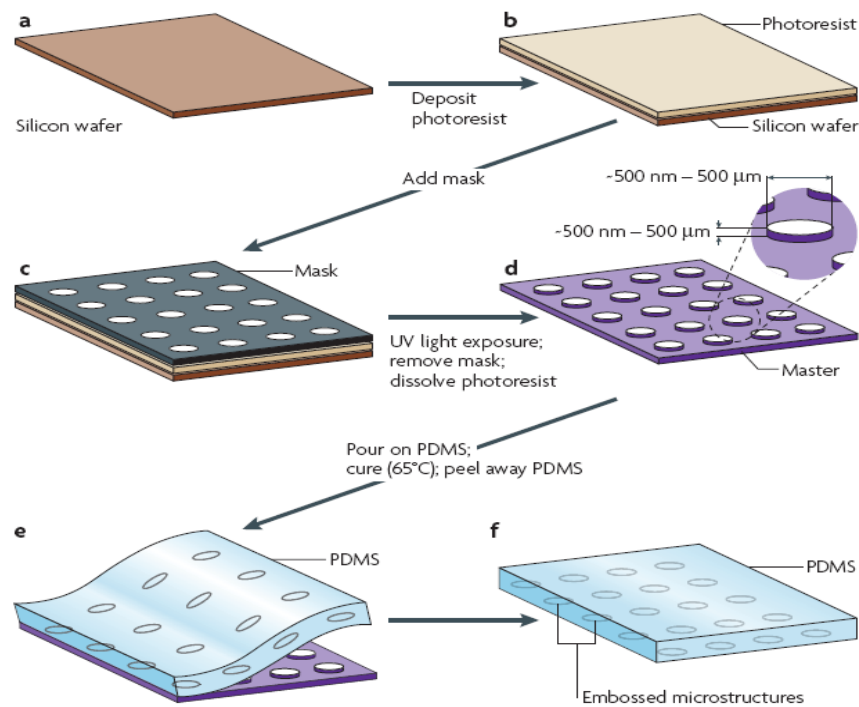


Figure 2: The fabrication of micropatterned slabs of PDMS. a–b | Photoresist is spincoated on a silicon wafer. c | A mask is placed in contact with the layer of photoresist. d | The photoresist is illuminated with ultraviolet (UV) light through the mask. An organic solvent dissolves and removes photoresist that is not crosslinked. The master consists of a silicon wafer with features of photoresist in bas-relief. An expanded view of one of the microfabricated structures with its characteristic critical dimensions is shown. e | PDMS is poured on the master, cured thermally and peeled away. f | The resulting layer of PDMS has microstructures embossed in its surface. PDMS, poly(dimethylsiloxane)[17].

By focusing on acrylic, we were able to manufacture chips quickly, inexpensively, and to our design requirements due to its inherent material properties and manufacturability. Reducing the material cost of microfluidic chips helps make them more accessible in point of care applications. To truly function in a point-of-care location, however, the chip must contain an on chip pump to reduce the need for additional equipment.

## 2.2 Microfluidic Components: Pumps

### 2.2.1 Importance of Steady Flow Rate Pumps

The development of pumps within the field of microfluidics falls into two main categories- machine driven pumps and manual pumps. While machine driven pumps are important and useful for lab on a chip purposes requiring higher flow rates and uniform volumetric flow rates, manual pumps hold potential due to their ability to be utilized in the field and in point of care applications with little instrumentation.

### 2.2.2 Types of Pumps

There are three main handheld pumps found in literature that yielded steady flow rates without the addition of external forces such as magnetic forces or pumping forces. These three main kinds of pumps are membrane driven pumps, paper driven pumps, and gravity driven pumps.

#### 2.2.2.1 Membrane Driven Pumps

Membrane driven pumps utilize the elastic properties of given materials such as PDMS and silicone tapes that allow them to deform without suffering permanent damage. In these pumps, fluid is pumped into a membrane bound reservoir by a syringe or other device and the membrane expands to accommodate the increase in fluid pressure. As the membrane returns to its original shape, it exerts a varying force on the fluid thus pumping it out at a constant flow rate. Due to the pressure and force that a human thumb can exert on the microfluidic system while using the syringe to insert the fluid into the

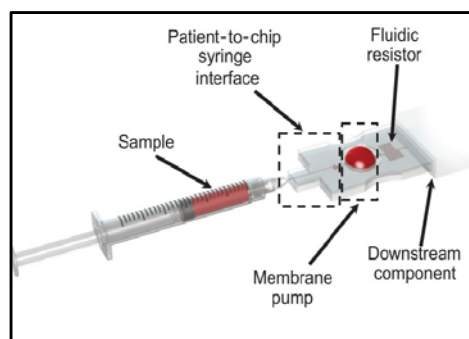


Figure 3: Membrane Driven Pump [18]

chip, many chips utilizing this kind of pump also include a curved fluidic resistor portion as shown to the right in Figure 3 to separate the analytic portion of the chip from the pumping force [18].

There are several different membrane driven chips in literature. While the majority of the components of a membrane driven pump (as discussed above) remain the same amongst these pumps, there are subtle differences and advantages to each. Each of the designs include an inlet and an outlet to the pump followed by the analytic fluid. The region between the inlet and the outlet varies between the pumps. Some of these differences are as a result of limitations in the designs of a membrane based pump. For example, the fluid membrane can hold only a set amount of fluid before plastically deforming [19]. Therefore, some pumps have integrated a safety valve and reservoir to absorb excess fluid in the membrane and protect the membrane from plastically deforming [19].

Another design includes passive flow regulators downstream of the fluid inlet to deliver a constant fluid flow rate regardless of varying pressure in the fluid channel. This is mainly achieved through a flexible layer, such as a normally closed membrane valve, that deforms under varying pressures [20].

#### 2.2.2.2 Paper Driven Pumps

There are three main paper driven pumps researched for this project. All three of these pumps utilize the adhesion properties of water and the tendency of capillary action to draw water into paper once initial contact is made. Capillary action draws the water into the filter paper thus creating negative pressure in the working liquid chamber pulling the water through the analytical channel [21].

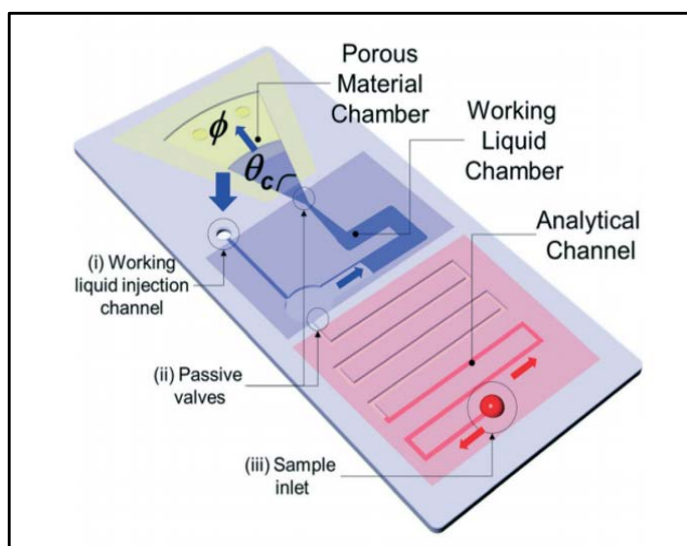


Figure 4: Paper Driven SIMPLE Pump [21]

The three main sections of these pumps (as seen in Figure 4 to the right) are the working fluid region, the absorbing region (the

different shapes for this region are one of the main fields of development in this field and are discussed in further detail below), and the analytic fluid region. This last region is connected to the working fluid through a very thin channel. In some pump designs, the channel contained a passive microvalve to ensure no backflow while in others, the working fluid channel and the analytic fluid channel were entirely connected with no separation [21].

In these pumps, pressure is applied to the working fluid via either a syringe or finger pressure which pushes it down the channel causing it to come into contact with the paper. The water is then sucked into the paper at a rate predicted by Equation one below. This equation shows that the main variables affecting flow rate are central angle, porosity of the filter paper, thickness of the filter paper, and the wetting radius.

$$Q = \frac{dV}{dt} = \frac{\theta_c}{360^\circ} \phi 2\pi r h \frac{dr}{dt},$$

*Equation 1: Flow Rate within porous paper*

The main differences between these pumps are the ways the working fluid connects to the filter paper, connections between the analytic and working fluid, and the filter paper design. In the paper pump for passive transport, the connection between the working fluid and the filter paper is simple- the filter paper is set on top of the inlet as shown in Figure 5. However, in the other two pumps, there is a region of restricted flow to help control

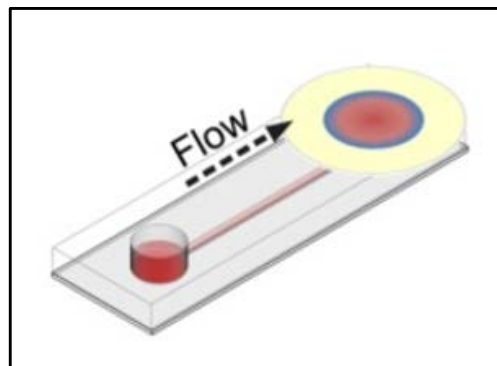


*Figure 5: Basic Paper Driven Pump [22]*

the flow into the paper and, thus, control the overall flow. In modular programming pumps, there is a region of higher flow resistance compared to the other regions at the inlet of the working fluid to ensure control of the flow. In the Self-Powered Imbibing Microfluidic Pump by Liquid Encapsulation (or SIMPLE Pump), the working fluid comes to a point with a passive valve between the working fluid and the filter paper to restrict and control the flow.

The connections between the analytic fluid and the working fluid also vary between pump designs. In the first two articles, there is no valve or separation of the fluids; however, in the

SIMPLE pump, there is a passive valve in a smaller channel that connects the two channels thus ensuring unidirectional flow.

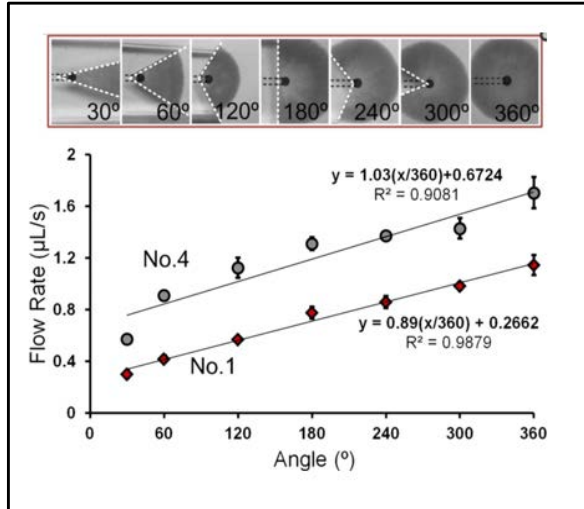


Figure 6: Flow Rate vs. Central Paper Angle [22]

Finally, the filter paper shape is different in all the pumps. Whatman #1 Chromatography Paper is used due to its high porosity lamination which mitigates excess evaporation [22]. However, all of the pumps change the central angle of the filter paper. In “Paper pump for passive transport” researchers Wang, Hagen, and Papautsky discuss the correlation of flow rate and angle of the fan in the paper used to absorb the working fluid thus initiating flow [22]. They found that increasing the angle in turn increased the flow rate in an almost linear fashion.

All of the three pumps had relatively steady flow rates with a sharp increase in flow rate at the very beginning which steadied out within 10 sections. However, the pumps themselves only ran until the filter paper became saturated after 30 seconds. Many of the differences in their flow rates came from the shape and angle of the absorbing paper [22]. Research into the SIMPLE pump in particular showed that reasonable flow rates for that particular pump would be 0.07 µL/s, 0.12 µL/s, and 0.17 µL/s in channels with a cross section of 200 µm × 600 µm [21].

### 2.2.2.3 Gravity Driven Pumps

Gravity driven pumps are driven by the hydraulic pressure differences caused by a height variation between fluid reservoirs. The pressure difference due to height difference can be described using Bernoulli’s equation which is a formula for energy conservation in fluid flow as shown in Equation 2 below [23].

$$P_1 + \frac{1}{2}\rho V_1^2 + \rho g h_1 = P_2 + \frac{1}{2}\rho V_2^2 + \rho g h_2$$

Equation 2: Bernoulli’s Equation

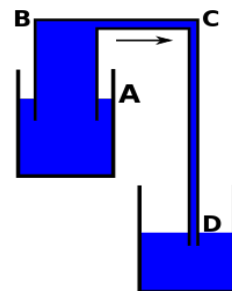


Figure 7: Gravity Driven Pump Based on Reservoir Height Difference [24]

This formula can be used to describe fluid flow within the tubes and channels of a gravitationally driven microfluidic pump. It can be rearranged to describe the pressure difference between two points in a microfluidic system. Assuming that the two points are at atmospheric pressure and stationary, the  $\Delta P$  will be zero and the velocities will cancel out meaning that the flow rate can be calculated from height difference as shown below [25].

$$\Delta P = P_2 - P_1 = \rho g(h_1 - h_2) = 0$$

However, due to the low Reynolds number and how slow the flow typically is in microfluidic systems, the pressure drop in tubes due to friction is not negligible and must be accounted for in the pressure difference equation. Pressure drop in a tube due to friction is dependent on the Reynolds number of the fluid as well as the viscosity and is shown below [25].

$$\Delta P_{friction} = f * \frac{L}{D_H} * \frac{\rho V^2}{2}$$

Equation 3: Pressure Loss due to Friction

In laminar flow, friction factor,  $f$ , can be approximated by  $\frac{64}{Re}$  [25].  $L$  refers to the distance traveled and  $D_H$  refers to hydraulic diameter. These must be added to the pressure drop formula to accurately predict the pressure drop thus yielding the equation:

$$\Delta P = P_2 - P_1 = \rho g(h_1 - h_2) + \frac{64}{Re} * \frac{L}{D_H} * \frac{\rho V^2}{2} = 0$$

There are two main gravity driven pumps, those with varying height differences in the fluid reservoirs and those with constant height as shown in Figure 8. In “Gravity- Driven Micropump with a Steady Flow Rate”, researchers were able to maintain a constant hydraulic pressure between the reservoirs by keeping the

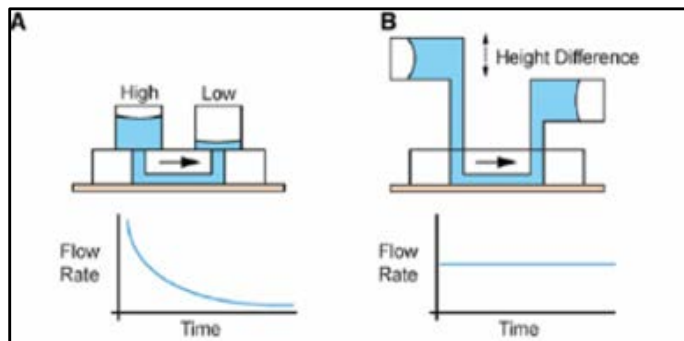


Figure 8: Comparison of Gravity Driven Pump Flow Rates [24]

reservoirs constantly horizontal and at the same heights [26]. They achieved this by replenishing the vertical tubes from horizontal tubes kept at a constant height. This ensures a constant height difference of the liquid in the reservoir regardless of the amount of liquid in the reservoir. This maintenance of height in turn guarantees difference in hydraulic pressure which is the driving force for fluid flow in this design.

Furthermore, this design is able to pump fluid for a chip for up to several hours with only a few centimeters difference necessary between the inlet and outlet reservoirs [26]. However, by increasing the height difference between the inlet and outlet, one can increase the flow rate. The other ways to change the flow rate would be to vary the total fluid resistance or by changing the fluid viscosity (although this last option yields a much smaller difference in flow rate than the first two.)

#### *2.2.2.4 Spring Driven Syringe Pumps*

Syringes are a common method of introducing fluid into microfluidic systems. In many cases where constant flow is desired, outside mechanical pumps are used to control the movement of the syringe piston at a constant speed. Outside of mechanical pumps, where the force is constantly adjusting slightly to ensure constant flow rate, there are several ideas in literature that produce quasi-constant flow such as a spring driven syringe pump.

In order for a spring to drive the piston at a constant speed, there would need to be no acceleration of the syringe head- meaning a zero net force. The relation governing the force exerted by a spring is Hooke's law which says that the force of a spring is varied depending on the displacement of the spring from its equilibrium position [27]. The equation is described below:

$$F = k\Delta x$$

*Equation 4: Hooke's Law*

In order to ensure a constant flow rate from a spring driven syringe, one would have to ensure a constant net force of zero. In order to achieve this, the amount the spring moves over the duration of flow would need to be minimized. The more the spring moves, the more the force varies over a given amount of time.

The main spring driven syringe on the market is named Springfusor<sup>®</sup> and is sold by several medical device companies [28]. It is a component that can be added to the top of a syringe similar to the schematic shown to the right and utilizes a pre-compressed spring to drive the syringe piston. When the spring expands as it moves back to equilibrium, it pushes down the piston in the syringe.

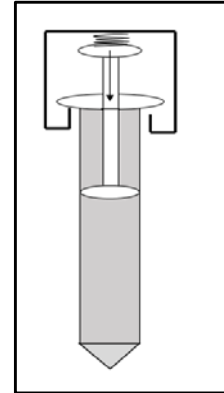


*Figure 9: Spring Driven Syringe Pump Diagram*

The company sells them at specific mean flow rates. However, due to the varying nature of the force exerted by a spring, the instantaneous flow rate varies by as much as 10% in any given direction from the mean flow rate [29].

It has a higher flow rate the fuller the syringe (due to the higher amount of compression in the spring when the syringe is full), and it decreases linearly with length along the syringe [29].

The estimated mean flow rate in these kinds of spring pumps is based on standard values of properties of the syringe and fluid including the viscosity of saline, the temperature, and elevation of the Springfusor<sup>®</sup> syringe above injection site, and back pressure above normal intravenous blood pressure [29].

The fluid flow rate calculations are based on the assumption that the spring powered syringes are going to be used with saline. When other fluids such as antibiotics are used that have different viscosities than saline, the mean flow rate has to be re-estimated. The relationship between the mean flow rate, the new flow rate, and the changes in viscosity is linear such that an antibiotic with 6.4 times the viscosity of saline (eg. Phenytoin IV) would take 6.4 times the original time that would have been required to dispense the saline [29].

The accuracy of the flow rate calculations is also affected by a 2.5% difference for every degree change in temperature Celsius [29]. The higher the Springfusor<sup>®</sup> is above the injection point (whether intravenous or otherwise) the higher the flow rate. The flow rate increases by 2.4% of the initial calculation for every 30cm height the Springfusor<sup>®</sup> has [29]. Finally, the back pressure of the reservoir into where the syringe is pumping fluid also affects the estimated flow rate. The flow rates were calculated assuming normal intravenous back pressure of 5mmHg (666.6 Pa.)

### 2.2.3 Limitations of Pumps with Current Lab on a Chip Devices

Currently, most lab-on-a-chip applications require extra laboratory equipment and external pumps to propel the fluid through the chip. Handheld pumps enable the chip to be used without extra laboratory equipment thus allowing for point-of-care usage where the chip can be used to deliver a diagnosis on site. Most point-of-care chips currently are cheaply made disposable paper based microfluidic devices instead of plastic based devices which give them different fields of applications such as pathogen detection rather than cell separation and cell culturing [30].

In order to systematically and repeatedly realize a variety of desired applications with plastic based microfluidics (such as predictable droplet generation, microscale particle sorting, etc.) a pump with steady flow rate is required for a variety of reasons. With regards to droplet generation, different kinds of droplets are formed in different flow regimes as determined by the velocity and viscosity of the two fluids in question [31]. These two fluids then meet in cross flow at a T-junction to form droplets (See Section 2.3 for more information). A handheld portable pump that produces steady flow rates for such junctions would allow reliable and predictable droplet generation for people using point-of-care chips which in turn would allow for reliable experiments and diagnoses.

### 2.3 Droplet Formation

One of the key concepts in microfluidics is droplet formation. Droplets are created when two immiscible fluids are combined [32]. Three different methods of combining fluids can be used to form droplets and are defined depending on how the fluids move in relation to one another. These three mechanisms are called co-flow, flow focusing, and cross flow [31]. In co-flow one fluid is injected into a stream of the second fluid. Flow focusing works in a similar way to co-flow, except that the two flows then jointly enter a smaller channel. This paper, however, will primarily focus on cross flow, in which the two flows collide at a junction [31]. A graphic showing all three flow types can be found below.

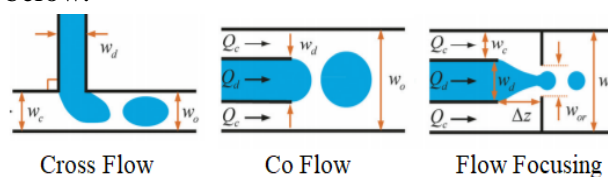


Figure 10: Diagram of Cross Flow, Co-Flow, and Flow Focusing [30]

In all three types of relative motion, the timing of droplet formation and the shape of the resultant droplet are governed by the interactions of gravity, capillary force, inertial force, and viscous force [31]. Based on the different ways these forces interact, five different flow regimes have been observed. These regimes are called squeezing, dripping, jetting, tip streaming, and tip multi-breaking [31]. Droplets can be formed in any one of the five different flow regimes, but will differ from one another in shape and in timing of their formation [31]. In squeezing, droplet formation occurs due to the buildup of pressure from the continuous flow. Droplets formed by squeezing tend to be plug shaped, with their length being primarily dependent on device geometry and the continuous flow rate. In dripping the droplet breaks off at the intersection of the two flows, primarily due to viscous forces. By breaking earlier than squeezed droplets, dripped droplets are more spherical with their diameter being determined primarily by the capillary number. The capillary number is defined as  $Ca = \mu V / \sigma$ , where  $\mu$  is dynamic viscosity,  $V$  is the characteristic velocity, and  $\sigma$  is the surface or interfacial tension [33]. In jetting a small stream enters the continuous phase and droplets break off the end of this stream as a result of Rayleigh-Plateau instability. Due to the relative lateness of droplet formation, jetted drops also tend to rely on channel geometry to determine their length. Tip streaming and tip multi-breaking have not yet been demonstrated in cross-flow and were, therefore, not considered in this project [31]. Figure 11 demonstrates cross flow droplet formation in squeezing, dripping and jetting.



Figure 11: Photographs of Droplets in the Squeezing, Dripping, and Jetting Regimes [30]

Droplets are an important concept in microfluidics because they allow for the creation of a consistent sample volume. Knowing the volume of the sample allows for uniform and reproducible results. In addition to being used to create unfluctuating sample volumes for testing droplets created on microfluidic chips can be used to conduct small scale chemical reactions. These reactions have been used to determine the correct dosage of certain medications by mixing the drugs into the droplets and observing the reactions. Droplets have also been used to cure cells in biological experiments. The cells were separated into droplets and allowed to grow for a period of time prior to continued testing [32]. Another exciting potential application for microfluidic droplets is their potential use in the creation of nanomaterials. In these chips, multiple flows would

be utilized, allowing two materials to mix in a single droplet setting off a chemical reaction resulting in nanoparticles [32].

The intent of this project is to experiment with the angles of a modified T-junction in an effort to create spherical droplets on an acrylic chip. The spherical droplet is desired because of the relative ease in measuring the volume contained within a sphere. Spherical droplets are most likely to be created in the dripping regime. It was determined through research that dripping is most likely to occur when the capillary number is between 0.013 and 0.1 [33]. Knowing the range in which the capillary number produces dripping allowed us to determine the flow rate in the channels which should yield dripping. Research indicated that a modified T-junction was most likely to yield spherical droplets. The T-junction is generally two streams which meet at a 90 degree angle where interfacial tensions cause the fluid from one of the channels to form droplets [31]. The modified T-junction varies the angle of one of the branches to be between 0 and 90 degrees. Although a modified T-junction was identified as the best method of creating spherical droplet generation, no previous research was found detailing what angle was optimal for spherical droplets.

## Chapter 3: Fabrication Methods and Parameters

Although each microfluidic chip was fabricated using slightly different procedures in this project, the same general fabrication method was used for all of the chips. This general method followed four steps:

1. A 2-D channel pattern was designed using AutoCAD
2. The pattern was printed onto a piece of acrylic using a CO<sub>2</sub> laser cutter
3. Tape or acrylic was used to form the fourth wall of the channel with various methods of bonding
4. The chip was prepared for testing, including the addition of hardware such as inlet and outlet tubing as needed.

The first step in this process was designing the channels using Solidworks or AutoCAD as shown to the right in Figure 12. Due to the fact that designs could be so easily modified using this software, iterations could be altered quickly reducing the time between design modifications.

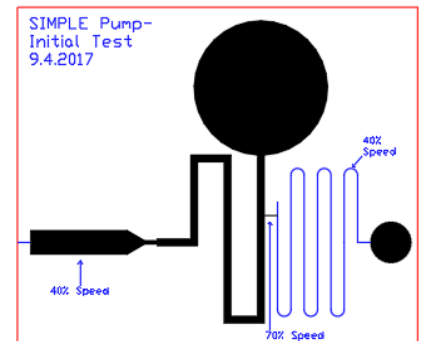


Figure 12: Microfluidic Chip Channel AutoCAD Design

The second step of the fabrication process was cutting the design onto acrylic. The laser cutter used in this project was a VLS4.60 CO<sub>2</sub> Laser Cutter. Once the design was complete, it was transmitted to a pre-installed software accompanying the laser cutter that converted the design into a file the laser cutter could print.

The third step, creating the final walls of the channels after the chips had been laser cut, was where the most variation in our process existed. This was due to the need for us to create a robust method to fabricate either the fourth or third and fourth walls of the channels in a way that would be most conducive to successful operation of our chips. The fourth wall was made out of either acrylic or tape. When chips were only vector engraved and rastered, only the fourth wall of the channel needed to be formed because the first three were cut from a single piece of acrylic. When the acrylic was through cut using vector cutting the third and fourth walls of the channels needed to be formed. In this method, they were always formed out of acrylic although the method to adhere the pieces of acrylic together varied between iterations. Several methods were tested to

determine the best method to create the final channel walls during this project as well as how to bond the walls together. The fourth and final step of chip fabrication was connecting any additional hardware to test the chips. This often including adding silicone or glass tubing to pump various fluids through the channels.

Since the second step, laser cutting, was the initial manufacturing process after the chip had been designed, our team wanted to determine the effect of the laser cutter’s settings on the outcome of the cuts including parameters such as channel depth, channel width, and cross-sectional shape. We performed a parametric study of the laser cutter speed, power, and number of passes to gain a better understanding of the laser cutter and its abilities to fabricate on acrylic.

### 3.1 Laser Cutter Parametric Study

Due to variations between lasers in individual laser cutters, a parametric study was valuable to determine the exact settings that were necessary to achieve desired channel parameters. Based on our literature review, we decided to vary power from 10% to 100% while holding speed constant (at the default speed setting for each kind of cutting) and conversely varied speed from 10% to 100% while holding power constant at default. We tested the effects of multiple passes on depth and channel width for vector engraving and rastering. We fabricated chips that included lines with between 1 and 7 passes.

<b>Parametric Study DoE</b>	<b>Vector Cutting</b>	<b>Vector Engraving</b>	<b>Rastering</b>
<b>Varying Power</b>	10%-50%; 10% Step	10%-100%; 10% Step	10%-100%; 10% Step
<b>Varying Speed</b>	10%-100%; 10% Step	10%-100%; 10% Step	10%-100%; 10% Step
<b>Number of Passes</b>		1-7; 1 Step	1-7; 1 Step

Table 1: Laser Cutter Parametric Study Design of Experiment

Machine Defaults	Vector Cutting	Vector Engraving	Rastering
Default Power	100%	64.6%	48.2%
Default Speed	7%	100%	100%

Table 2: Laser Cutter Machine Defaults

Once we had created these chips, we measured both the channel width and channel depth as well as noted the surface irregularities and deformities as the different combinations of settings affected them. Detailed graphs of the results of this study can be seen in the sections below.

### 3.1.1 Vector Cutting Parametric Study Results

Laser power and speed were varied in the vector cutting parametric study. Power was only adjusted up to 50% because the acrylic had been through cut at that point. By varying the laser power, we determined that the channel depth increased and the channel width did not noticeably change as power increased, as can be seen below.

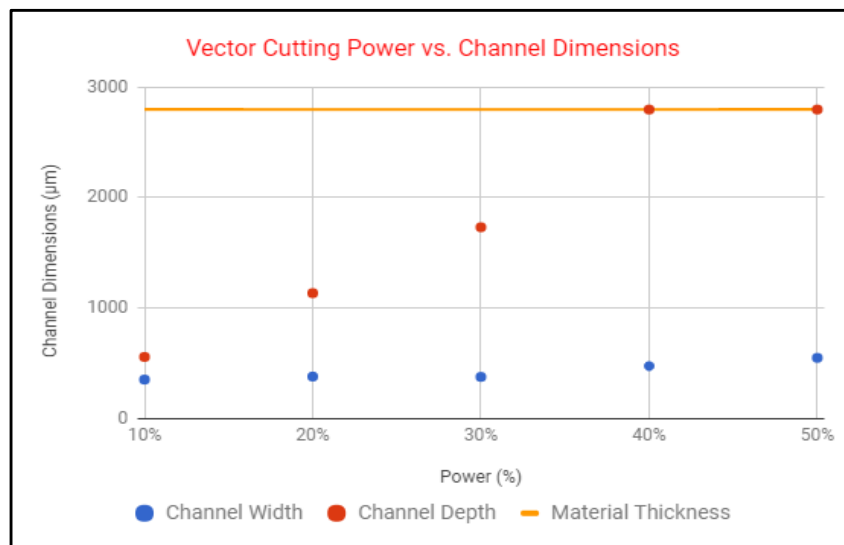


Figure 13: Vector Cutting Power vs. Channel Dimensions

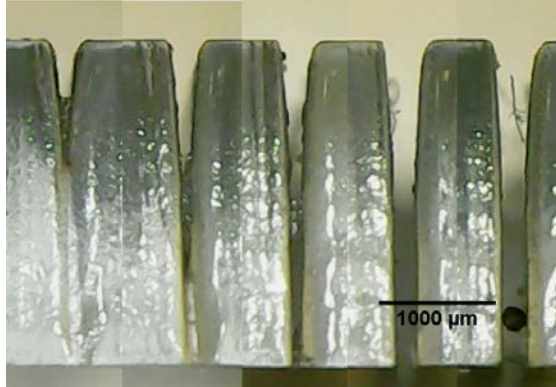


Figure 14: Increasing Vector Cutting Power

By varying the laser speed, we determined channel depth decreased and channel width did not noticeably change as power increased as can be seen below.

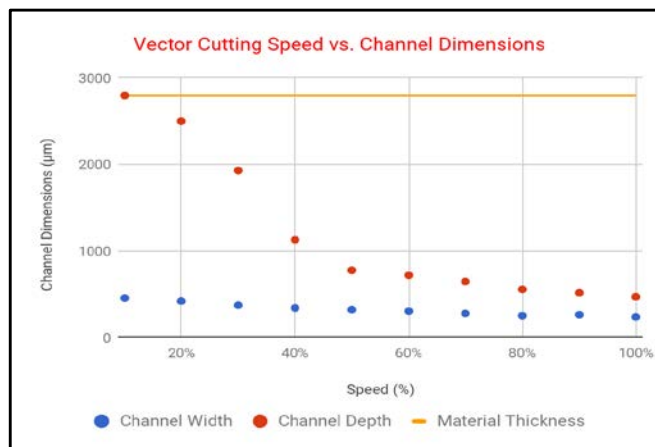


Figure 15: Vector Cutting Speed vs. Channel Dimensions



Figure 16: Vector Cutting Increasing Speed

### 3.1.2 Vector Engraving Parametric Study Results

Laser power, speed, and number of passes were varied in the vector engraving parametric study. By varying the laser power, we determined channel depth slightly increased and channel width did not noticeably change as power increased as can be seen below.

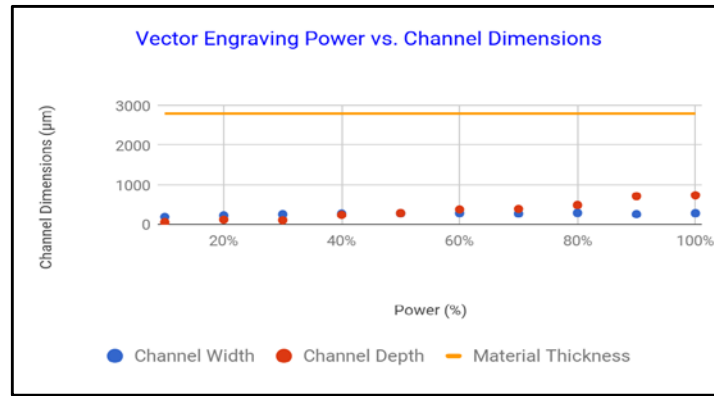


Figure 17: Vector Engraving Power vs. Channel Dimensions

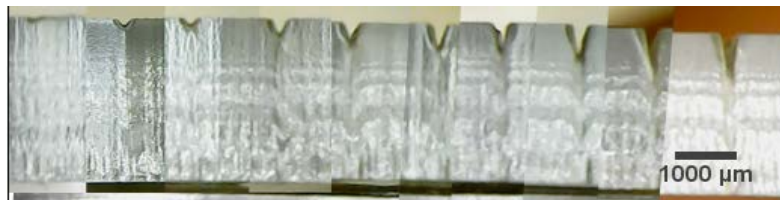


Figure 18: Vector Engraving Increasing Power

By varying the laser speed, we determined channel depth quickly decreased and channel width did not noticeably change as speed increased as can be seen below.

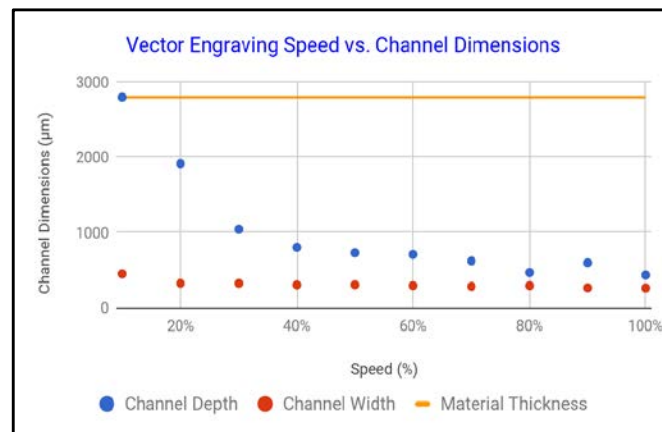


Figure 19: Vector Engraving Speed vs. Channel Dimensions



Figure 20: Vector Engraving Increasing Speed

By varying the number of passes completed by the laser cutter we determined channel depth increased and channel width did not noticeably change as the number of passes increased as can be seen below.

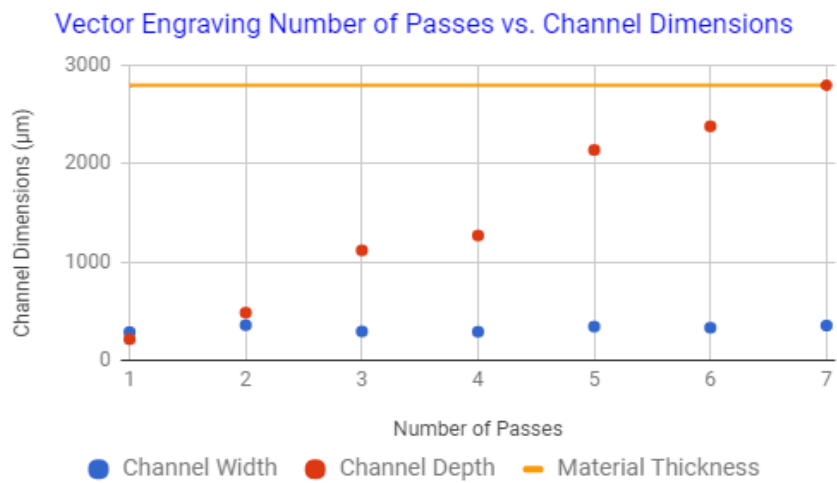


Figure 21: Vector Engraving Number of Passes vs. Channel Dimensions



Figure 22: Vector Engraving Increasing Number of Passes

### 3.1.3 Rastering Parametric Study Results

By varying the laser power, we determined channel depth slightly increased, channel width did not noticeably change, and channel cross sectional area was more visibly trapezoidal as the number of passes increased as can be seen below.

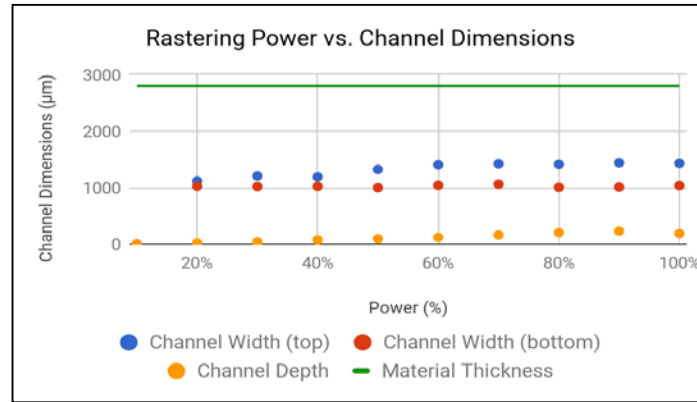


Figure 23: Rastering Power vs. Channel Dimensions

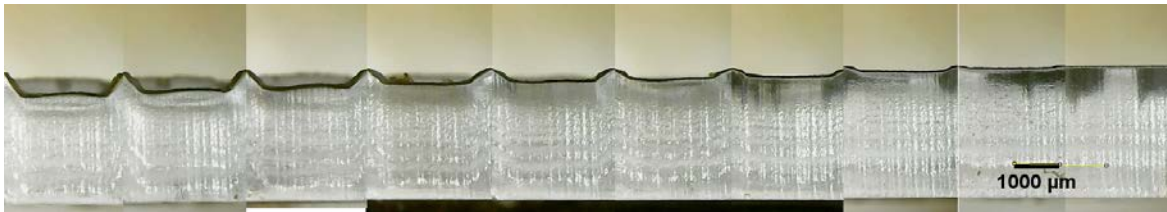


Figure 24: Rastering Increasing Power

By varying the laser speed, we determined channel depth decreased, channel width did not noticeably change, and left and right channel walls became more vertical as speed was decreased as can be seen below.

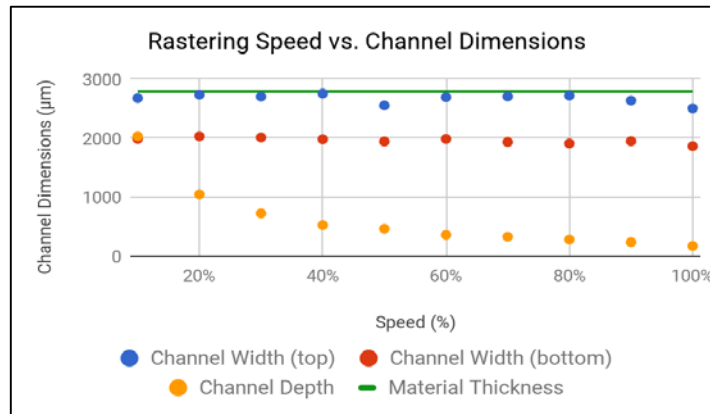


Figure 25: Rastering Speed vs. Channel Dimensions

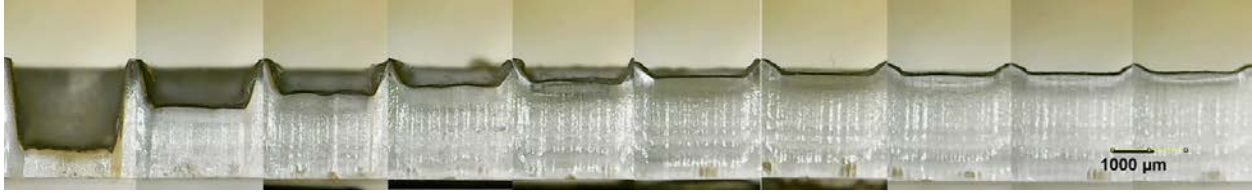


Figure 26: Rastering Increasing Speed

By varying the number of passes, we determined channel depth increased, channel width did not noticeably change, and channel cross sectional area was more visibly deformed as the number of passes increased as can be seen below.

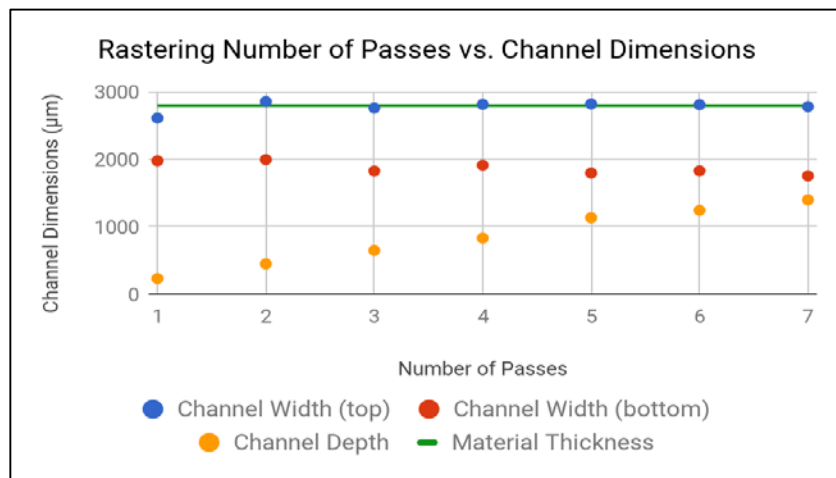


Figure 27: Rastering Number of Passes vs. Channel Dimensions



Figure 28: Rastering Increasing Number of Passes

### 3.1.4 Laser Cutter Parametric Study Conclusions

In general the results of the parametric study matched the trend in our literature review regarding speed and power's effects on depth. Our results revealed that lowering the speed at which the laser cutter was moving, increasing the power of the laser cutter, and increasing the number of passes all increased the depth of the channels. Channel width between vector engraving and cutting was essentially unchanged. The only change in the width of a cut came from rastering. This follows

logically due to the set width of the laser. From the results of our parametric study, we visually noticed a high surface roughness in rastered channels. Therefore, we decided to perform a surface roughness study to determine the effects of select chemical treatments on the channel surfaces.

### 3.2 Surface Roughness Study

In order to explore possibilities for reducing surface roughness in the fluid channels, we conducted an experiment to determine if surface roughness could be reduced with an additional step in the manufacturing process of our chips.

Table 3 shows the design of experiment for this surface roughness study. Our team decided to test the effects of water, isopropyl alcohol, and acetone on the surface of the rastered channels. Test acrylic that had not been used for another study was cut using the same parameters for each chip and each piece underwent its respective treatment. A control piece of acrylic was retained for each of the treatments so the surface roughness could be compared. An image of each treated and control chip were imaged using an LEXT OLS4000 Laser Confocal Microscope. The 3D images were decomposed into 2D profiles, five of which were taken from 100, 300, 500, 700, and 900 micrometers along the surface and analyzed for their Ra values using Mountains Map. Ra was selected for use due to its widespread use and understanding in the scientific and industrial community. The five Ra values were averaged for each treated surface and its respective control. An outlier filter was not used on this data. The results can be seen in Table 3. Microscope scans and additional data can be found in Appendix A and Appendix B: Surface Roughness Study Ra Values, respectively.

<b>Treatment</b>	<b>Control Average Ra (<math>\mu\text{m}</math>)</b>	<b>Post-Treatment Average Ra (<math>\mu\text{m}</math>)</b>
Water Rinse	9.594	10.652
Alcohol Rinse	9.446	9.854
Acetone Rinse	11.54	8.21
Acetone 30 Second Soak	9.258	3.122
Acetone 60 Second Soak	9.914	2.618

*Table 3: Surface Roughness Study Results*

As can be seen from the data above, the most significant result came from soaking the acrylic in acetone. However, leaving the chips soaking for too long resulted in chip disintegration. Additionally, when the acrylic came in contact with the alcohol and acetone, micro-fractures appeared around the fluid channels. When testing, these micro-fractures only became an issue when the tape could not properly adhere to the acrylic because of the fractures. In light of this data, our team began experimenting with treating fluid channels with alcohol or acetone to determine if reduced surface roughness would improve fluid flow or droplet generation.

After concluding this parametric study, we began designing and fabricating chips. The results from the laser cutter parametric and surface roughness studies allowed us to choose the initial fabrication parameters for our designs based on desired channel parameters. These two studies also allowed us to modify the laser cutter settings in subsequent iterations because we had an understanding of their effects on channel parameters.

## Chapter 4: Droplet Generation: Design and Optimization

Using the fabrication methods and parameters discussed in Chapter 3, we designed and fabricated microfluidic devices and worked to optimize the formation of spherical droplets. We tested each device, and continued improving the design and fabrication process for each device based on observations and results. The generation of droplets was realized through the use of cross flow and a modified T-junction. Parameters such as channel angle and fluid flow speeds were varied to determine their effect on droplet sphericity.

### 4.1 Droplet Generation

From the laser cutter parametric and surface roughness studies, we were able to determine the required laser cutter settings to create chips with the initial channel parameters determined by our literature review to be suitable for droplet generation.

### 4.2 Initial Droplet Chip Design and Fabrication

As mentioned in our background section, no research had yet been conducted to determine the angle which maximized the sphericity of a droplet formed by a modified T-junction, so this was a primary focus of our initial research. To determine the optimal angle for spherical droplet formation, a chip, shown in Figure 29, was fabricated with two channels which met at an angle. The goal was to fabricate chips with modified T-junctions, as shown in Figure 29, and vary the angle of the two inlet channels between 0 and 90 degrees with a step value of 15 degrees.

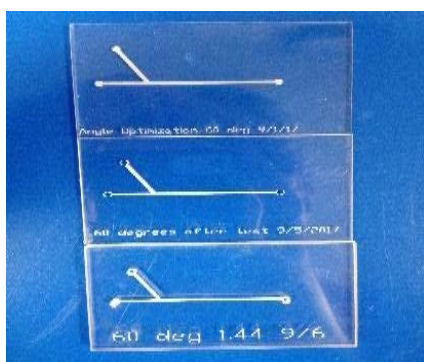


Figure 29: Microfluidic Chip

Using the parametric study, laser parameters were selected so that our finished channels were a similar size to the study we planned to follow. The design used channels that were intended to be 0.325 mm in width and 80  $\mu\text{m}$  in depth. After the fabrication of one chip, it was realized that

not only were the dimensions for the inlet too small for the tubing needed to connect to the pump, but that the channels were too small in general. The design of the channels were then scaled to be twice as large as the initial design. After measuring the tubing again, the outlet and inlet were adjusted to be 1.45 mm, a little smaller than the outer diameter of the tubing to allow for an interference fit. The designed channels were 0.65 mm in width and 80  $\mu\text{m}$  in depth. Once fabricated, a chip was cut in half to determine how true the dimensions were to the design. The fabricated chip had a width of 687.487  $\mu\text{m}$  (+5.77%) and a depth of 127.247 (+59.06%)  $\mu\text{m}$ . The cross section of this chip is shown in Figure 30 below.



*Figure 30: Channel Cross Section*

### 4.3 Initial Droplet Testing

Once the chips were fabricated, we began testing. Testing was conducted by adding two immiscible fluids to the chip through tubing and syringes attached to mechanical pumps, which kept the flow rate constant. The mechanical pumps used in this experiment were a Fusion series Precision Syringe Pump by Chemyx and a Longer Pump Model ISP02-1B. The two fluids this experiment used to test were water and VWR Vacuum Pump Oil 19. The water was colored using food dye to allow us to see the droplets as clearly as possible. Testing using the chips described above, with channels that were 687  $\mu\text{m}$  wide and 127  $\mu\text{m}$  deep, was unsuccessful early on due to leaking around the inlet holes. Multiple chips were fabricated with a variety of different sized inlet holes, but the leakage continued to occur.

### 4.4 Revised Material and Fabrication Technique

We observed chips fabricated by previous projects and noted that previous chips were all cut in much thicker acrylic than we had been using, so we switched to fabricating our chips on  $\frac{1}{8}$  inch thick acrylic. Once we made this switch, several other small changes were necessary. For example, we greatly reduced our inlet diameter- going from 1.45 mm to 1.27 mm. We also began to cut the inlets on the opposite side of the chips from our rastered channels at the suggestion of a graduate student in the lab. Flipping the chips prior to cutting the inlets allowed us to take advantage of the conical shape created by the laser cutter. The inlet was widest where the tubing

enters and narrowed as it approached the channels enabling a better interference fit. Cutting from the back into thicker acrylic also allowed us to take full advantage of the thickness of the acrylic by increasing the distance the tubing could go into the chip before it reached the channels.

#### 4.5 Initial Fabrication and Testing for Droplet Angle Optimization

Once we had chips that were functioning we cut chips at 15, 30, 45, 60, 75, and 90 degrees for testing. We analyzed the droplets we produced using a USB Digital Microscope 1-500x Continuous Portable Electron Microscope. In looking at the droplets created in these chips under the microscope, all of them were visibly much longer than they were wide. Images of some of the droplets formed can be found in the images below.

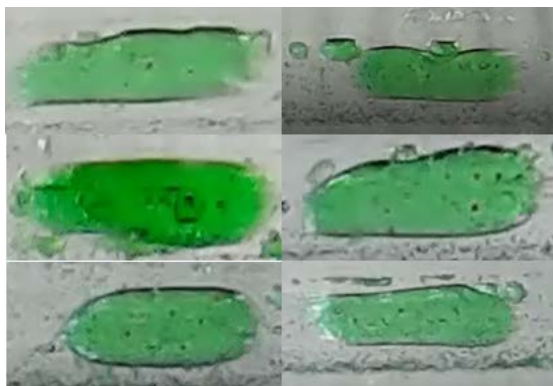


Figure 31: Droplets formed at 15, 30,45,60,75 and 90 degrees (left to right)

Analysis of the droplets in ImageJ showed that the droplets were between 2.6 and 6 times longer than they were wide. As can be seen in the graph below, the droplets formed at 45 degrees had the lowest length to width ratios.

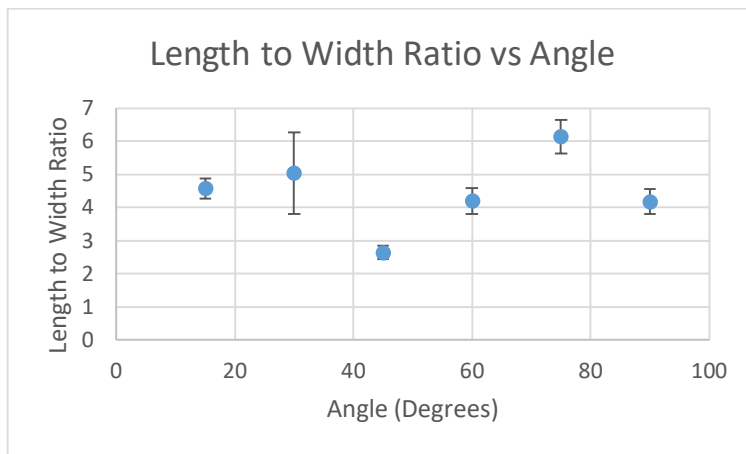
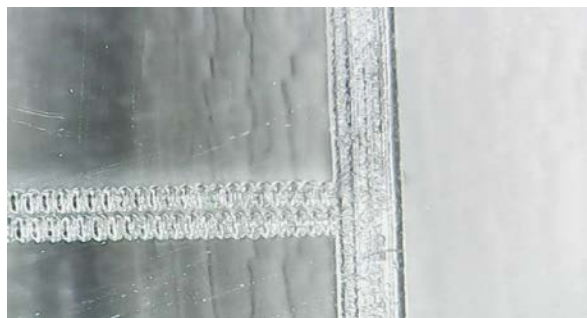


Figure 32: Graph Showing Average l/w ratio versus degrees (Oil speed 5 $\mu$ L/min-water speed 4 $\mu$ L/min)

Despite the fact that we were able to gather results from these chips, the sphericity of the droplets we were receiving was unideal. Feedback from Professor Liu confirmed our belief that a narrower channel might produce more spherical droplets, so new chip designs were created for fabrication.

#### 4.6 Scaling Down Channel Size

Our group first attempted to scale down our chips so that all the channels would be smaller than originally designed, but the water inlet channel would be smaller than the main channel. We changed our design so the water inlet channel was 250  $\mu\text{m}$  in width and the same depth as before. The main channel was scaled down as well and designed to have a width of 350  $\mu\text{m}$ . Testing began on this chip the next day, but we quickly realized that the rastering for the water inlet channel had not created a channel but cut two small jagged lines, as shown in Figure 33 below. The channels were too small for fluid to flow through and the inlet for the water began to leak due to pressure buildup in that channel.



*Figure 33: Incorrectly Rastered Channel*

After consulting with the professor again, we decided to scale down the whole chip rather than having a smaller water inlet channel. We made all the channel widths 350  $\mu\text{m}$  and kept the same depth as previous chips fabricated.

#### 4.7 Continuing Issues with Inlet and Outlet Leakage

Chips with the water inlet channel at 30, 60 and 90 degrees were fabricated to do an initial test of the design and to assure flow was possible through this size channel. We began testing these chip but had problems with the inlet hole for the water channel leaking. We decided to try two methods to fix this issue. First we fabricated three new chips with tubing connection diameters of 1.24mm, 1.25mm, and 1.26mm respectively. Each of these chips was tested and the 1.26mm

diameter chip worked best. The tubing did fit into the 1.25mm and 1.24 mm tubing but the tubing did not go far enough into the acrylic so the tubing pressurized and slowly pushed its way out of the chip until the inlet was no longer sealed properly. We decided to use the 1.26mm inlet diameter, but because we were still experiencing some leaking on the chip we decided to try another method to seal the channels.

After speaking with Professor Liu, we learned that graduate students in his lab occasionally glued the tubing in place. The glue used was NOA 68T manufactured by Norland Products, Inc. and was set with a UV light. This method of sealing the channels kept the inlets and outlet from leaking and also, in an initial trial, produced the most spherical and consistent droplets seen up to that point as seen in Table 1 below.

	Average l/w	Standard Deviation
Glued	2.724444	0.134476
Unglued	3.718629	0.983925

*Table 4: Length/Width Ratios and Standard deviation comparison between glued and unglued chip*

#### 4.8 Angle Optimization for Unglued and Glued Chips

While initial testing showed a benefit from the use of glue, this had only been demonstrated on one chip, and we wanted to confirm these results through the collection of more data at a wider spread of angles. This required a two-fold testing approach. First, chips with a 1.26 mm inlet diameter were fabricated at 15, 30, 45, 60, 75, and 90 degrees. These chips were then tested without glue using 5  $\mu\text{L}/\text{min}$  flow rates for the oil and 4  $\mu\text{L}/\text{min}$  flow rates for the water. Each chip was run until two good tests where droplets formed at the intersection with no leaking had been achieved and videotaped. Next, still images of the droplets were collected, three from each video, and measured using ImageJ. The length and width of the droplets were collected into an Excel spreadsheet which calculated the length to width ratios of each individual droplet as well as the average length to width ratio. The spreadsheet also calculated the standard deviation of the ratio,

these standard deviations are represented in the graph as error bars. The top view area of each droplet was also measured, and the standard deviation calculated. The image below shows an idealized version of the droplet with length, width, and top view area labeled.

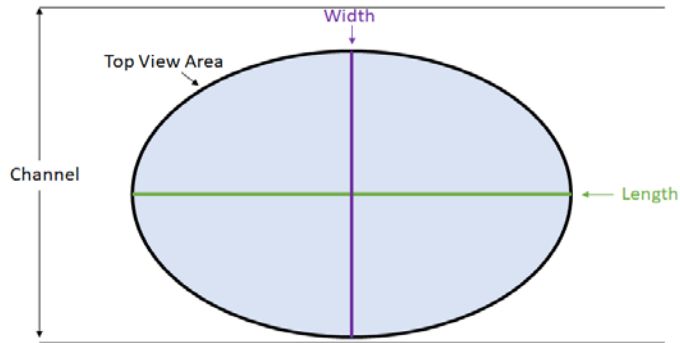


Figure 34: Droplet with measures labeled

Second, once we had gathered all of the necessary data from the chips without glue, all tubing was glued into place and the same testing procedure was followed again. The same data was collected in the same way, and placed into the Excel sheet. This data was graphed alongside the data collected from the unglued chips and is shown in the figures below. Gluing the tubing in place resulted in a much stronger correlation between angle and droplet size, with higher angles generally giving smaller droplets. Gluing did not, however, provide the overall improved ratios and lower standard deviations that we had hoped it would, so testing continued.

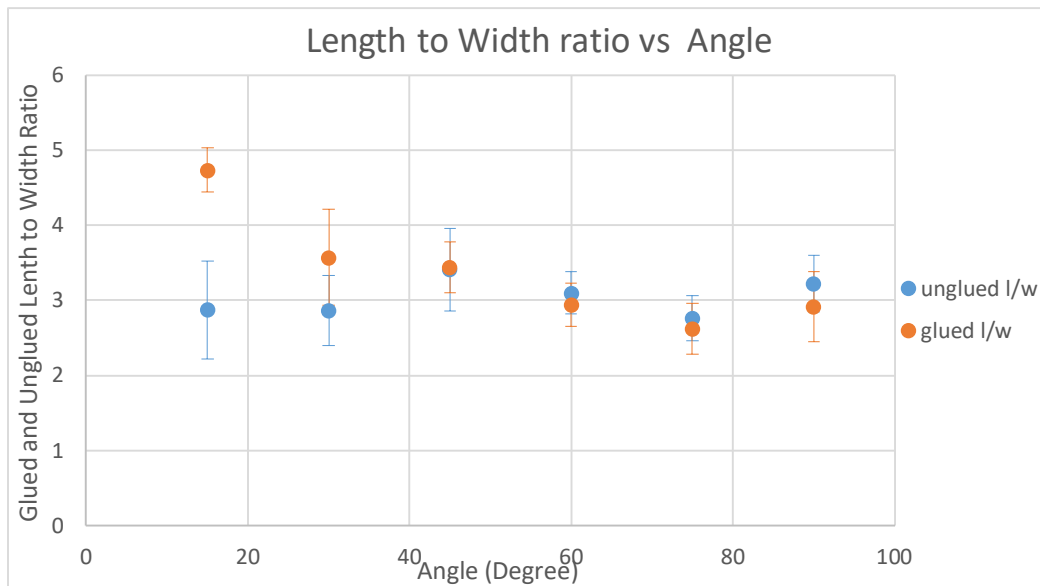


Figure 35: Graph Depicting Length to Width Ratio in comparison to angle (Oil flow rate 5 $\mu$ L/min-Water 4 $\mu$ L/min)

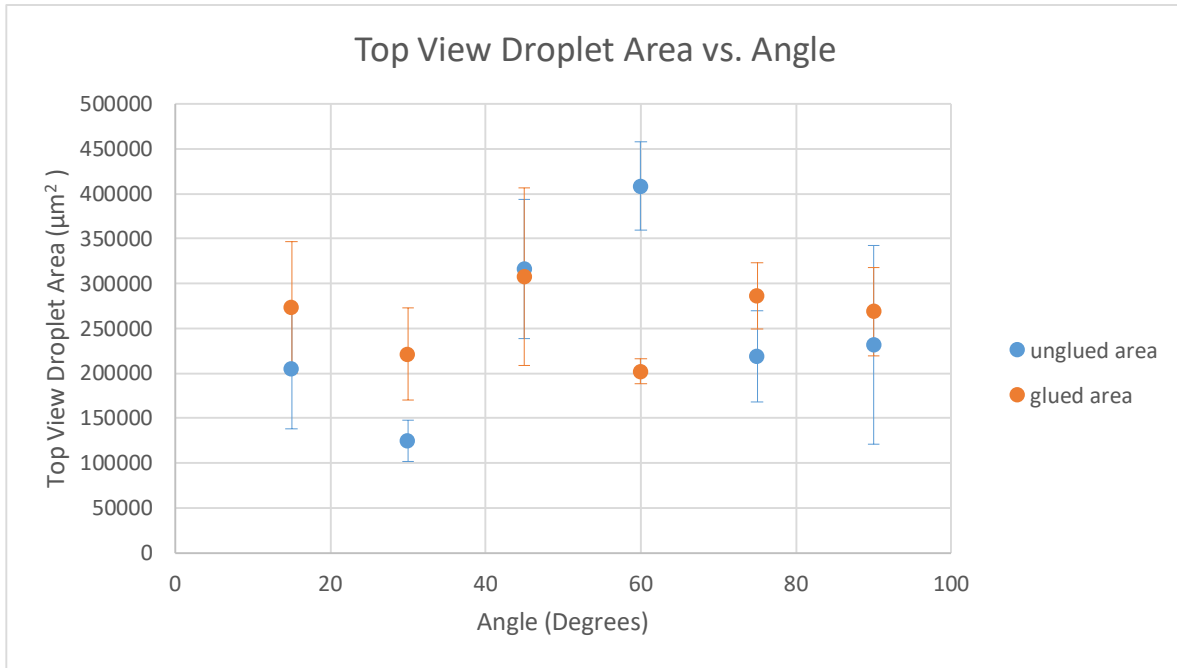


Figure 36: Graph showing area versus degree for glued and unglued chips (Oil flow rate 5µL/min-Water 4µL/min)

There is no clear relationship between chip angle and a droplet's length to width ratio. One possible reason is that droplet formation is governed primarily by other factors, such as the flow rates of the fluids.

#### 4.9 Flow Rate Optimization for Glued and Unglued Chips

In addition to studying how angles would impact droplet formation, we recognized that flow rates were another important factor influencing droplet sphericity. During our testing we noticed that when we turned the water pump off the droplets visually appeared to become more spherical. After this observation, we realized that the water flow rate either needed to be slower or the difference between the oil and the water flow rate needed to be greater. First, we tested increasing the difference between the oil and water flow rates by increasing the oil flow rates. This reduced the size of the droplets, but the ratio of length to width on average was still above 2, and there was a significant standard deviation. Next, we decided to try only reducing the flow rate of water. This yielded smaller droplets with a significantly smaller standard deviation as seen in Figure 37 below.

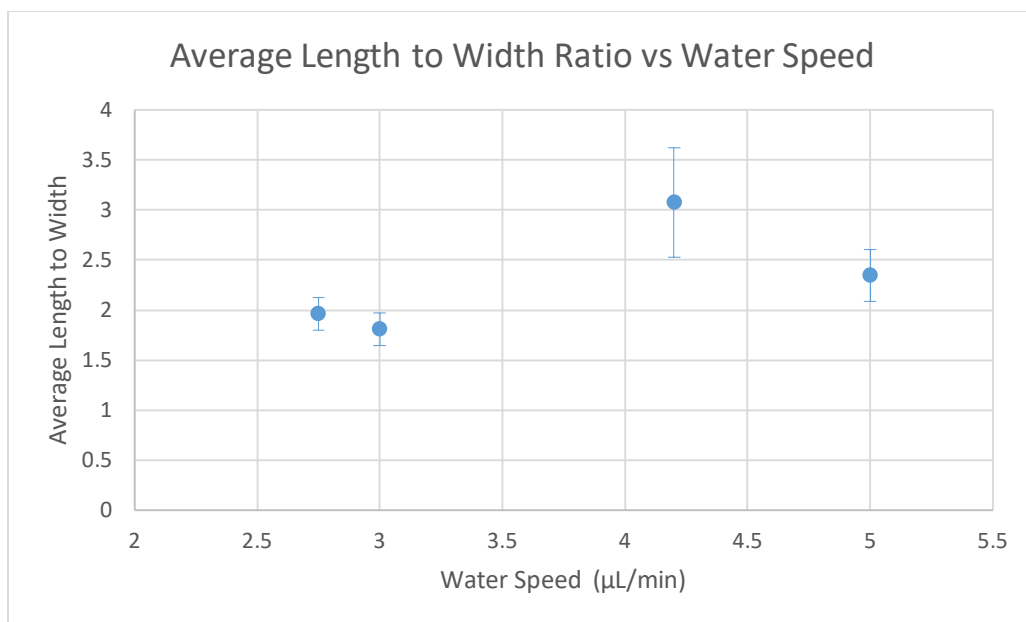


Figure 37: Graph showing Average L/W Ratio vs. Water Speed, Oil Speed constant at 7.2 µL/min

After seeing these results, we realized that further testing need to be performed with flow rates to optimize the sphericity of the droplets. Additionally, we wanted to test the new flow rates on chips that had the tubing glued to them. The oil flow rate was kept constant at 7.2 µL/min, and the water flow rate was varied between 2.25 and 3.25 µL/min with steps of 0.25 µL/min. This flow rate range was confirmed to be in the dripping regime through capillary number calculations. A MathCad file of these calculations can be found in Appendix C. Our research indicated that dripping occurred when the capillary number for the continuous flow needed to be less than 0.01. We tested the numbers with which we intended to test using the viscosity and surface tension of water and found that this would result in capillary numbers on the order of  $10^{-8}$ , putting us solidly in the dripping regime. This testing was performed on one glued 45-degree chip and one unglued chip. Tests were run until two trials were recorded without leaking or any other issues. The size of three droplets was measured per video to make a total of six droplets per flowrate. Figure 38 below shows the average ratio of length to width of each of the flow rates tested.

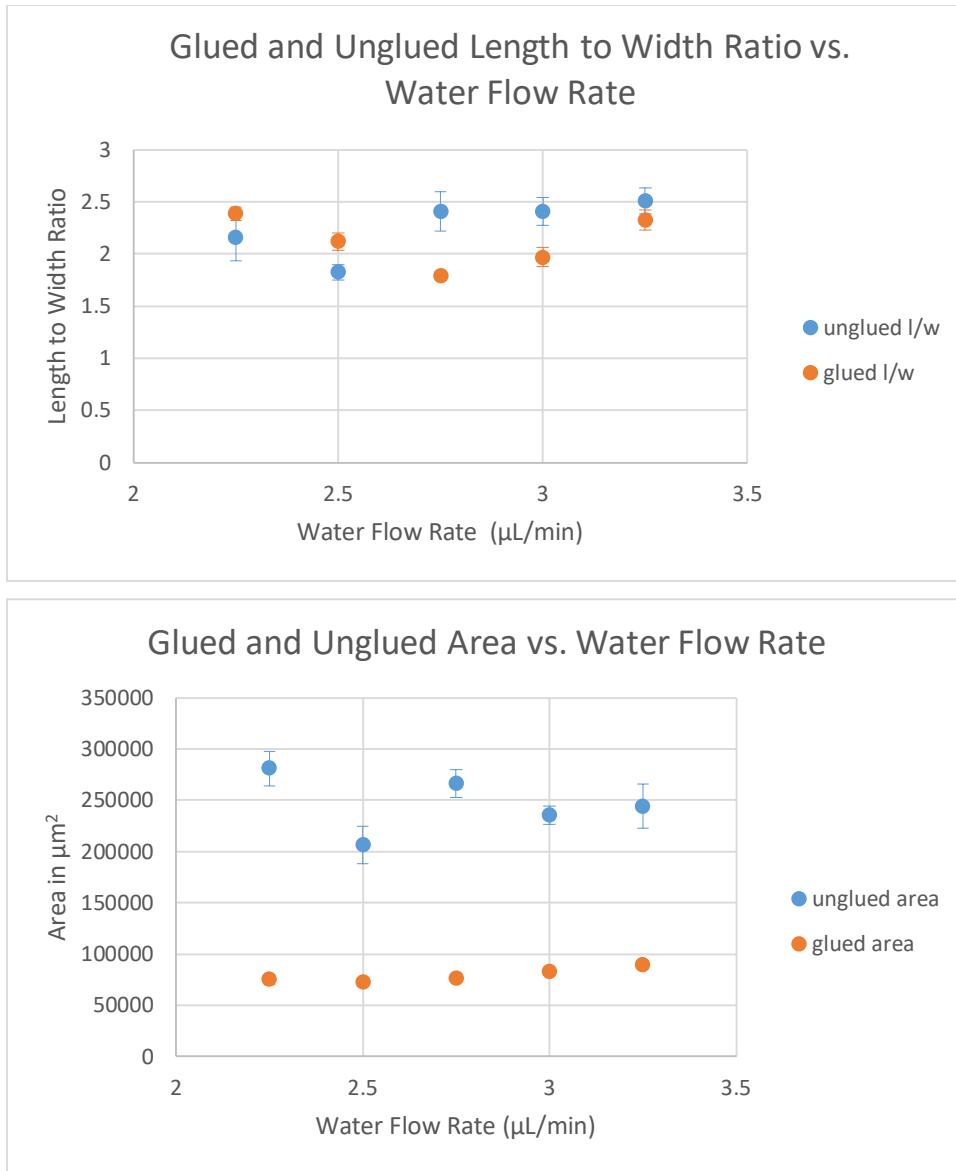


Figure 38: Graphs showing Average l/w and Area vs. Water Speed, Oil Speed constant at 7.2  $\mu\text{L}/\text{min}$  for glued chip

For the glued chips, the chip with the lowest ratio of length to width was the chip tested at a flowrate of 2.75  $\mu\text{L}/\text{min}$  for water and 7.2  $\mu\text{L}/\text{min}$  for oil. This droplet had an average ratio of length to width of 1.79 and a standard deviation of 0.042. There is no clear correlation between water flow rate and the length to width ratio. One possible reason is that droplet formation is governed by other factors, such as surface roughness or channel defects, which are difficult to control.

#### 4.10 Considerations for Integration with the On-Chip Pump

In the process of this testing a few ideas not directly affecting droplet sphericity were also tested. These ideas were intended to ease the combination of pumps and droplet generation towards the end of our project. One of the ideas was the use of hydrophilic tape, rather than hydrophobic tape, as the fourth wall of the channel. This idea failed, as the water simply flowed along the tape and did not create droplets. Another idea tested was that of through cutting the acrylic to improve the surface roughness of the channel. This created issues when we attempted to bond the chip we created with an additional piece of uncut acrylic to create the bottom of the channel. Gluing the chips together failed because it was nearly impossible to get the glue close enough to the channels for a proper seal without some of the glue entering and obstructing the channel. Acetone bonding, the method recommended to us by one of the graduate students, also failed because as the chips bonded together a residue was created which obstructed our channel. We were finally able to bond the chips together using a double sided adhesive layer between the chips, however the droplets formed in this chip were unmeasurably long, and the flowrates necessary to achieve more reasonable droplets were going to be infeasible when combined with our on-chip pump.

#### 4.11 Optimized Droplet Generation

After running tests to determine the optimal angle and flow rate, we began testing using optimized parameters. From our angle optimization trials, we determined that the 75-degree chip created the drops with a length to width ratio closest to 1. From our glued and unglued flow rate testing, it was determined that the optimal flow rates for the system were 2.75  $\mu\text{L}/\text{min}$  for water and 7.2  $\mu\text{L}/\text{min}$  for oil. We also decided to use the glued 75-degree chip for this testing. Glued chips were chosen because, although the droplets from the unglued chip are slightly smaller, it takes a significantly larger number of attempts to get a usable trial. Additionally, we wanted to simulate as closely as possible the setup we would use when we began testing with blood, and the glued chips almost completely eliminated the chance of leaking near the inlet and outlet tubing.

Because the flow rates for our optimized droplets were conducted on a 45 degree chip and our optimized angle was 75 degrees, we decided to test some flow rates around the optimized flow rate of 2.75  $\mu\text{L}/\text{min}$  obtained during flow rate testing performed on the 45 degree chip. As the droplets formed at lower flow rates had smaller areas, flow rates were tested between 2.25  $\mu\text{L}/\text{min}$

and 2.75  $\mu\text{L}/\text{min}$  with steps of 0.125  $\mu\text{L}/\text{min}$ . The results of this testing can be found in Figure 39 below.

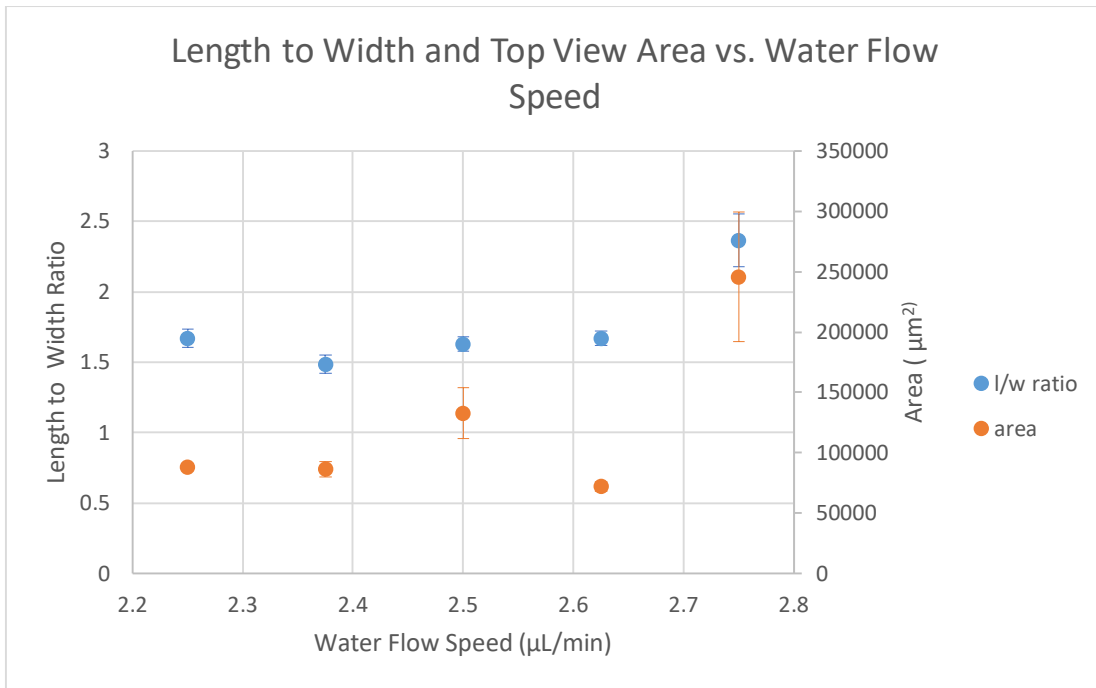


Figure 39: Graph showing l/w and area vs water flow speed, Oil speed constant at 7.2  $\mu\text{L}/\text{min}$  for glued chip

For our optimized testing the droplet with the lowest length to width ratio was formed at 2.375  $\mu\text{L}/\text{min}$ , with a ratio of 1.48 and a standard deviation of 0.064.

From our experiments on unglued chips:

- Length to width ratio is not impacted by intersection angle
- Top view area is not predictably impacted by intersection angle
- The best flow rates are 7.2  $\mu\text{L}/\text{min}$  for oil and 2.5  $\mu\text{L}/\text{min}$  for water

From our experiment on a glued chip:

- Length to width ratio is impacted by intersection angle
- Top view area is not predictably impacted by angle
- The best flow rates are 7.2  $\mu\text{L}/\text{min}$  for oil and 2.375  $\mu\text{L}/\text{min}$  for water

#### 4.12 Blood Testing

Once our group had determined our most optimized water droplets, we began testing the ability of our chip to generate blood droplets. Early in the process, this testing was complicated because the pump oil we were testing with was not allowed in the biohazard disposal bins. Biologically based cooking oils, such as vegetable or olive oil, were allowed. The viscosity of olive oil is closest to that of the pump oil so new testing was conducted using olive oil. The capillary number calculated for the pump oil at 7.2  $\mu\text{L}/\text{min}$  was 0.016. That number was combined with the olive oil viscosity and surface tension to calculate an appropriate volumetric flow rate for the new, less viscous olive oil. The calculated flow rate to create a capillary number of 0.016 using olive oil was found to be 16.3  $\mu\text{L}/\text{min}$ . Testing was conducted at 7.2, 12.2, and the calculated 16.3  $\mu\text{L}/\text{min}$  to ensure that the droplets formed were comparable to the droplets formed using the pump oil. The results from these tests can be found in the graph below.

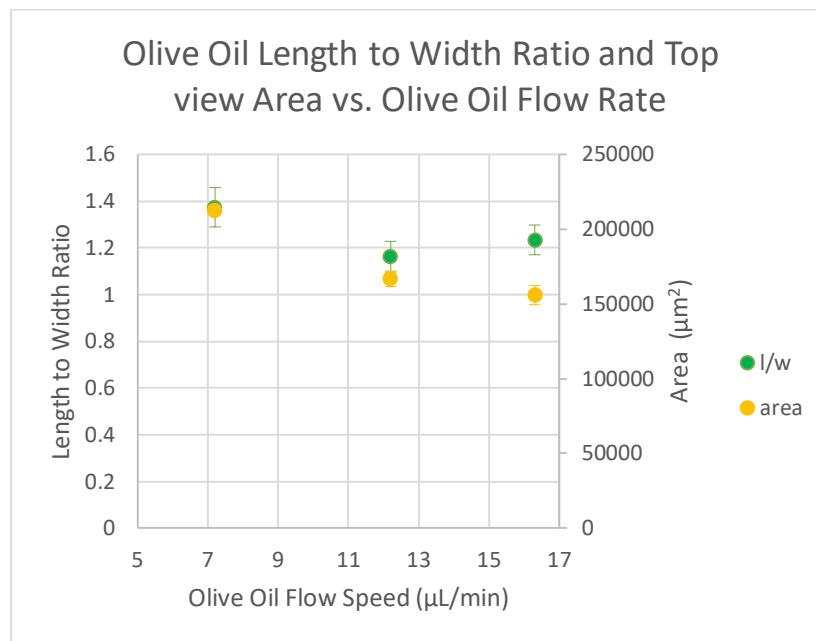


Figure 40: Graph Showing l/w and area vs. oil flow speed water held constant at 2.5  $\mu\text{L}/\text{min}$

Once we had proven that reasonably spherical droplets could be produced using the olive oil at higher flow rates, we began testing with blood. The original blood cell concentration of our sample was 800,000 red blood cells per microliter of blood. As this was already fairly diluted, our first set of testing was run at a dilution of 1 part blood to 9 parts saline for a cell concentration of 80,000 cells per microliter. This dilution unfortunately did not produce consistent droplets, and

instead seemed to allow the blood solution to stream down the channel uninterrupted. In an effort to combat this a second round of testing was conducted, this time with the blood diluted farther down, 1 part blood to 12 parts saline, resulting in a cell concentration of 61,538 cells per microliter of blood. As the camera can only capture two dimensional images, a photo was taken of the diluted blood and a cell count was performed. 88 cells were counted in 31552 square micrometers for an approximate concentration of 0.002789 cells per square micrometer. This number was multiplied by the area of each cell to determine the approximate number of cells per droplet. Testing at this concentration was successful with droplets being formed. The data from these droplets, as well as images of them in the outlet tubing and under the microscope can be found below.

	Length	Width	L/W	Area	Cells per Drop
Drop 1	569.983	280.466	2.032271291	141187.397	393.7773472
Drop 2	556.817	284.449	1.957528415	136816.727	381.5873722
Drop 3	505.887	298.709	1.693578031	131071.013	365.562344
Drop 4	532.268	299.949	1.774528336	138583.638	386.5153583
Drop 5	548.525	301.851	1.817204515	139714.138	389.6683684
Drop 6	523.202	310.06	1.687421789	136571.183	380.9025401
Average	539.447	295.914	1.82708873	137324.016	383.0022217
Standard Deviation	23.48738362	11.22085081	0.14093023	3525.597529	9.833033768
% Deviation	0.04353974277	0.03791929684	0.0771337635	0.02567356848	0.02567356848

Table 5: Length, width, l/w, and area of blood droplets

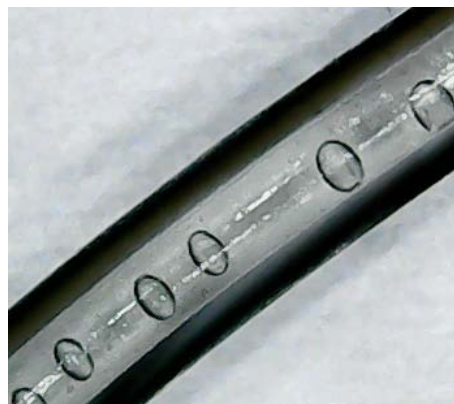


Figure 41: Droplets captured in outlet tubing



*Figure 42: Droplet seen under a microscope. Arrows show examples of individual blood cells.*

## Chapter 5: On Chip Pump Design, Prototyping, and Characterization

In order to produce droplets entirely on chip, our team investigated several kinds of microfluidic pumps to be integrated onto our acrylic based system. After concluding our background research, we selected the design criteria that needed to be met by our pump designs. The first of these criteria was that the pump must be handheld and require no outside mechanical device for operation. The second criterion was for the chip to be reusable. For this, we examined paper based pumps, gravity-driven pumps, and weight driven syringe pumps.

### 5.1 Paper Based Pumps

A paper based pump fit our criteria because it utilizes the capillary action of paper on a microfluidic chip to cause constant flow. It is handheld and has the potential to be reusable if constructed with acrylic and pressure sensitive adhesive. For these reasons, we created multiple designs and test iterations to adapt the “Self-Powered Imbibing Microfluidic Pump by Liquid Encapsulations” or SIMPLE pump found in the literature review to make it compatible with acrylic based microfluidic chips to capitalize on the benefits of this alternate material [21].

#### 5.1.1 Paper Based Pump 1.0

Our first acrylic chip design, Paper Based Pump 1.0, shown in Figure 43 was a pump modeled after the SIMPLE pump and modified based on other research conducted into paper based pumps [21].

This design was modified to include a semi-circle paper shape and working fluid channel tapering in the section immediately prior to the working fluid meeting the paper as shown in Figure 44. The working fluid channel was printed to allow a wider path than the analytical fluid in order to yield less fluidic resistance than the analytic fluid path, thus keeping the working fluid in its respective channel (Exact laser cutter setting can be found in Appendix C: Capillary Number Calculations and Appendix D: Paper Pump Design Pictures and Settings.) Between the analytic and working fluid channels, our team vector engraved a line

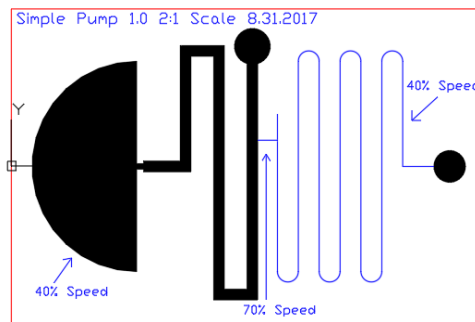


Figure 43: Paper Based Pump 1.0 AutoCAD Drawing

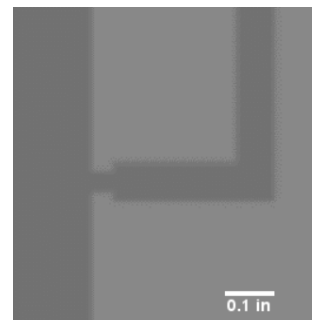


Figure 44: Paper Based Pump 1.0 Tapered Working Channel

shallower than the working fluid channel to pull the analytic fluid into its respective channel. This was added in place of the passive valve used in the original SIMPLE Pump so that the chip could be fully fabricated using a laser cutter. Once printed, it was determined that the dimensions of the finger pressed membrane were too small and thus not conducive to human interaction.



Figure 45: Photograph of Paper Based Pump 1.0 The chip size is about 57x38x3 mm

### 5.1.2 Paper Based Pump 2.0

We chose to revise our design to Pump 2.0 with a modified paper chip shape to ensure constant flow rate by eliminating the varying wetting radius,  $\Phi$ , present in the semi-circle design of Pump 1.0 that can be seen in Figure 46: Wetting Radius Depiction. We used a rectangular prism that tapers to a point where it contacted the working fluid. The rest of the settings remained the same as Pump 1.0.

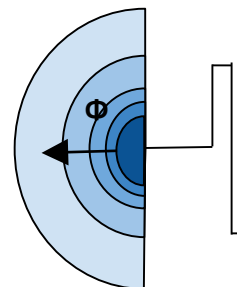


Figure 46: Wetting Radius Depiction

The working and analytic fluid used in these tests were water mixed with food coloring so test results could be visually observed. The fluid was dispensed into the inlet reservoirs of the chip using syringes. A piece of Whatman 1 Filter Paper was trimmed to fit the shape of the paper chamber on the chip and placed in it. The entire chip was then covered with hydrophobic Adhesives Research ARCare 92734 tape (MSDS sheet can be found in Appendix E [34]) and the working fluid was then activated with a finger push.



Figure 47: Photograph of Paper Based Pump 2.0 with Leakage

Because multiple pieces of tape were used instead of a solid piece, there was leakage between the layers as can be seen in Figure 47. Although the working fluid made it to the paper, when the finger was removed, a suction force was created as the tape returned to its unstressed state, and the working fluid was pulled back into the holding chamber. Because of the initial leaking issue, the trial was conducted again with a single piece of tape. However, the vacuum issue was not solved and the liquid still returned to the working fluid channel.

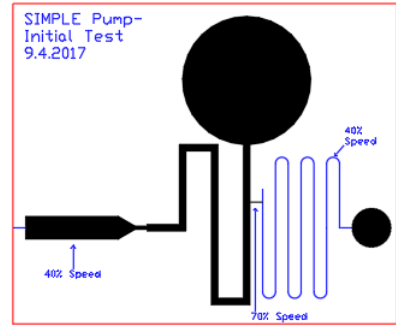


Figure 48 : Paper Based Pump 2.0 AutoCAD Design

### 5.1.3 Pump 2.1

In order to combat the vacuum issue, vents were added in the next design iteration. They were created with single vector engraved lines connecting the working fluid entrance, analytic fluid entrance, and paper chip to the outside environment at the top, right, and left edge of the chip, respectively. When the tape was adhered to the top, the vents allowed the respective parts of the chip to remain open because the tape adhered only to the top of the chip. The filter paper was widened to absorb working fluid for a longer duration and the finger activation area was further reduced to more closely match the size of a finger.

The same fabrication steps were completed as during the testing of Pump 2.0, and the same vacuum issue occurred limiting the ability of the working fluid to be steadily drawn into the filter paper. There was now also leakage of the working fluid through the vent connecting it to the top of the chip.

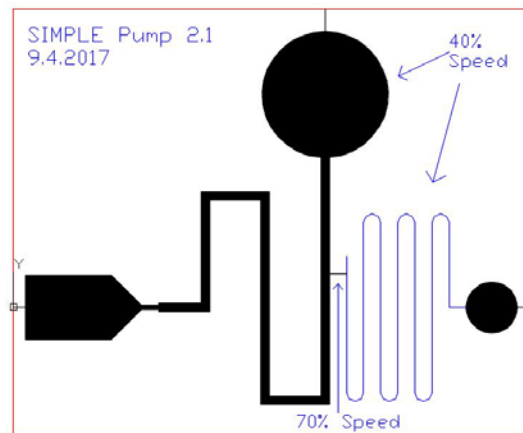


Figure 49 : Paper Based Pump 2.1 AutoCAD Design



Figure 50: Photograph of Paper Based Pump 2.1 Sealed with Scotch Tape

During testing, it was examined that the tight PET liner of ARCare 92734 was separating from the adhesive on the hydrophobic tape in certain areas of this chip causing leakage throughout the chip surface. To immediately test if the separation of adhesive was

causing an issue, Scotch Magic Tape that was available in the lab was tested on the chip as can be seen in Figure 50. The working fluid was successfully drawn into its channel after finger activation using the wicking force of the paper. The analytic fluid, however, did not move- indicating there was not sufficient negative pressure in the analytic fluid channel. This was attributed to the Scotch tape being applied in multiple layers, allowing for air leaks between layers.

#### 5.1.4 Pump 2.2- 2.4

Pumps 2.2, 2.3, and 2.4 were all designed and tested at the same time to reduce the time between iterations and to test multiple ideas in parallel. All of these pumps were designed with the intention of making it easier for the analytic fluid to flow- although, they all achieved this in a different way. Pump 2.2 had a shortened analytical fluid resistor, shortened and widened working fluid channel, smaller analytic fluid entrance, a larger paper chip, and a

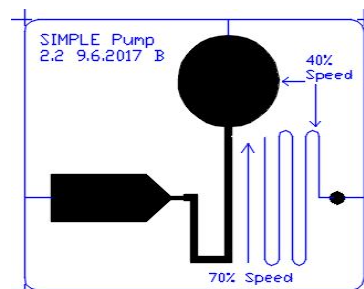


Figure 51 : Paper Based Pump 2.2 AutoCAD Design

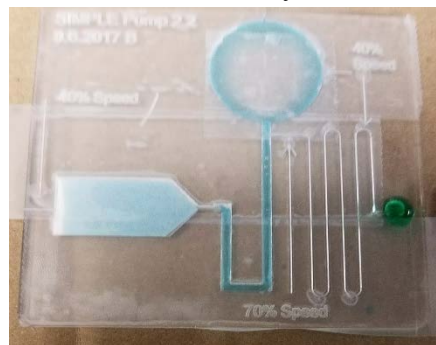


Figure 52: Photograph of Paper Based Pump 2.2 during Testing

smaller overall chip size. All of these changes were made to more closely mimic the original SIMPLE pump design.

During testing, we had similar results to Pump 2.1 as we were able to get the working fluid to flow by the wicking force of the paper, but were unsuccessful at achieving analytic fluid flow as can be seen in Figure 52.

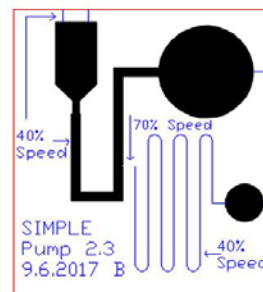


Figure 53 : Paper Based Pump 2.3 AutoCAD Design

Pump 2.3 had an even shorter working fluid channel than Pump 2.2 and two vents connecting the paper to the edge of the chip. We added these two vents instead of one to allow more air to be released when the paper drew in the working fluid. When we tested this iteration, the working fluid was successfully moved via wicking force from the paper, but the analytic fluid did not flow into the channel.

Pump 2.4 was identical to Pump 2.3 except for an even wider working fluid channel. The pump was able to successfully move working

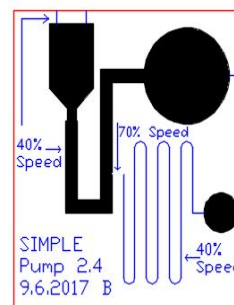


Figure 54 : Paper Based Pump 2.4 AutoCAD Design

fluid, but the analytic fluid was not pulled into the channel. We took note of the fact that the vents in the finger press area were a probable cause to the analytic fluid not flowing due to the fact that air is a less viscous fluid and therefore would be more likely to flow than the analytic fluid.

These results led us to re-examine our channel parameters and material properties. We also developed pumps with simplified analytic channels to test in parallel to test additional designs.

### 5.1.5 Pump 2.5

Pump 2.5 was drafted with no fluidic resistor in the analytic fluid channel and only one bend in the working fluid channel. This was done to decrease the hydraulic resistance in the analytic channel to make it easier for the analytic fluid to flow. The paper chamber was extended to the edge of the chip to ensure the air from the paper was able to leave the pump to allow the working fluid to saturate the paper. The vent on the analytic fluid entrance was removed to ensure air, a less viscous fluid and

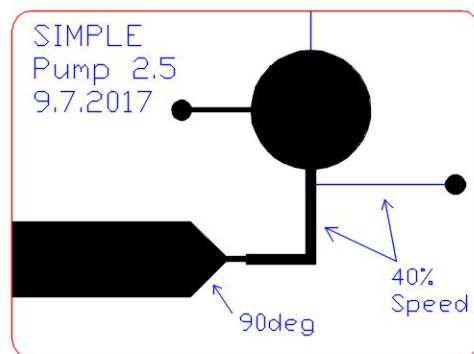


Figure 56 : Paper Based Pump 2.5 AutoCAD Design

therefore a fluid more susceptible to being drawn into the channel, did not do so in place of the



Figure 55: Photograph of Paper Based Pump 2.5 during Testing

analytic fluid. An additional working fluid channel segment was added to the left of the finger activation area so working fluid could be pushed into the finger activation area with a syringe.

We were unable to test Pump 2.5 when covered with hydrophobic tape because we could not successfully fill the finger activation area with working fluid via the syringe inlet. We then covered the chip with hydrophilic tape and both the working and analytic fluid immediately began flowing without pump activation (seen in Figure 55) - necessitating design changes to increase hydraulic resistance in the analytic channel.

### 5.1.6 Pump 2.6- Pump 2.9

Pumps 2.6- 2.9 were iterations designed similarly to Pump 2.5 with slight modifications based on the hydrophilic tape results from Pump 2.5. Our team added different elements to increase

the hydraulic resistance of the channels (especially the analytic fluid channel) to discourage the fluid from flowing prior to activation. We tested these iterations using hydrophilic tape and all of the subsequent iteration design changes were made based on the fact that we were using hydrophilic tape. While running these pump tests, another subset of our team was simultaneously running tests on droplet generation with hydrophilic tape. We found that even though hydrophilic tape helped our pump run, it was not conducive to droplet generation. Therefore, we terminated our use of hydrophilic tape, and results from these pumps were not useful in further iterations. However, these results can be found in Appendix D.

#### 5.1.7 Pumps 2.10- 2.17

After we had determined that we should not be using hydrophilic tape in our pumps due to its effect on droplet generation, we went back to our base design of 2.10 which was a reflection of the design iteration changes made between Pumps 2.6 and 2.9 as well as being influenced by the SIMPLE Pump found in literature. The main influence from the SIMPLE Pump in literature was moving the analytic fluid channel up to the finger activation area. The idea behind this move

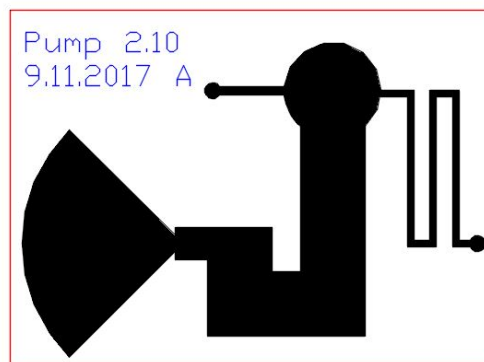


Figure 57 : Paper Based Pump 2.10 AutoCAD Design

was to utilize the vacuum created in the finger activation area to draw in the fluid from the analytic channel. We widened the shape and angle of the filter paper to increase the central angle and total absorptive capacity of the paper. This was done to increase the pull that the paper had in the channel. However, when we tested it with hydrophobic tape, we could not get the working fluid into the working fluid channel due to the resistive properties of the tape.

We also began using a syringe with a needle tip to ensure the working fluid would reach the finger activation area. This kind of syringe was necessary due to the results from Pump 2.5. However, when we used a syringe to pump the fluid into the channel, the fluid would leak under the tape we were using to seal the top of the chip due to the pumping force of the syringe. We realized that the seal between the tape and the acrylic chip was not strong enough so the force from injecting the fluid via needle-tipped syringe was ripping the tape off the chip. Therefore, we decided that in future iterations, we needed to pre-fill the working fluid channel. In order to ensure

that the working fluid would not fill the analytic fluid channel or the paper area before we pressed the working fluid into the channel, we added thinner channels between the working channel and the analytic channel as well as the working channel and the paper area in our new design 2.16 as discussed below.

The design for Pump 2.16 can be seen in Figure 60 to the right. When we pre-filled the channel, we did not encounter problems with the working fluid going into the paper area or the analytic channel. However, when we pressed the finger activation area to initiate fluid flow, the working fluid moved for a short amount of time until we let go of the finger activation area and the fluid flowed back to the finger activation area to fill the vacuum created by the lack of fluid.

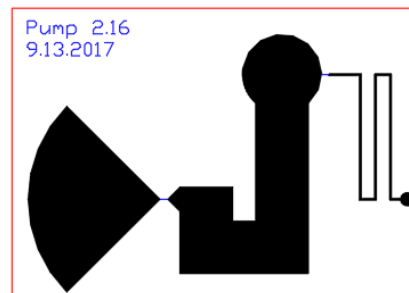


*Figure 58 : Paper Based Pump 2.16  
AutoCAD Design*



*Figure 59: Photograph of Paper Based  
Pump 2.16 during Testing*

We also had problems with leakage between the tape and the working channel once we placed the tape on top of the chip. Additionally, the tape stuck to the bottom of the working fluid channel as it was deformed due to the vacuum created by the wicking force of the paper. A picture of this trial can be seen in Figure 59. We decided to try to fill the channel to its maximum capacity in order to mitigate this problem. Therefore, in design 2.17, we added back in our channel inlet to allow our team to pre-fill the working channel and then fill the rest of the channel fully using a syringe. The inlet did not prevent our issues with leakage, and prefilling did not prevent the tape from sticking to the bottom of the working fluid channel. From this, we decided to pursue other, less deformable materials to use to cover the working channel to mitigate this problem.

#### 5.1.8 Pumps 2.18- 2.21

Our team decided to cover the working fluid and analytic fluid channels with another piece of acrylic due to its increased rigidity compared to tape. We tried several different methods to bond the two pieces of acrylic together. Our team tried double sided 3M Scotch tape attached directly

to the acrylic, sealing the channel first with the hydrophobic tape used in earlier iterations and then attaching the upper piece of acrylic with double sided 3M Scotch tape, bonding the two pieces of acrylic with acetone, bonding the two pieces of acrylic with UV hardened glue, and using the hydrophobic tape as double sided tape to adhere the two pieces to each other.

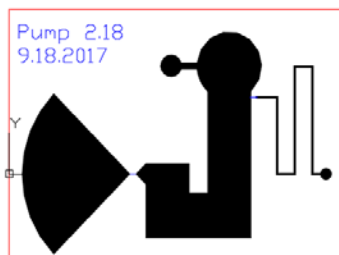


Figure 60 : Paper Based Pump 2.18 AutoCAD Design

The first iteration, Pump 2.18 is shown to the left and is very similar to Pump 2.17 except in this design, our team moved the junction between the working and analytic fluid down to below the finger press to reduce the influence of the finger pressure on the analytic fluid. In this design, the majority of the working and analytic fluid channels were covered by acrylic, leaving the rest of the chip solely covered with tape. When our team tested this design we had problems with leakage both during testing as well as when we filled the working fluid channel at the beginning. A picture of this trial can be seen in Figure 60. Additionally, the vacuum continued forming in the finger press area despite the majority of the chip being covered in acrylic.



Figure 61: Paper Based Pump 2.18 during Testing

Therefore, in Pump 2.19 (shown in Figure 62), we made the design change of extending the paper area to the edge of the chip, allowing us to fabricate an acrylic top piece that would cover the entire chip except the working fluid inlet, the analytic fluid inlet, and the finger activation area. These areas would be sealed with other kinds of tape. The rest of the iterations in Pump 2.19 focused on how to ensure leakage would not occur in the channels during operation as this leakage was detrimental to our chip operation.

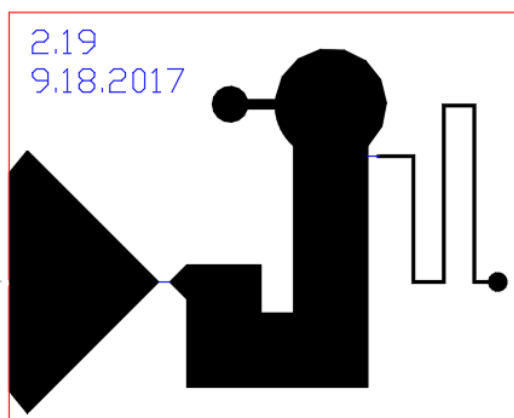


Figure 62 : Paper Based Pump 2.19 AutoCAD Design

The first way we tried attaching the upper acrylic chip to the base was using only double sided 3M Scotch tape. This led to many leakage issues as the tape was narrow so the fluid would run along the junctions of the tape instead of in the channel as can be seen in Figure 63. We then tried sealing the channels with the hydrophobic tape and then used double sided tape to attach the upper acrylic piece. This also led to leakage problems, similar to issues seen when the channels were sealed exclusively with hydrophobic tape, where the fluid would have enough pressure to push up the tape and flow between the tape and the acrylic.

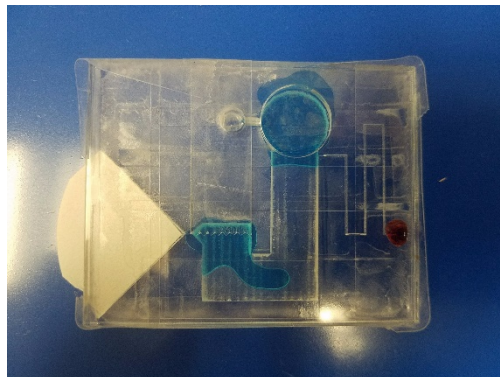


Figure 63: Paper Based Pump 2.19 during Testing- Bonded with Double Sided Tape

Then we decided to try to use methods other than tape to attach the two pieces. We first tried acetone bonding which had been used previously in our lab. To do this we applied a thin layer of acetone between the upper and lower acrylic chips and pressed them together. The acetone dissolved parts of the two chips thus bonding them together. The issue with this was that the acetone and acrylic mixture obstructed both the working and analytic fluid channels making them impassable. However, when bonded using this method there was not much leakage in the areas where the working fluid could flow. Thus, our team decided to pursue an option to attempt to utilize this bonding while not obstructing the channels.

We designed Pump 2.20 similar to 2.19 but with a different junction between the working fluid channel and the filter paper area. It was to be cut out of 1/16” acrylic and acetone bonded to two pieces of acrylic- one the same as the top acrylic chip mentioned earlier and one a blank acrylic rectangle to act as the bottom of the channels. When we tested this, we acetone bonded the middle layer to the bottom acrylic chip and then used a knife to cut out any blockage in the channels. We then acetone bonded the middle to the top layer. We still had issues with the acetone-acrylic mixture in the channels which blocked the fluid flow. A picture of this chip can be seen in Figure 64.

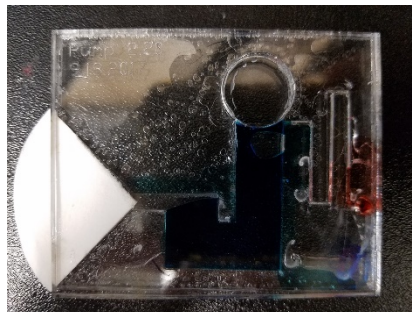


Figure 64: Paper Based Pump during Testing 2.20- Bonded with Acetone

We then went back to our 2.19 design and tried other methods to bond the two pieces of acrylic together. Our next iteration used UV hardened glue to permanently attach the two pieces together. This iteration did not yield useable results due to the inability to get the glue close enough to the channels to provide a sufficient bond to seal the two chips and still allow for proper flow within the channels. Due to the difficulties applying the glue precisely, the leakage problem worsened when we used this method. Next, we tried using the hydrophobic tape as a double sided adhesive and adhered the top and bottom acrylic pieces together. We put the tape on the bottom piece containing the fluid channels and then cut out the areas over the channel to make sure the tape was not touching and impeding flow within the channels. We used a clamp to apply more pressure between the two pieces of acrylic after we added the tape. In this iteration, we were able to successfully solve the leakage issues within our pump.

We did, however, encounter problems where, even though the working fluid flowed without issue, the analytic fluid would not flow. Subsequently, our team wanted to reduce the hydraulic resistance in the analytic fluid channel to help the analytic fluid flow. We changed the design to chip 2.22 as shown to the right where the analytic fluid channel was reduced to a straight line to mitigate the minor losses due to bends in the channel. We tried this design with the straight line both beneath the finger press area and connecting to the finger press area to see the results. When we tested these designs, we found that we still had problems with the working fluid properly flowing. Our team observed that when we applied pressure to the finger activation area, the working fluid would come into contact with the filter paper

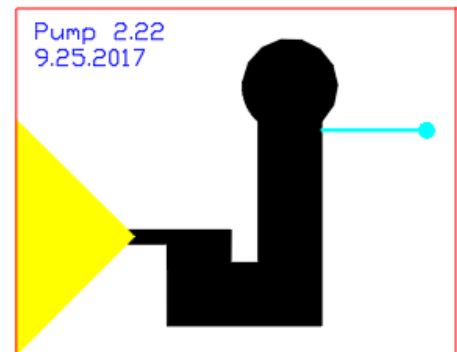


Figure 66 : Paper Based Pump 2.22  
AutoCAD Design



Figure 65: Paper Based Pump 2.22  
during Testing

and then would draw back into the working fluid channel as soon as the finger activation area was not being pressed as can be seen in Figure 65. However, when we would press down and force the working fluid to come into contact with the paper, the red analytic fluid would be drawn into the channel but it would stop flowing when the finger pressure was released. This was due to a vacuum being formed in the finger press area as soon as it was released thus drawing the working fluid back into its channel.

### 5.1.9 Pumps 2.24

This vacuum was an issue due to the wicking force from the paper not being stronger than the formed vacuum.

Therefore, the working fluid was being drawn back up into the channel. Our team wanted to work on increasing the draw of the paper to counteract this vacuum. We did this by trying to increase the



Figure 68: Paper Based Pump 2.24 during Testing

central angle of the paper by making the paper a semi-circle as shown in Figure 68. When tested, the same issue as before was encountered and increasing the central angle of the paper did not help counteract the vacuum as can be seen in Figure 67.

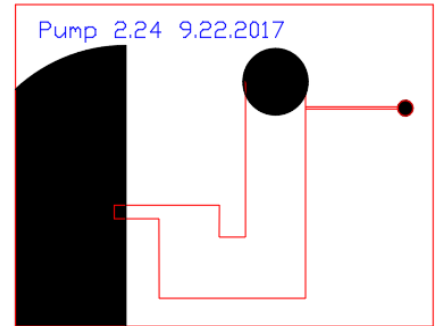


Figure 67 : Paper Based Pump 2.24 AutoCAD Design

We were unable to utilize this vacuum to draw in the analytic fluid due to the relatively high hydraulic resistance in the analytic fluid channel compared to the hydraulic resistance in the working fluid channel. Therefore, we changed our design to include a section of the working fluid above the finger press with the intent that the vacuum formed due to a release of finger pressure would draw in the fluid from above the finger press as opposed to below.

### 5.1.10 Pump 2.25

By adding the additional length of working fluid above the finger activation portion of the chip, we hoped to utilize the vacuum that was forming at the top of the working fluid channel. The analytic fluid channel was positioned to connect to the upper portion of the working fluid channel as well. We also deepened the depth of the paper chip area from  $527\mu\text{m}$  to  $727\mu\text{m}$  to include additional pieces of paper, thus increasing the wicking force of the paper pump.

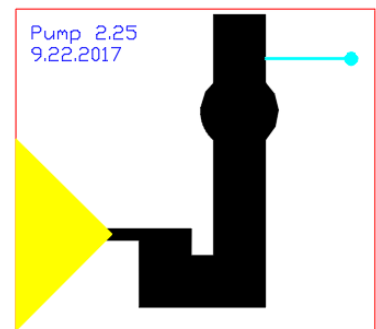


Figure 69 : Paper Based Pump 2.25 AutoCAD Design



Figure 70: Paper Based Pump 2.25 during Testing

During testing, the fluid was not drawn from the added portion of the working fluid but continued to be pulled from the finger activation area as can be seen in Figure 70. This resulted in no impact on the analytic fluid. From this design, we learned that the fluid would begin flowing from the point of activation. In order to reduce this problem in our next iteration, we removed the finger activation area altogether and replaced it with a syringe fill location on the top chip of acrylic.

#### 5.1.11 Pump 2.26

In order to ensure the analytic channel was at the activation area of the working fluid, we designed a syringe inlet on the top chip of acrylic. This was done to ensure that any vacuum formed could be used to draw in the analytic

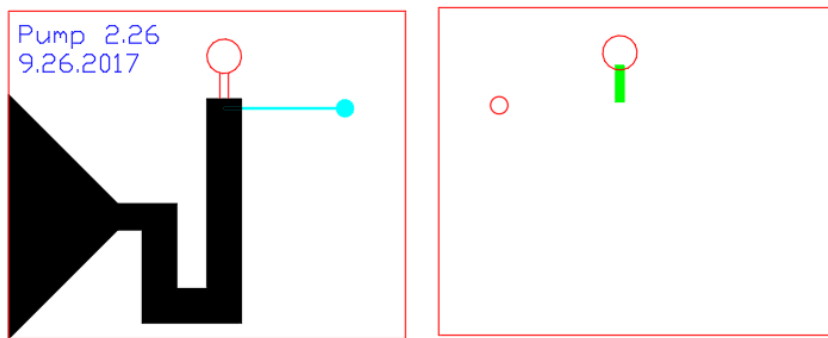


Figure 71 : Paper Based Pump 2.26 AutoCAD Design

fluid. This design also allowed us to reduce the amount of surface area that could be deformed if covered with flexible tape and that would need to be sealed from the outside air. The width of the working fluid channel was also reduced to decrease the ratio between the widths of the two channels. This would decrease the amount of hydraulic resistance needed to be overcome by the paper's wicking force. This reduction also decreased the volume of the working channel to make it match more closely with the volume of liquid the filter paper was able to absorb.



Figure 72: Paper Based Pump 2.26 during Testing

When testing, we performed multiple iterations using both a small acrylic chip covered in EL-92892 hydrophobic tape (MSDS sheet can be found in Appendix E) and a piece of packing tape to cover the syringe inlet. The vacuum formed in the working fluid channel was, again, too strong for the force of the filter paper to overcome and the working fluid did not properly flow through the channel as can be seen in Figure 72.

In order to determine if this issue was caused by the surface roughness created by rastering, our next design iteration compared the results of rastering and through cutting.

#### 5.1.12 Pump 2.27

Pump 2.27 was manufactured both as a two layer rastered chip and as a three layer through cut chip. The bottom piece of the rastered chip was cut on 1/8th inch acrylic. The top of the rastered chip and all three layers of the through cut chip were cut from 1/16th inch acrylic. Two stacked pieces of paper fit into the chips when rastered, and four stacked pieces of paper fit into the through cut chips.

When testing these iterations, there was a successful result when using the through cut of design 2.27 when the syringe activation area was covered with a small piece of acrylic adhered to

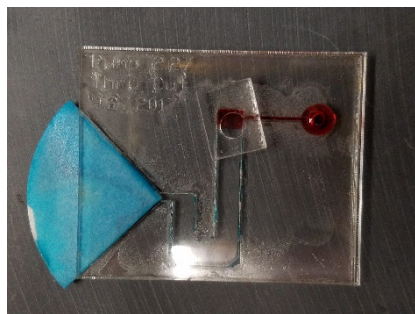


Figure 73: Paper Based Pump 2.27 during Testing

the chip using EL-92892 adhesive as can be seen in Figure 73. However, this testing trial was unique because of when the syringe area was sealed. The working channel was only sealed once about half of the working fluid had soaked the paper chips. The analytic fluid was then pulled into the working fluid channel because of the created vacuum. The rastered chip test was unsuccessful.

After seeing these results, three theories were formed about why this through cut trial was successful- the decreased surface roughness of the channels, the increased wicking force in the paper and the decreased vacuum force at the inlet of the working fluid channel.

The first theory was that the hydraulic resistance of the analytic fluid channel had been sufficiently decreased due to decrease in surface roughness to allow the analytic fluid to overcome to resistance and flow through the channel. Due to there being other varied parameters between the two chips such as thickness of filter paper and wetting radius when the working channel was sealed, our team re-ran the experiment with the filter paper thickness and wetting radius held constant between the two chips. One unavoidable difference between these two setups was the amount of air in the paper area. Because the through cut chip's paper area is inherently thicker than on the rastered chip, two pieces of filter paper did not completely fill the paper area as they do on the rastered chip. Both the rastered and through cut acrylic chips were tested with two pieces

of paper and an acrylic square was adhered with EL-92982 tape to the syringe inlet after the working fluid had reached a 10 mm wetting radius on the paper. Once the syringe inlet was covered with acrylic on the rastered chip, the working fluid stopped flowing. When the inlet was covered on the through cut chip, the working fluid continued to flow and the analytic fluid began flowing through its respective channel. However, the analytic fluid stopped flowing after the paper pieces were nearly saturated.

The second theory was that the fact that the channel was sealed a given time after the water had started to be absorbed into the paper caused the wicking force of the paper to be higher than the vacuum force in the front of the working fluid channel. It was therefore able to overcome the vacuum force created in the working channel due to the increased wetting radius of the paper at the time of vacuum formation and the thickness of the paper. The wetting radius, thickness of the paper, and wicking force are directly proportional as shown in Equation 1 in the literature review. In order to test this theory, twelve trials were completed where the working fluid was allowed to partially soak the filter paper, increasing its wetting radius, before the syringe inlet of the chip was sealed. Of these twelve trials, three were partially successful. The analytic fluid was somewhat drawn into the working fluid channel, but the working fluid stopped flowing into the paper and the analytic fluid would stop as can be seen in Figure 74. This was most likely due to the vacuum force becoming stronger than the wicking force of the paper after some of the analytic fluid flowed because of the increased wetting radius. The wetting radius was not increased further because increasing it limited the volume of working fluid the filter paper was able to absorb. Therefore, increasing the wetting radius further would not have yielded successful trials because the filter paper would have been nearly saturated before the vacuum was formed.

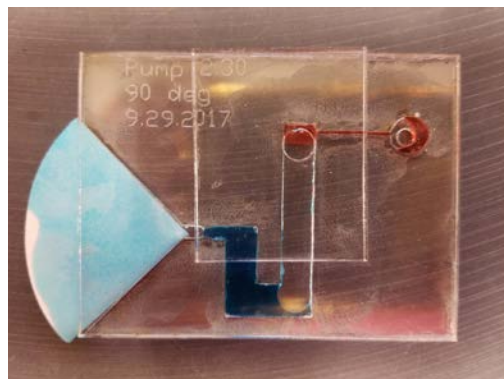
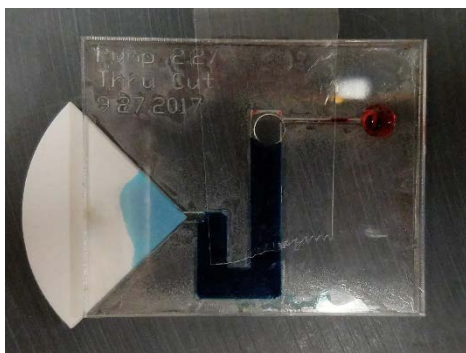


Figure 74: Photograph of Paper Based Pump 2.30

This was most likely due to the vacuum force becoming stronger than the wicking force of the paper after some of the analytic fluid flowed because of the increased wetting radius. The wetting radius was not increased further because increasing it limited the volume of working fluid the filter paper was able to absorb. Therefore, increasing the wetting radius further would not have yielded successful trials because the filter paper would have been nearly saturated before the vacuum was formed.

The third theory was that the acrylic chip placed on top of the syringe inlet did not fully seal and led to a weakened vacuum force allowing the wicking force to draw in the working fluid. This theory was supported by the success of the original SIMPLE Pump manufactured from PDMS, a somewhat more breathable material than acrylic. This breathable material may have

allowed for slight air leakage in the microfluidic chip leading to a decreased vacuum pressure. In order to test the third theory, six other sealing methods were used to cover the syringe inlet. These included: the original small piece of acrylic with EL-92892 (with no time to increase wetting radius), a piece of packing tape, a larger piece of acrylic with EL-92892, a larger piece of acrylic with double-sided Scotch tape, a larger piece of acrylic with water, and a larger piece of acrylic with soap. All of these, with the exception of the water seal, were not able to successfully move the working fluid, and, thus, did not move the analytic fluid. The water seal successfully moved the working fluid, but the analytic fluid did not move- most likely because there was not a strong enough seal to create a vacuum in the working fluid channel. After these trials, we determined the third theory was not plausible. The chips sealed with packing tape and water can be seen in Figure 76 and Figure 75, respectively.



*Figure 76: Paper Based Pump 2.27 during Testing- Syringe Inlet and Top Acrylic Chip Sealed with Packing Tape*

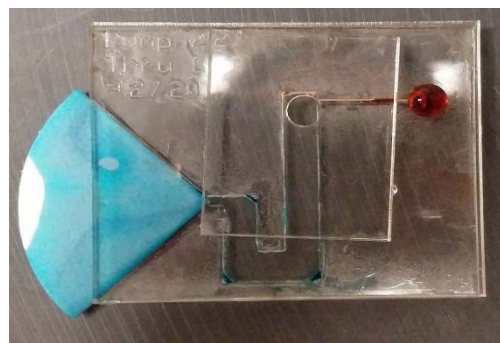


*Figure 75: Paper Based Pump 2.27 during Testing- Syringe Inlet and Top Acrylic Chip Sealed with Water*

## 5.2 Gravity Driven Pumps

As we continued our research into hand held pumps, we realized that the paper based pump would not be as conducive to droplet generation due to the difficulty in trying to collect the droplets in a usable fashion before they were absorbed by the paper.

Therefore, our team researched other methods for droplet generation such as gravity driven pumps. In our planning for this pump, we used Bernoulli's equation to describe fluid flow in a pipe as discussed in the background.

We decided that instead of having an additional, raised reservoir at the other end, we would leave our collection at the same height as the chip face. This was achieved by rastering a small rectangle at the end of the continuous fluid channel, shown in Figure 77 to the right.



*Figure 77: Photograph of Gravity Driven Pump 5.3 with Borosilicate Tube Attached Via UV Hardened Glue*

### 5.2.1 Material Selection

An initial test was completed before chips were fabricated to determine the effect of hydrophobicity on fluid flow in the tubes. Hydrophobicity is an important factor in allowing fluid to flow because if there is a water-air interface within a hydrophobic tube, there is an added Laplace Pressure for the fluid to overcome. As denoted by Young's law, the fluid would have to be pushed until the contact angle between the hydrophobic surface and the water was over 90 degrees before the fluid will flow [35]. This extra required force is detrimental to the flow of water through hydrophobic tubes.

We wanted to test if gravity force was sufficient to overcome the Laplace pressure in the two kinds of tubing to determine which material could be used in our pump design. Two types of tubing were used to complete this test- silicone and borosilicate. Both had an internal diameter of 0.5 mm, but silicone tubing was hydrophobic while borosilicate was hydrophilic. Both tubes were oleophilic, so the flow of oil through either tube was not affected by the hydrophobicity of the tube. We attached the tubing to medicine cups so oil or water could be run through the tubes.

The oil was able to flow through both types of tubing while the water was only able to run through the borosilicate glass tube. Theoretically, the Laplace pressure only exists in a hydrophobic tube if there is a water-air interface. If there is no air within the tube, there would be no added pressure to overcome. In order to attempt to overcome the higher Laplace pressure present in the silicone tubing with water, we pre-filled the silicone tube to lessen the existence of a water-air interface. However, the water still did not flow. This was most likely due to small air bubbles being present in the tube when it was pre-filled, causing high surface tension between the air bubbles and water to prevent flow. After seeing these results, we decided to complete further testing using borosilicate glass tubing.

### 5.2.2 Fabrication Process

In order to create strong bonds between the chip and reservoir tubing and the reservoir and reservoir tubing, UV hardened glue was used at the junctions. Initially, we faced fabrication issues because the glue would get into the tubing and fluid would be unable to flow. To circumvent this, a reliable fabrication process was created. To begin, the tubing was marked with a marker at the desired location to meet the reservoir. We used medicine cups for our reservoirs because of immediate availability in the lab. A small hole was poked in the bottom of the reservoir and the tube was inserted to the marked line. Glue was then placed at the junction and hardened. The reservoir was then supported using an adjustable height microscope stand and the tubing was lowered into the acrylic chip .06 inches (half the thickness of the acrylic chip). Glue was applied at the junction and hardened. Hydrophobic tape was then applied on the bottom side of the chip to form the fourth wall of the channels. Pictures of this process can be found in Appendix F. Before implementing this improved process, 50% of chips we fabricated with gravity pumps were unusable. After process creation, all chips were usable.

### 5.2.3 Calculations for Pump Height

The pressure drop in a pipe (or other channel) is described by Bernoulli's equation, adjusted for pressure drop due to friction as shown below. Given this formula, our team calculated the required height of the tubes of the pump to allow for the required flow rates to optimize droplet sphericity as found in the droplet section of this paper.

$$\Delta P = P_3 - P_1 = \rho * g * (-z_1) + \frac{64}{Re} * \frac{z_1}{D_H} * \frac{\rho * V^2}{2} + \frac{64}{Re} * \frac{L}{D_H} * \frac{\rho * V^2}{2}$$

In order to ensure the required flow rates, we needed to calculate a height that ensured this pressure drop to be equal to zero because both reservoirs were at atmospheric pressure. We chose the flow rates (used to calculate the velocity in this equation) from the optimal flow rates found in the droplet generation analysis. These volumetric flow rates were 12.2  $\mu\text{L}/\text{min}$  for the continuous flow in the main channel which contained olive oil and the second flow rate was 2.5  $\mu\text{L}/\text{min}$  for the dispersed flow made of water. We calculated the pressure drop in both the main channel and in the water channel separately to calculate the needed height of each fluid in order to generate different flow rates.

In our calculations, we assumed minor losses due to tube bends to be negligible because of our low Reynolds numbers as minor losses are generally more significant in turbulent flows. Other assumptions include estimating the friction factor for each portion of the fluid's path as  $\frac{64}{Re}$  due to our laminar flow.

Before we started testing our pumps, we wanted to test the accuracy of our mathematical model to take note of possible discrepancies between the model and the actual system. We set up two gravity pump systems, one with water and one with olive oil. These systems were fabricated at the same heights (10.4cm) and allowed to flow. We measured their velocities through the channel and used those velocities to back calculate an experimental volumetric flow rate. We compared our experimental flow rates with the theoretical flow rates our model predicted we should have achieved. Our calculations can be seen in Appendix G. The table below shows the analytic flow rates we calculated and the actual flow rates we were able to achieve with the gravity pump for both water and olive oil.

	<b>Water</b>	<b>Olive Oil</b>
Analytic volumetric flow rate (μL/min)	93.19	.861
Experimental gravity pump volumetric flow rate (μL/min)	77.1	2.392

*Table 6: Comparison of Analytic and Experimental Volumetric Flow Rates of Different Fluids*

Possible causes for discrepancies between analytic and actual volumetric flow rates include slight variations in the heights of the starting liquid, air bubbles in the tubes, and minor losses. We then tested pumps to achieve experimental volumetric flow rates that matched the volumetric flow rates desired for spherical droplet generation. In order to do this, we first analytically found the required heights, assuming we were using the tubing already present in the lab with a diameter of 0.5 mm. However, there was no way to get the continuous fluid (whether pump oil, olive oil, or soybean oil) to flow at the desired rate using solely gravity due to the high pressure drop in the thin tube. The main variables that would decrease required height of the pump tubing were increased diameter of the tubing, decreased viscosity of the fluid, and decreased velocity of the

fluid. Due to the viscosity and velocity being prescribed by the requirements for droplet generation, we could not change these variables and instead increased the diameter of the tubing by 10 times to 5 millimeters. From this we analytically found that the required height for the olive oil would be 1.45 meters.

Due to the fact that this height was too large to be feasible for use in a microfluidic device, we tried to see if we would be able to produce droplets from lower, more reasonable heights. We ordered new tubing with diameters of 1.2mm, 2.7mm, and 3mm with which to test.

#### 5.2.4 Pump Testing

After we ordered the new tubing, we wanted to test our experimental flow rates with respect to our theoretical flow rates with the new diameters. We also wanted to test our ideas about allowing for cross flow with the gravity pumps by trying several different methods of activation.

First, we tested the new flow rates for the olive oil in larger diameter tubes. These tests were performed on the chips fabricated to be droplet generation chips at a 75° angle modified T-junction in order to ensure the same parameters between our flow rate study and the droplet generation tests. We then glued the 75° channel shut as we did not want the opening at the end of that channel to affect the flow rate testing. The comparison between the expected and the theoretical rates can be found in the chart below. The calculations for the theoretical flow rates- which are the same as performed above- can be found in Appendix H.

<b>Tubing</b>	<b>Experimental Flow Rate (<math>\mu\text{L}/\text{min}</math>)</b>	<b>Theoretical Flow Rate (<math>\mu\text{L}/\text{min}</math>)</b>
6mm OD - 1.2mm ID	10.56	3.295
6mm OD - 2.7mm ID	9.78	3.312
7mm OD - 3mm ID	12.69	3.312

*Table 7: Comparison of Analytic and Experimental Volumetric Flow Rates of Different Tube Diameters*

These flow rates are roughly three times higher than the theoretical flow rates calculated. This follows relatively closely with the percent difference in flow rates with our initial oil calculations with the 0.5mm diameter tube. In the testing with the 0.5mm borosilicate tube, experimental flow rates are 2.78 times the theoretical flow rate. With the larger diameters, the percent different was an average of 3.33 times. Due to the large (and yet similar) percent differences with all of these trials, the most likely causes of the discrepancy between theoretical and experimental values was the use of the wrong density and viscosity of the oil because there is a large range of densities and viscosities of olive oil within literature. Other possible causes for the error in our theoretical flow rate are variations in surface roughness as well as slight errors in measuring the height of the reservoir (and fluid within the reservoir) as well as unexpected influences from the modified T-junction.

After we performed these trials, we started to test our gravity pumps' capability to achieve sustainable cross flow that would yield droplets. We realized that the order in which the fluids were added to the channels would affect the pressure at the end of the channel and, ultimately, the flow. During previous, erroneous flow rate testing we noted that the olive oil in the main channel was likely to move up the angled channel if there was nothing in the channel or if there was only an empty medicine cup attached by a tube. Therefore, our first iteration in testing this pump was to add the water before adding the oil to allow it to flow through the channel and to mitigate the olive oil going up the angled channel and preventing water flow. In this iteration, the water was able to flow unrestricted, however, when we added the olive oil, it did not flow through the tube due to the lack of pressure differential. Our second iteration was to add the oil first and then add the water once the oil had reached the junction. When we did this, we were unable to add the water before the oil had fully covered the junction and some of the olive oil moved up the angled channel and prevented the flow of the water.

Therefore, our next iteration was to add the water to its reservoir after the olive oil had reached the height of the water cup. In this trial, the water and olive oil met at the modified T-junction at almost the same time. The oil and water were able to interface briefly before the oil began flowing up the angled channel as well as continuing to flow in the main channel. The olive oil flowed up the angled channel and pushed the water backwards into the glass tube and, eventually, the medicine cup. When we increased the height of the water from 5cm to 10cm in an

effort to prevent the oil from flowing into the angled channel, we noted that, while the oil still moved up into the water channel, it moved noticeably slower than when the water was at a height of 5cm. After seeing these results, we determined the pressure difference between the oil and water was too high, and we decided to increase the pressure of the water at the junction to more closely match the pressure of the oil.

We did this by determining that the only way the oil will not flow up into the angled channel is if the pressures at the junction is the same. Based off of observations, we hypothesized that the pressure differential would be more equalized as the height of the water reservoir increased. We modeled the pressure of each side, the water and the oil, and set them equal to each other to calculate the required height of the water. When we attempted to model this pressure equalization of the water and the oil (full calculations found in Appendix I), given our current diameters and heights, we calculated that the height of the water would have to be 0.83 meters tall. While there were possible design changes, such as diameter change and tube height change, that could yield a pressure equalization, they were outside of the feasibility of a hand held pump and would yield non-desirable flow rates.

### 5.3 Weight Driven Syringe Pump

While the gravity pumps had potential, the required heights of the tubes and the diameters required to obtain the desired flow rates were not feasible to be paired with microfluidic devices. We therefore sought to replace the gravity portion, which was the dominant term in the Bernoulli's equation used to describe the flow in our gravity driven pump, with a different force that was more compact.

Due to the slightly varying flow rate created by the spring driven syringe pump found in our literature review, our team decided to pursue syringe pumps powered by other means than springs. The linearly decreasing force in the spring driven pump provided a problem because the force created by the spring continued to decrease as the spring expanded, thus slowing down the fluid and yielding a non-constant flow rate. Our team decided to explore the possibility of attaching a constant weight to the top of the syringe and using the constant gravitational force on that weight to drive the piston of the syringe down.

In the same way the spring driven pump required zero net force, in order to keep the velocity constant, the net force on the head of the syringe needed to be zero. In this scenario, the forces on the head of the syringe would be the weight pushing down on the syringe, the pressure of the fluid in the syringe acting against the syringe plunger, and the frictional force between the rubber lining on the plunger and the plastic syringe. This can be seen in Figure 78.

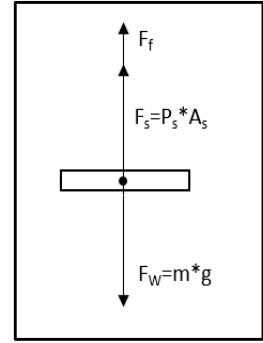


Figure 78: Force Diagram of Weight Driven Syringe Pump

The pressure in the syringe can be determined by Bernoulli's equation. By setting the starting point at where the plunger contacts the top of the liquid in the syringe and the end point at where the fluid leaves the chip and becomes atmospheric pressure, the pressure can be back calculated by adding atmospheric pressure to the pressure drops described in the below equation.

$$\Delta P_t = \frac{64}{Re} * \frac{L_c}{D_H} * \frac{\rho V_c^2}{2} + \frac{64}{Re} * \frac{L_t}{D_t} * \frac{\rho V_t^2}{2} + \frac{64}{Re} * \frac{L_n}{D_n} * \frac{\rho V_n^2}{2} + \frac{64}{Re} * \frac{L_s}{D_s} * \frac{\rho V_s^2}{2}$$

Assuming the desired flow rate for olive oil to be 16.9  $\mu\text{L}/\text{min}$  and using the predetermined channel parameters, we calculated our pressure drop in our system to be what is seen below thus yielding the below force:

$$\left( P_1 + \frac{1}{2} \cdot \rho_{\text{olive}} \cdot V_s^2 + \rho_{\text{olive}} \cdot 9.81 \cdot h_1 - \frac{1}{2} \rho_{\text{olive}} \cdot V_c^2 - h_L \right) \text{ solve, } P_1$$

$$P_1 := 31160.16755 \quad \text{Pa}$$

$$F_1 := P_1 \cdot A_s = 0.559 \quad \text{N}$$

The frictional force in the system was the friction between the rubber lining of the syringe and the plastic walls of the syringe. After substantial research, we were unable to find an exact frictional force between the walls of the syringe and the rubber lining. Therefore, we chose to experimentally find a value we could use for friction in our calculations. We tested for kinetic friction by adding weights to the piston as shown in Figure 79 and seeing at which weight, the friction did not stop the motion of the piston. This occurred at 72g.



Figure 79: Setup of Experiment to Measure Frictional Force in a Syringe

Thus, we determined that the kinetic friction acting against the movement of the syringe was 0.706N.

We then performed flow rate tests of the oil and the water to see how well our theoretical models operated. The desired flow rates for both water and oil were so small that we started by adding higher weights to achieve much higher flow rates. This would allow us to be able to visually see the change in distance within the syringe. We found the flow rates by adding a specified amount of weight (250g for the water syringe and 450g for the oil syringe) and recording the change in the position of the syringe piston over time. We then plotted it on a graph and the slope of the plotted line was the volumetric flow rate (in mL/sec.)

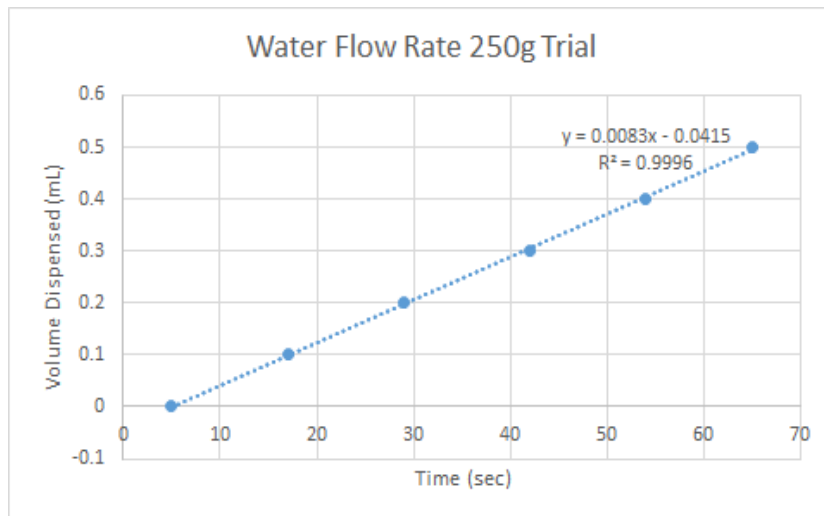


Figure 80: Water Volumetric Flow Rate in Gravity Driven Pump Trial with 250g Weight

The results can be seen below. The tests yielded relatively linear flow rates as shown by the linearity of the graphs each with an  $R^2$  value of at least 0.9948. These graphs clearly show a linear trend of the displacement meaning an almost constant velocity. This follows from our mathematical calculations because the weight pushing down on the top of the syringe is always constant. While there are slight variations in the hydraulic resistance in the syringe due to the change in the wetted surface area within the syringe, the change in pressure inside the syringe (and therefore the force pushing up on the syringe piston head from the inside pressure) is negligible in comparison to the amount of resistive force from the friction between the rubber syringe head and the side walls of the syringe.

The differences between our calculated mathematical model and the experimental flow rates can be seen below.

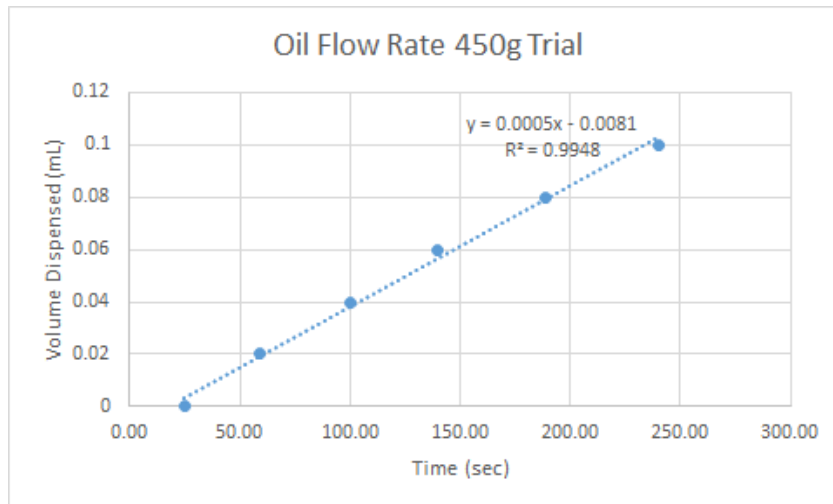


Figure 81: Oil Volumetric Flow Rate in Gravity Driven Pump Trial with 450g Weight

	<b>Weight Added (g)</b>	<b>Theoretical Flow Rate (μL/min)</b>	<b>Experimental Flow Rate (μL/min)</b>
Water	250	4,851	500
Olive Oil	450	111.782	27.78

Figure 82: Theoretical vs. Experimental Volumetric Flow Rates of Gravity Pump Trials

The error in our experimental versus theoretical flow can be attributed to slight errors on both sides. The experimental flow rate was calculated solely based on visual note of change in volume over the course of the fluid flowing. This visual measurement, in combination with possible slight measurement errors in length of channel, height of syringe, etc. could have led to some errors in our experimental flow rates.

The other large factor in the difference between the two flow rates could be attributed to the fact that a large portion of the force used to calculate theoretical flow was the friction force which was experimentally found instead of found in our research due to the large differences in friction in different syringes. When analyzing these numbers, we realized how we might have possibly incorrectly calculated the friction force due to our set up. We therefore performed our

experiment for a second time, this time we calculated the friction plus the force of the fluid in the syringe and needle for both water and oil. We performed the test very similarly to our initial friction experiment except that this time we set up the syringe pointing down and added weights to the top. When we performed this experiment, we found new friction forces of 1.08N for the water syringe and 2.16 for the oil syringe.

We then recalculated our estimated flow rates for oil and water using these new friction forces and the compared results can be seen in the table below. When we performed these calculations, we took into account the fact that the friction had been calculated to include the pressure drop in the syringe and needle and adjusted our calculations accordingly (full calculations can be seen in Appendix J and K)

	<b>Weight Added (g)</b>	<b>Theoretical Flow Rate (<math>\mu\text{L}/\text{min}</math>)</b>	<b>Experimental Flow Rate (<math>\mu\text{L}/\text{min}</math>)</b>
Water	250	3,932	500
Olive Oil	450	65.084	27.78

After testing flow rates and adjusting calculations, we started droplet generation testing with varying weights. We calculated the theoretical flow rates for the continuous fluid- olive oil- to be able to characterize the continuous flow capillary number and flow regime. The different trials included weights of oil of 220g, 250g, 350g, and 450g. The table below discusses the olive oil weight and the resulting experimental sphericity.

	<b>Oil Weight (g)</b>	<b>Theoretical Flow Rate</b>	<b>Average L/W Ratio</b>
Trial 1	220	0.413	2.534
Trial 2	250	8.849	1.754
Trial 3	350	36.966	1.120
Trial 4	450	65.084	1.045

The graph of this data can be seen below. Clearly, as the flow rate of the continuous fluid-olive oil- increases, the sphericity of the droplet produced improves.

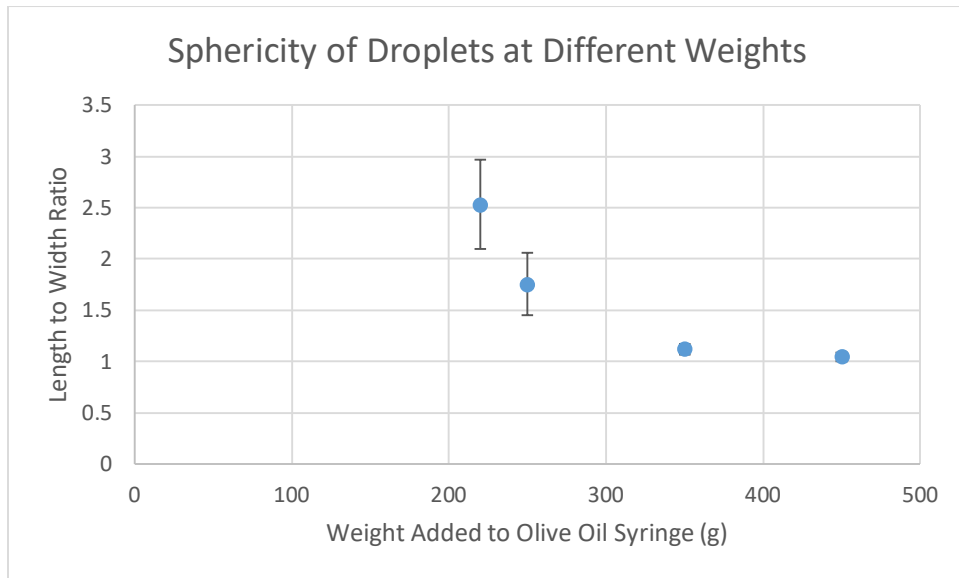


Figure 83: Length to Width Ratio for Droplets at different Olive Oil Weights

We then calculated the capillary number of the continuous flow to characterize into which flow regime each trial fell. Given that the capillary number of the continuous fluid should be between 0.013 and 0.1 for dripping regime, the flow regimes of each trial are also listed in the chart below. The results of these calculations as well as the corresponding flow regime can be found below.

	<b>Oil Weight</b>	<b>Theoretical Flow Rate</b>	<b>Capillary Number</b>	<b>Flow Regime</b>
Trial 1	220	0.413	0.000465	Squeezing
Trial 2	250	8.849	0.00871	Squeezing
Trial 3	350	36.966	0.036	Dripping
Trial 4	450	65.084	0.064	Dripping

## Chapter 6: Final Results Summary and Recommendations

The goal of this project was to create spherical droplets from a manual handheld pump with a steady flow rate. We achieved this by working in two sub-teams to both optimize the junction at which the two fluid flows met and by working on hand held pump development and testing. In this chapter, we discuss the final deliverables we were able to achieve in each sub-team. It also includes the final weight driven pump and in which we combined the optimized droplet junction and the handheld pump to create spherical droplets. We then provide recommendations on how to continue this project and further it in the future.

### 6.1 Droplet Results

The goal of the droplets sub-team was to optimize junction parameters to ensure consistent spherical droplets. From our background research we tested the effects of junction angle and flow speed on droplet formation. Once we had optimized the sphericity of the droplets produced we also did testing to show our design was capable of creating droplets using a blood sample. The following section contains a summary of our results and recommendations.

#### 6.1.1 Measurement and Leakage Issues

One of the first challenges of our project was how to determine the sphericity of an object based on the two dimensional information we were able to capture using the microscope camera. The method we decided on was measuring two perpendicular lines on the top view of the droplet seen by the camera. These lines were the length and width of the droplet. A ratio of these measures was then taken, this helped determine how round the droplet was. As in a circle, the two measures should be the same leading to a ratio of one. Therefore, our goal was to create droplets with a ratio as close to one as possible. Once testing began we encountered issues with our chip leaking around the inlet and outlet holes where the tubing attaching our chip to the pumps connected. This issue was eventually reduced through the use of thicker acrylic, and eventually prevented through the use of glue to seal the tubing attachment areas. As a result, we recommend using acrylic at least  $\frac{1}{8}$  in thick for droplet formation and gluing the tubing in place to absolutely prevent leaks.

#### 6.1.2 Angle Results

Our literature review did not reveal any studies showing which angle of a modified T-Junction would produce the most spherical droplets, so we conducted our own study. Our results,

shown graphically below in Figure 84, indicated that on the glued chip we recommend a 75-degree angle which produces the most spherical droplets.

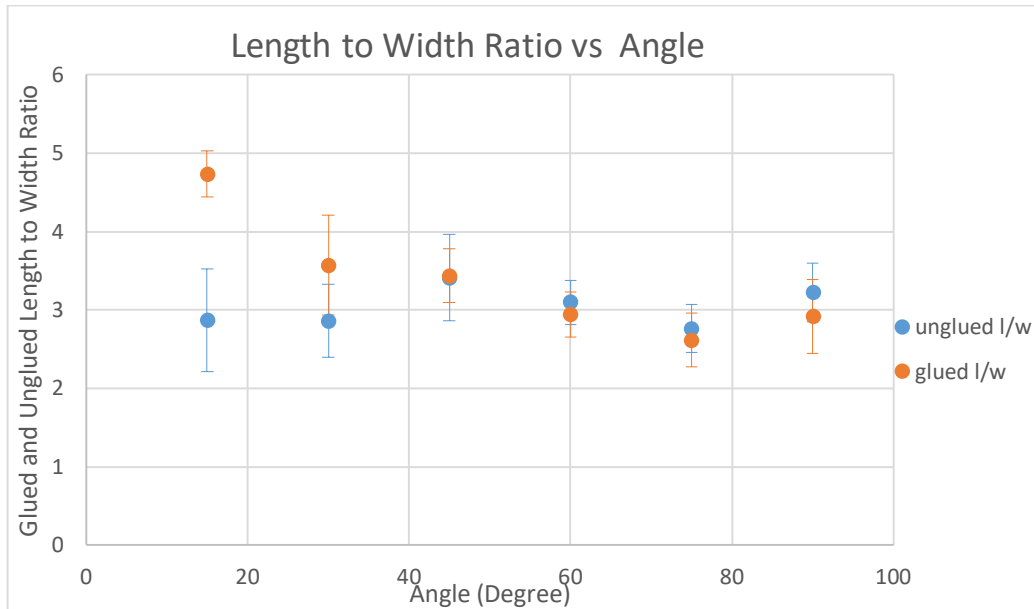


Figure 84: Length/Width Ratios of Glued and Unglued Chips by T-junction Degree

### 6.1.3 Flow Speed Results

In addition to optimizing the angle of the junction, our research indicated that the flow speeds of the two fluids would also have a major impact on the sphericity of the droplets. As a result, a study was conducted to determine the optimum flow rates for spherical droplets. Our results, shown below, indicated that on the glued chip we recommend a 7.2  $\mu\text{L}/\text{min}$  flow rate for oil and a water flow rate between 2.25 and 2.75  $\mu\text{L}/\text{min}$  flow rate to produce the most spherical droplets.

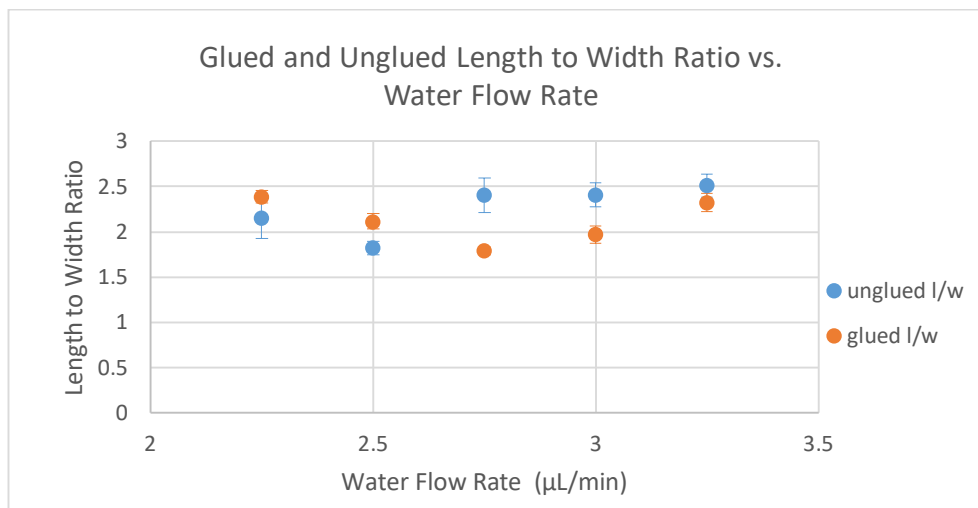


Figure 85: Length/Width Ratios for Glued and Unglued Chips for Various Flow Rates

#### 6.1.4 Optimized Droplets

From results determining the optimum flow speed and angle for droplet generation, we began testing to create our optimized droplets. Since our flow speed testing was conducted on a different angle chip than our angle optimization test indicated was ideal, a small spread of flow speeds was tested to ensure that switching the angle would not impact flow speed recommendations. The results, shown in Figure 86 below, indicate that while there is a small difference in overall sphericity the general trends remain the same. As such our most spherical droplets were produced with a 75 degree junction angle with the inlet tubing glued in place, and oil flow speeds of 7.2  $\mu\text{L}/\text{min}$  and water flow speeds of 2.375  $\mu\text{L}/\text{min}$ .

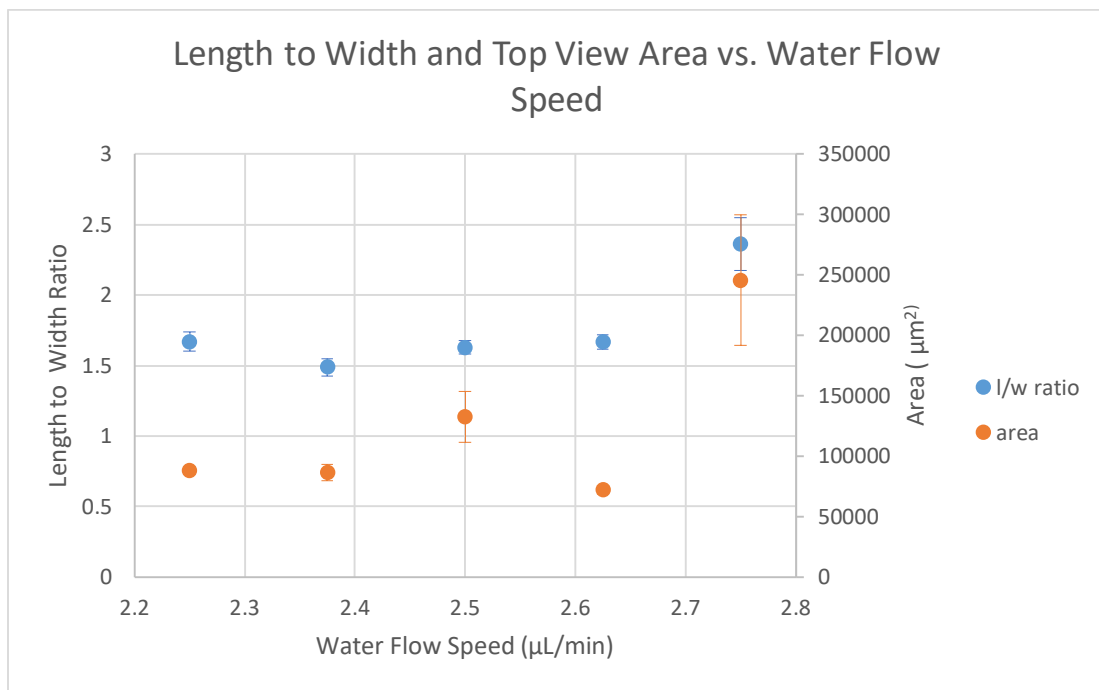


Figure 86: Length/Width Ratios and Top View Areas for Various Flow rates

#### 6.1.5 Blood Separation Testing

With our optimal droplets formed we began testing to attempt to separate a blood sample into smaller droplets. The original blood cell concentration of our sample was 800,000 red blood cells per microliter of blood. Prior to testing we diluted the blood sample at a ratio of 1 part blood to 12 parts saline, resulting in a cell concentration of 61,538 cells per microliter of blood. A photo was taken of the diluted blood and a cell count was performed. 88 cells were counted in 31,552 square micrometers for an approximate concentration of 0.002789 cells per square micrometer. This number was multiplied by the area of each cell to determine the approximate number of cells per droplet. Droplets were formed using a 2.5 $\mu\text{L}/\text{min}$  flow rate for the blood solution and

7.2 $\mu$ L/min for the oil. The droplets formed had a ratio of about 1.8 with standard deviation of 0.14. The droplets had an average area of 137,324  $\mu\text{m}^2$ , which should result in approximately 383 cells per droplet. The data gathered about each droplet can be found in the table below.

	Length	Width	L/W	Top View Area	Cells per Drop
Drop 1	569.983	280.466	2.032271291	141187.397	393.7773472
Drop 2	556.817	284.449	1.957528415	136816.727	381.5873722
Drop 3	505.887	298.709	1.693578031	131071.013	365.562344
Drop 4	532.268	299.949	1.774528336	138583.638	386.5153583
Drop 5	548.525	301.851	1.817204515	139714.138	389.6683684
Drop 6	523.202	310.06	1.687421789	136571.183	380.9025401
Average	539.447	295.914	1.82708873	137324.016	383.0022217
Standard Deviation	23.48738362	11.22085081	0.14093023	3525.597529	9.833033768
% Deviation	0.04353974277	0.03791929684	0.0771337635	0.02567356848	0.02567356848

*Table 8: Blood Droplet Length, Width, Length to Width Ratio, Top View Area, and Cells per Droplet*

#### 6.1.6 Recommendations for Future Work:

From our time working on this project, we have identified areas for future research that we would have liked to address but did not due to time limitations. One suggestion for further research would be to do more experimentation using through cut acrylic chips and creating the third and fourth walls with either tape or acrylic. We did some testing using this method of fabrication but chose to focus on the rastered channels as we had more success with them. However, surface roughness caused some irregularities in our testing and a through cut could be advantageous because of the low surface roughness on the bottom the channel.

In addition to further testing with through cut chips, we think more testing with blood samples could prove useful. We did much of our testing using water and oil, and although we diluted the blood it does not have the exact same fluid properties as water. Further testing with blood samples would allow the flow rates used to be optimized further. In addition, the inclusion of a person with a background in biology would be useful in continued testing.

## 6.2 Pump Results

The goal of this sub-team was to create a manual, hand held pump that produced steady flow capable of producing spherical droplets. From our background research, we tested the feasibility of four kinds of pumps- paper based pumps, gravity driven pumps, and weight driven syringe pumps. In the end, we were able to produce droplets from the weight driven pumps. The following section contains a summary of our results and recommendations from each pump.

### 6.2.1 Paper Pump Results

We first tried to replicate a modified microfluidic pump found in the literature review- Self-Powered Imbibing Microfluidic Pump by Liquid Encapsulation (SIMPLE). Our goal was to modify it to allow us to utilize it for droplet generation within the analytic channel. This goal was unique to replication of the pump due to the new platform on which we were making this pump- acrylic. In literature, all the paper based pumps are made out of PDMS which, while also a polymer material, has different material properties than acrylic. Thus, using acrylic presented its own challenges both due to the material properties and results yielded by a different fabrication method. The two main challenges we encountered when working with this pump were how to fabricate them to prevent leakage and the difference in vacuum force and wicking force of the paper.

#### 6.2.1.1 Leakage issues

One of the biggest issues we had at the onset of our pump design was how to fabricate acrylic chips without allowing leakage like that which can be seen in Figure 87. The PDMS chips were fabricated with photolithography and therefore all four of the walls of the channels were made with PDMS. However, we tried to use tape to seal the channels and create the fourth wall. We ran into many problems with the tape not being strong enough to properly withstand the pressure provided by the fluid in the channels. Thus, we experimented with many other ways to seal the channels including other kinds of tape, acetone bonding the two pieces of acrylic together, and using double sided tape to adhere two pieces of acrylic together.



Figure 87: Paper Based Pump with Leakage

In the end, the leakage issues were solved by utilizing the original tape we were using, ARcare® 92892, as a double sided adhesive bonding two pieces of acrylic together. However, in order to solve the leakage problem, we had to use a c-clamp to provide enough force. We were

able to visually see the effects of added pressure to the adhesive between the chips. When pressed down further, the layer between the two chips became clear. When the chip was pressed to the point of being clear, we were able to achieve a pump with no leakage problems.

#### 6.2.1.2 Vacuum Issues

The other main issue that our team encountered while testing these pumps was the creation of a vacuum at the beginning of the channel. The vacuum was occurring in the finger press area as shown circled in red to the right in Figure 88. This vacuum was a desired phenomenon as that was the means to move the fluid through the analytic channel. However, it became an issue when the wicking force in the paper was not strong enough to overcome the vacuum,

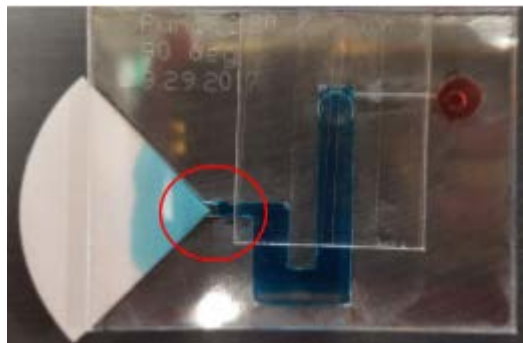


Figure 88: Photograph of Paper Based Pump with Gap between Working Fluid and Paper Filter Circled in Red

and the working fluid was

not pulled into the paper as opposed to the vacuum pulling in the analytic fluid. An example of the working fluid not being pulled into the paper and a gap forming between the filter paper and working fluid can be seen in Figure 89 circled by red. We had two main hypotheses as to why this was occurring and how to counteract it.

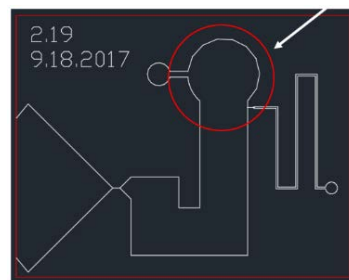


Figure 89: Paper Based Pump Design with Area Where Vacuum Formed Circled in Red

The first was that the hydraulic resistance in the analytic channel was too high and therefore the wicking force could not overcome the resistance nearly as easily as it could overcome the resistance in the working channel. When we tested how much easier it was for the analytic fluid to be pulled through the channel when we used through cut chips which had lower surface roughness than rastered chips, the fluid required much less force to flow through the through cut chips than the rastered chips. Therefore, we started only testing through cut chips- which gave us better results for flow.

The second idea we had was to change variables to increase the wicking force of the filter paper. We did this by testing increased wetting radius of the filter paper (by delaying when we sealed the channel) and increasing the filter paper thickness (by adding several layers of paper). The increasing of the wetting radius worked approximately 50% of the time. Increasing the filter paper thickness delayed how long it would take before the vacuum in the top of the working fluid

channel stopped the flow of the working fluid. However, it never successfully kept the working fluid flowing the entire time, nor did it pull in any analytic fluid.

#### 6.2.2.3 Paper Pump Component Integration Issues

Our team did not successfully replicate the paper powered pump. However, we terminated testing of this pump due to the fact that, through our testing, we learned that this pump's operation would not align with our goals of producing droplets. This was due to the inability of this design to allow for cross flow to produce droplets and the inability of this pump to collect usable droplets after production- even if we had been able to produce them.

First, through trials, we learned that this pump only starts drawing in the analytic fluid after the working fluid has passed the junction between the analytic fluid channel and the working fluid channel due to the fact that it uses a vacuum as its driving force. While this design works for many microfluidic applications, it would not allow for cross-flow because by the time one fluid starts flowing, the other has already flowed entirely past the junction and there is no co-flow produced.

Secondly, through the droplet team's experiments and research into reservoirs and how to collect the droplets after production, we learned that, because the paper pump relies on a pulling force at the end of the channel, the fluid would need to end up being sucked into the filter paper at the end, it cannot be diverted elsewhere or the wicking force becomes zero and there would be no force pulling the fluid. Therefore, we would be unable to collect usable droplets before they were absorbed by the filter paper.

Due to these two main issues with integrating this pump design with the application of droplet generation, we decided to terminate testing with this pump and pursue other pump ideas that allowed for cross flow and relied on a pushing force at the beginning of the channel instead of a pulling force at the end.

#### 6.2.2 Gravity Driven Pump Results

This pump was our second idea to produce droplets generated by cross-flow, and an example can be seen in Figure 90. We calculated required heights to achieve desired flow rates using MathCad. Feasibility became one of the largest issues with this pump. While we theoretically could calculate the required heights, we could not fabricate them due to their extreme height (for example, 1.8 meters high for the oil tube.) Furthermore, these heights would not be feasible for an in the field hand held pump.

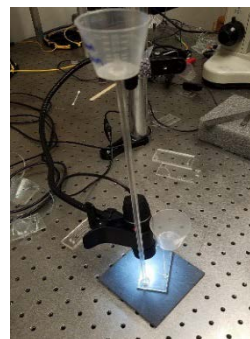


Figure 90: Example of Fabricated Gravity Pump

However, our team wanted to test the models we had created for these pumps regardless so we decreased the height from the desired height to 0.3048m which we were able to fabricate. We were able to test the discrepancy between our theoretical flow rates and our experimental flow rates. We found a very small error between the experimental and theoretical rates for water. However, our team found that our experimental flow rates for the olive oil were around 3 times as large as the theoretical flow rates. This factor of about 3 stayed consistent throughout the continuation of our testing with larger diameters.

Our team also tried cross-flow with this pump. We encountered issues when the fluids met at the junction- the olive oil would start to travel up the angled channel. We deemed this issue to be due to the pressure differential between the two channels at this junction. We, therefore, performed calculations to find the height required to equalize the pressures. Our calculations led to a height that was not feasible for fabrication either.

Due to the infeasibility of the gravity driven pump as a whole, our team decided to focus on another pump that would yield constant flow- the weight driven syringe pump.

### 6.2.3 Weight Driven Syringe Pump Results

Weight driven pumps were started as a derivative of the Springfusor® spring driven syringe found in our literature review. We chose to use weight, instead of a spring, in order to ensure a constant force on our syringe and therefore a more constant flow.

We performed initial calculations about the relationship between weight and flow rate in our system as well as ran flow rate tests and droplet generation tests. At the onset of working with this pump, we needed to determine the friction in the syringe as that was a large portion of the resistive force in the system that the weight was counteracting. Our team did this by running experiments with the relationship between weight and whether or not the syringe would continue to move. We performed this experiment once for the olive oil filled syringe and water filled syringe to be able to take into account the different effects the liquid would have on the friction. We measured the frictions in the system to be:

<b>Fluid</b>	<b>Friction (N)</b>
Water	1.08N
Olive Oil	2.16N

*Table 9: Experimental Frictions of Syringe Piston for Water and Olive Oil*

With these frictions calculated, we ran experimental trials to compare theoretical flow rates and analytical flow rates. The differences between the flow rates are shown below:

	<b>Weight Added</b>	<b>Theoretical Flow Rate (μL/min)</b>	<b>Analytic Flow Rate (μL/min)</b>
Water	250	3,932	500
Olive Oil	450	65.084	27.78

Table 10: Theoretical and Analytic Volumetric Flow Rates for Water and Olive Oil

The differences were notable but much closer with this new friction. The errors in our theoretical and analytic flow rates could be attributed to human error as well as some differences in surface roughness and the extent to which surface roughness affects a system at such a small size.

### 6.3 Combined Droplet Optimization and Handheld Pump Testing

With these calculations done, we attempted cross-flow in our system by attaching two syringes to the same chips used by the droplet sub team to run their angle optimization tests. The set up can be seen in the photo to the right in Figure 91. We added a varying amount of weights to the oil syringe ranging from 220 grams to 450 grams. While the experimental flow rate was too slow to be able to visually take note of due to the short time frame of our experiments, we noted the theoretical flow rate during our experiments.



Figure 91: Weight Driven Pump Setup



Figure 92: Droplets Formed in Tube from Weight Driven Pump

In all of these trials, we were able to produce droplets as seen in the collection tube at the end of the system to the left in Figure 92. The sphericity of these droplets varied with the weights added to the continuous flow and therefore varied with respect to the continuous fluid flow rate. A graph of the results can be seen to the right.

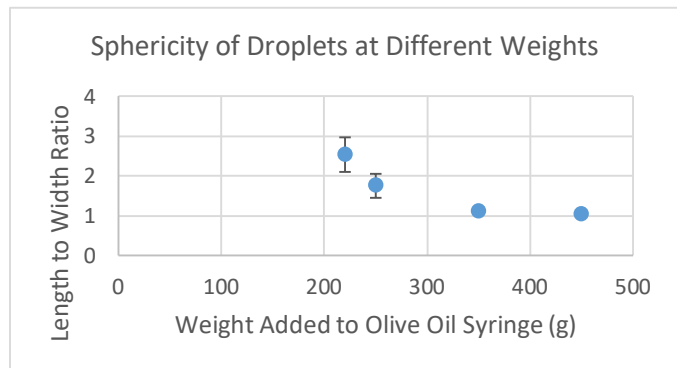


Figure 93: Sphericity of Droplets Produced by Weight Driven Pump at Given Weights

We also calculated the capillary numbers of the continuous flow to characterize the flow regime of the continuous fluid. This was done to check what flow regime these droplets were produced at as the flow regime affects what shape the droplets take (spherical as opposed to plug shaped.) In our calculations, we found that the capillary numbers ranged from 0.000463 in the first trial to 0.064 in the last trial. The flow was in the squeezing regime for the first two trials and was in dripping in the last two trials which was why the last two trials yielded such better sphericity.

### 6.3.1 Future Recommendations for Weight Driven Pumps

Due to the time constraints of our project, we were unable to perform further testing on the weight driven pumps. If we had more time, we would have run additional experimental flow rate testing where we allowed the syringe to entirely empty. Our team was unable to run these tests as they would require several hours to be able to fully dispense the contents of a syringe and for us to be able to see a change in position. Unfortunately, we did not have time at the end of our project to perform these tests. We would recommend that any team in the future working on this project complete those tests to properly evaluate the accuracy of our analytic models. This flow rate testing could be performed for systems containing only one fluid- either oil or water- but also should include discrepancies given by the water and oil interaction at the junction.

Furthermore, in order for this pump to be commercially viable, it would require a mechanism to hold the weights on the top of the syringe therefore eliminating the need for the operator to hold the weights in place. This would mitigate any force variations on the head of the syringe due to slight changes in the force of the human hand holding the weights on the syringe head. (While most of the force applied from human hands in this system and in our testing was perpendicular to the force down on the head of the syringe, there was the possibility of accidentally applying weight down on the syringe.) Therefore, a mechanism to be added to the top of the syringe would ensure constant force on the piston head and would achieve more consistent results. If this device could be designed for an operator to be able to change the weights on the syringe, this pump could achieve different flow rates with relative accuracy (assuming all weights and flow rates were previously confirmed prior to commercialization.)

## Chapter 7: Conclusion and Outlook

This MQP was completed in a seven-week term. During the course of this project, we learned several things about teamwork, time management, and record keeping that can be carried into our future work as engineers and team members.

Teamwork is vital for the success of a Major Qualifying Project. In order to complete everything for this project, we had to work in a group of four to accomplish more work more efficiently than a single person could achieve on their own in a seven-week period. Our team learned a lot about the importance of communication within teamwork- especially due to the unique subgroup set up of our team. The two main topics of our project were pump development and droplet generation. We divided our four-person project team into two sub-teams comprised of two people to complete the necessary trials in our short time frame. Although there were two sub-teams, we met every day and often worked concurrently in the lab to allow for cross team collaboration. We also extensively communicated through electronic means within and between the sub-groups to coordinate logistics and discuss project ideas. This communication was necessary to keep everyone on the same page and aid in discussion and brainstorming when a problem was encountered. Additionally, we met once a week with our advisor for at least an hour to update him on the project and get suggestions. We also occasionally had smaller ad hoc meetings with him between the formally scheduled ones to discuss specific questions or difficulties we were facing. Due to this extensive and open communication channel between our two sub teams and our professor, our team was able to work together much better and all contribute ideas to the final project that would have been lacking without proper communication. This communication and teamwork was an important skill to develop as we will all partake in extensive teamwork in the future and it was essential for our short project timeline.

Time management was also extremely important to the timely execution of our project. Completing this project in seven weeks required proper preparation and time management throughout its duration in order to finish in time. Due to the fact that, between the four of us, we had completed a significant number of projects and courses on a seven-week term, we were confident we could be successful completing this MQP in one term. Because the MQP is the most academically intensive project completed by WPI students, we began preparing for it at the end of D term of our junior years and continued that preparation throughout the summer preceding the

MQP. Over the summer we completed our entire literature review as well as formulated our specific project goals, divided up the teams, and worked through the logistics. This allowed us to begin design and fabrication immediately when the project officially began at the end of August.

Another issue we faced with time management was machine availability at WPI. Although one of the major advantages of fabricating our microfluidic chips with a laser cutter was a reduction in manufacturing time, one of our biggest limitations in this project was being able to schedule time on the laser cutter available for student use at WPI. Because the laser cutter available in our machine shop was shared by the entire university, it was sometimes difficult to use it when we desired. We quickly learned to counteract this issue by scheduling the laser cutter for the time we needed in advance.

We also needed to use these time management skills when taking shipping time of materials into account. Although there were some companies that could provide our materials overnight, some could take up to week which was a significant portion of our project timeline. Even overnight shipping was a larger delay, percentage wise, than it would have been in a twenty-one-week project. This was rarely an issue because we ordered our materials in advance of when they were needed; however, it needed to be carefully managed during the project.

The last main topic we learned while working on this project was the importance of proper record keeping. Record keeping during a project is important regardless of its time frame. Throughout the project, our entire team focused on keeping detailed records of each meeting. However, we did not initially do a sufficient job of keeping records of our testing trials. The pump sub-team ran several trials of pump 1.0 and 2.0 before realizing we had not always recorded the data we needed to make informed design iteration changes. As the term progressed, we constantly improved our record keeping process as we learned what information would be more relevant to making the next design change as well as how detailed the documentation needed to be to properly make design changes. The most noticeable side effect of learning the importance of data collection and organization is some inconsistencies in the pump iteration numbering system. Changing how pumps were numbered part way through the project led to some gaps in the numbering system. By quickly learning to make this change and adapting it to fit our needs, we were able to include what we believed to be the most relevant and understandable information in our final report without having to rely on memory or strictly photographic records. The droplet team learned a similar lesson in terms of how we named the video files of testing. Originally these file names contained

only the degree of the chip being tested, however, as the term progressed and testing became more involved so did the file names. File names were used to store information about the angle, flow speeds, and whether or not the chip had glued tubing. This allowed us to more easily group and analyze our results. This lesson on the importance of proper data labeling will be applicable in future projects and prevent the need for data reconciliation and the additional time it takes.

## References

- [1] G. M. Whitesides, "The origins and the future of microfluidics," *Nature*, vol. 442, no. 7101, pp. 368–373, 2006.
- [2] C. D. Chin, V. Linder, and S. K. Sia, "Commercialization of microfluidic point-of-care diagnostic devices," *Lab on a Chip*, vol. 12, no. 12, p. 2118, 2012.
- [3] Z. Nie, C. A. Nijhuis, J. Gong, X. Chen, A. Kumachev, A. W. Martinez, M. Narovlyansky, and G. M. Whitesides, "Electrochemical sensing in paper-based microfluidic devices," *Lab Chip*, vol. 10, no. 4, pp. 477–483, 2010.
- [4] H. Wei, B.-han Cheuh, H. Wu, E. W. Hall, C.-wing Li, R. Schirhagl, J.-M. Lin, and R. N. Zare, "Particle sorting using a porous membrane in a microfluidic device," *Lab on a Chip*, vol. 10, no. 4, pp. 238–245.
- [5] "PDMS: A review," *Elveflow*. [Online]. Available: <http://www.elveflow.com/microfluidic-tutorials/microfluidic-reviews-and-tutorials/the-poly-di-methyl-siloxane-pdms-and-microfluidics/>. [Accessed: 12-Oct-2017].
- [6] G. Fiorini and D. Chiu, "Disposable microfluidic devices: fabrication, function, and application," *BioTechniques*, vol. 38, no. 3, pp. 429–446, 2005.
- [7] "Overview of materials for Acrylic, Extruded," <http://www.matweb.com/search/DataSheet.aspx?MatGUID=632572aef2a4224b5ac8fbd4f1b6f77&ckck=1>.
- [8] A. Hiznay, D. Gantulga, J. LaValley, and K. Lou, "Robust Assay to Study Associative Learning in *C. elegans*," (2016).
- [9] H. Klank, J. R. P. Kutter, and O. Geschke, "CO<sub>2</sub>-laser micromachining and back-end processing for rapid production of PMMA-based microfluidic systems," *Lab on a Chip*, vol. 2, no. 4, p. 242, 2002.
- [10] M. Rahbar, S. Chhina, D. Sameoto, and M. Parameswaran, "Microwave-induced, thermally assisted solvent bonding for low-cost PMMA microfluidic devices," *Journal of Micromechanics and Microengineering*, vol. 20, no. 1, p. 015026, Jul. 2009.

- [11] “McMaster-Carr,” *McMaster-Carr*. [Online]. Available: <https://www.mcmaster.com/>. [Accessed: 12-Oct-2017].
- [12] X. Han, X. Liu, L. Tian, and Z.-G. Mao, "A Non-Photolithography Fabrication for a Microfluidic Chip Based on PMMA Polymer," *Machines* 3, 107–122 (2015).
- [13] Z. K. Wang, H. Y. Zheng, R. Y. H. Kim, Z. F. Wang, and Y. C. Lam, "Improving surface smoothness of laser-fabricated microchannels for microfluidic application," *Journal of Micromechanics and Microengineering* 21, (2011).
- [14] C. A. Mack, “Semiconductor Lithography (Photolithography) - The Basic Process,” (2014).
- [15] “Introduction about soft-lithography for microfluidics,” *Elveflow: Plug & Play Microfluidics*. [Online]. Available: <http://www.elveflow.com/microfluidic-tutorials/soft-lithography-reviews-and-tutorials/introduction-in-soft-lithography/introduction-about-soft-lithography-and-polymer-molding-for-microfluidic/>. [Accessed: 12-Oct-2017].
- [16] M. Brown, J. Brown, and F. Alfayez, "Development of a stand-alone microfluidic device -- with fiber optical sensor, self-powered pump, and cellphone based imaging platform," <https://web.wpi.edu/Pubs/E-project/Available/E-project-042915-161214/>.
- [17] D. B. Weibel, W. R. DiLuzio, and G. M. Whitesides, "Microfabrication meets microbiology," *Nature Reviews Microbiology* 5, 209–218 (2007).
- [18] M. M. Gong, B. D. Macdonald, T. V. Nguyen, and D. Sinton, “Hand-powered microfluidics: A membrane pump with a patient-to-chip syringe interface,” *Biomicrofluidics*, vol. 6, no. 4, p. 044102, 2012.
- [19] K. Iwai, R. D. Sochol, and L. Lin, “Finger-powered, pressure-driven microfluidic pump,” *2011 IEEE 24th International Conference on Micro Electro Mechanical Systems*, 2011.
- [20] W. Zhang, S. Lin, C. Wang, J. Hu, C. Li, Z. Zhuang, Y. Zhou, R. A. Mathies, and C. J. Yang, “PMMA/PDMS valves and pumps for disposable microfluidics,” *Lab on a Chip*, vol. 9, no. 21, p. 3088, 2009.
- [21] T. Kokalj, Y. Park, M. Vencelj, M. Jenko, and L. P. Lee, “Self-powered Imbibing Microfluidic Pump by Liquid Encapsulation: SIMPLE,” *Lab Chip*, vol. 14, no. 22, pp. 4329–4333, 2014.

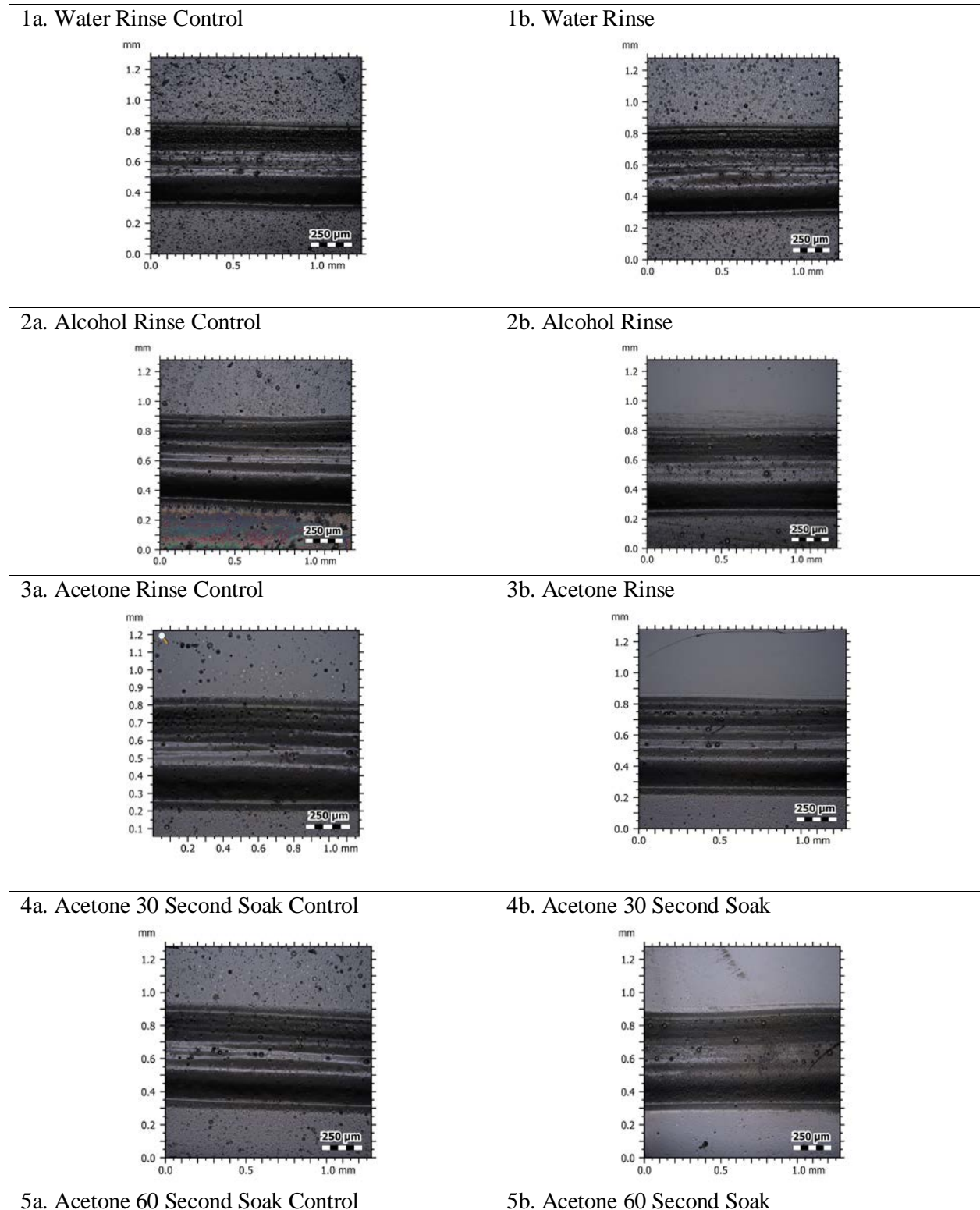
- [22] X. Wang, J. A. Hagen, and I. Papautsky, "Paper pump for passive and programmable transport," *Biomicrofluidics*, vol. 7, no. 1, p. 014107, 2013.
- [23] NASA. [Online]. Available: <https://www.grc.nasa.gov/www/k-12/airplane/bern.html>. [Accessed: 12-Oct-2017].
- [24] C.K. Byun, K. Abi-Samra, Y.-K. Cho, and S. Takayama, "Pumps for Microfluidic Cell Culture," *Electrophoresis*, vol. 35, no. 2-3, pp.245-257, Feb. 2014.
- [25] Y. A. Çengel and J. M. Cimbala, *Fluid mechanics fundamentals and applications*. New York, NY: McGraw-Hill Education, 2017.
- [26] X. Zhu, N. Phadke, J. Chang, B. Cho, D. Huh, and S. Takayama, "Gravity-Driven Micropump with a Steady Flow Rate," *Micro Total Analysis Systems 2002*, pp. 151–153, 2002.
- [27] V. E. Neie, *Introduction to physics, mechanics*. West Lafayette, IN: Purdue University, 1978.
- [28] "Springfusor® & Flow Control Tubing (FCT)," *Admedus*. [Online]. Available: <http://www.admedus.com/medical-products/infusion-systems/springfusor-flow-control-tubing-fct/>. [Accessed: 12-Oct-2017].
- [29] "Springfusor Data Sheet," *Springfusor Data Sheet*. [Online]. Available: <http://www.westbournemedical.co.uk/springfusor%20data%20sheet.htm>. [Accessed: 12-Oct-2017].
- [30] W. Jung, J. Han, J.-W. Choi, and C. H. Ahn, "Point-of-care testing (POCT) diagnostic systems using microfluidic lab-on-a-chip technologies," *Microelectronic Engineering*, vol. 132, pp. 46–57, 2015.
- [31] P. Zhu and L. Wang, "Passive and active droplet generation with microfluidics: A review," *Lab on a Chip*, vol. 17, no. 1, pp. 34–75.
- [32] L. Shang, Y. Cheng, and Y. Zhao, "Emerging droplet microfluidics," *Chemical Reviews*, vol. 117, no. 12, pp. 7964–8040.
- [33] T. Fu, Y. Ma, D. Funfschilling, C. Zhu, and H. Z. Li, "Squeezing-to-dripping transition for bubble formation in a microfluidic T-junction," *Chemical Engineering Science*, vol. 65, no. 12, pp. 3739–3748, 2010.

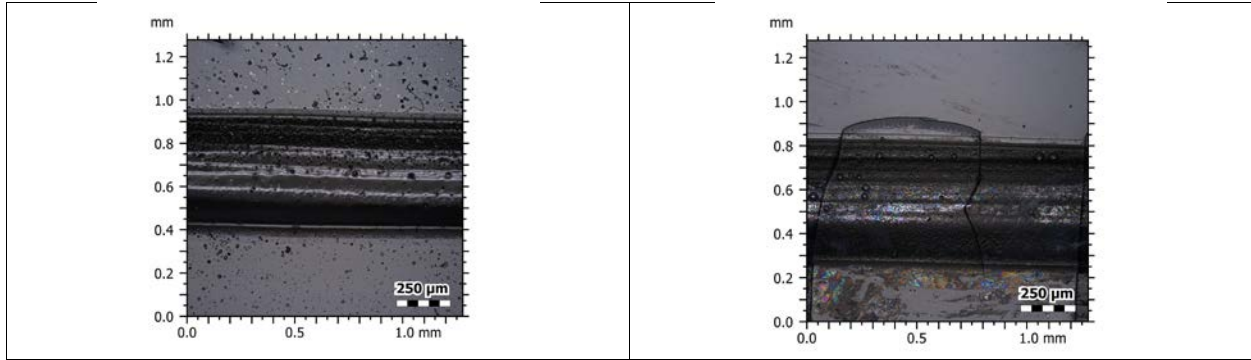
[34] “Pressure Sensitive Adhesives - Pressure Sensitive Tapes - Pressure Sensitive Films - Drug delivery Systems,” *Adhesives Research*. [Online]. Available: <http://www.adhesivesresearch.com/>. [Accessed: 12-Oct-2017].

[35] G. Bracco and B. Holst, Eds., *Surface Science Techniques*. Berlin: Springer, 2013.

# Appendices

## Appendix A: Surface Roughness Study Confocal Microscope Images





Appendix B: Surface Roughness Study Ra Values

**Water:**

	<b>Water Rinse Control</b>	<b>Water Rinse</b>
<b>Ra (100um)</b>	10.1	11.1
<b>Ra (300um)</b>	10.4	9.73
<b>Ra (500um)</b>	9.16	12
<b>Ra (700um)</b>	8.77	9.03
<b>Ra (900um)</b>	9.54	11.4
<b>Average Ra</b>	<b>9.594</b>	<b>10.652</b>

**Alcohol:**

	<b>Alcohol Rinse Control</b>	<b>Alcohol Rinse</b>
<b>Ra (100um)</b>	9	11.7
<b>Ra (300um)</b>	8.45	9.26
<b>Ra (500um)</b>	8.76	8.39
<b>Ra (700um)</b>	9.02	10.4
<b>Ra (900um)</b>	12	9.52
<b>Average Ra</b>	<b>9.446</b>	<b>9.854</b>

**Acetone:**

	<b>Acetone Rinse Control</b>	<b>Acetone Rinse</b>	<b>Acetone 30 Sec Control</b>	<b>Acetone 30 Sec</b>	<b>Acetone 60 Sec Control</b>	<b>Acetone 60 Sec</b>
<b>Ra (100um)</b>	10.2	8.09	8.68	3.86	10.8	3.49
<b>Ra (300um)</b>	12.2	7.32	9.36	3.44	10.7	2.88
<b>Ra (500um)</b>	12.8	7.35	9.6	3.12	8.96	2.06
<b>Ra (700um)</b>	10.6	8.92	8.98	2.03	9.54	2.31
<b>Ra (900um)</b>	11.9	9.37	9.67	3.16	9.57	2.35
<b>Average Ra</b>	<b>11.54</b>	<b>8.21</b>	<b>9.258</b>	<b>3.122</b>	<b>9.914</b>	<b>2.618</b>

## Appendix C: Capillary Number Calculations

To start, we calculated the bounds that velocity of the oil had to fall in between in order to be considered within the dripping regime.

### Variables

#### 1. Surface Tension

$$\sigma_{\text{oil}} := 21 \cdot 10^{-3} \frac{\text{N}}{\text{s}}$$

#### 2. Kinematic Viscosity

$$\nu_{\text{oil}} := 143.7 \cdot 10^{-6} \frac{\text{m}^2}{\text{s}}$$

#### 3. Density of oil

$$\rho_{\text{oil}} := 870 \frac{\text{kg}}{\text{m}^3}$$

#### 4. Dynamic Viscosity

$$\mu_{\text{oil}} := \nu_{\text{oil}} \cdot \rho_{\text{oil}} = 0.125 \text{ Pa} \cdot \text{s}$$

$$\mu_{\text{oil},2} := \mu_{\text{oil}} \cdot 10^3 = 125.019 \text{ mPa} \cdot \text{s}$$

#### 5. Cross-sectional area

$$h := 127 \cdot 10^{-6} \text{ m}$$

$$w := 350 \cdot 10^{-6} \text{ m}$$

$$A_c := h \cdot w = 4.445 \times 10^{-8} \text{ m}^2$$

### Calculate minimum velocities:

6. Known:

$$Ca_{\min} := 0.013$$

$$Ca_{\max} := 0.1$$

Solve for velocity boundaries:

$$V_{\min} := \frac{Ca_{\min} \cdot \sigma_{\text{oil}}}{\mu_{\text{oil}}} = 2.184 \times 10^{-3} \frac{\text{m}}{\text{s}}$$

$$V_{\max} := \frac{Ca_{\max} \cdot \sigma_{\text{oil}}}{\mu_{\text{oil}}} = 0.017 \frac{\text{m}}{\text{s}}$$

### Calculate minimum and maximum flow rates:

Minimum flow rate:

$$Q_{\min} := V_{\min} \cdot A_c = 9.706 \times 10^{-11}$$

$$Q_{\min, \text{oil}} := Q_{\min} \cdot 10^9 \cdot 60 = 5.824 \frac{\mu\text{L}}{\text{min}}$$

Maximum flow rate:

$$Q_{\max} := V_{\max} \cdot A_c = 7.466 \times 10^{-10}$$

$$Q_{\max, \text{oil}} := Q_{\max} \cdot 10^9 \cdot 60 = 44.799 \frac{\mu\text{L}}{\text{min}}$$

## Capillary Number Verifications- Oil

To verify that our flow rates were within the desired regime,

### Variables

$$Q_{\text{oil}} := 7.2 \frac{\mu\text{L}}{\text{min}}$$

$$Q_{\text{oil}.2} := .12 \cdot 10^{-9} \frac{\text{m}^3}{\text{s}}$$

$$V_{\text{oil}} := \frac{Q_{\text{oil}.2}}{A_c} = 2.7 \times 10^{-3} \frac{\text{m}}{\text{s}}$$

### Calculate capillary number

$$Ca_{\text{oil}} := \frac{\mu_{\text{oil}} \cdot V_{\text{oil}}}{\sigma_{\text{oil}}} = 0.016$$

## Capillary Number Verifications- Water

To verify that our flow rates were within the desired regime,

### Properties

$$\mu_w := 9.02 \cdot 10^{-4} \text{ Pa}\cdot\text{s}$$

$$\sigma_w := 72.8 \frac{\text{mN}}{\text{m}}$$

### Variables

$$Q_w := 2.5 \frac{\mu\text{L}}{\text{min}}$$

$$Q_{w.2} := \frac{Q_w \cdot 10^{-9}}{60} = 4.167 \times 10^{-11} \frac{\text{m}^3}{\text{s}}$$

$$V_w := \frac{Q_{w.2}}{A_c} = 9.374 \times \frac{\text{m}}{\text{s}}$$

### Calculate capillary number

$$Ca_w := \frac{\mu_w \cdot V_w}{\sigma_w} = 1.161 \times 10^{-8}$$

## Capillary Number Verifications- Olive Oil

To verify that our flow rates were within the desired regime,

### Properties

$$\mu_{\text{olive}} := 84 \cdot 10^{-3} \text{ Pa}\cdot\text{s}$$

$$\sigma_{\text{olive}} := 32 \cdot 10^{-3} \frac{\text{N}}{\text{m}}$$

### Variables

$$Q_{\text{olive}} := 12.2 \frac{\mu\text{L}}{\text{min}}$$

$$Q_{\text{olive.2}} := \frac{Q_{\text{olive}} \cdot 10^{-9}}{60} = 2.033 \times 10^{-10} \frac{\text{m}^3}{\text{s}}$$

$$V_{\text{olive}} := \frac{Q_{\text{olive.2}}}{A_c} = 4.574 \times 10^{-3} \frac{\text{m}}{\text{s}}$$

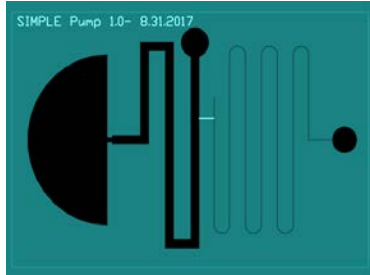
### Calculate capillary number

$$Ca_{\text{olive}} := \frac{\mu_{\text{olive}} \cdot V_{\text{olive}}}{\sigma_{\text{olive}}} = 0.012$$

## Appendix D: Paper Pump Design Pictures and Settings

### Pump 1.0

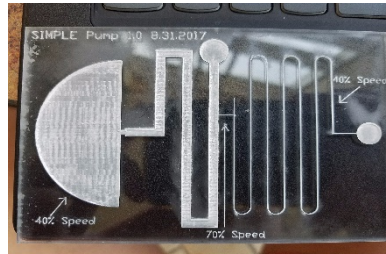
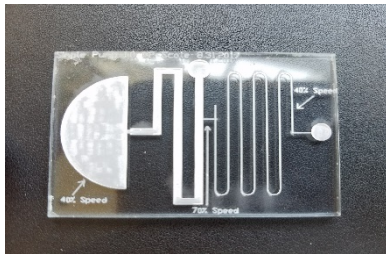
#### AutoCAD Drawing



#### Settings

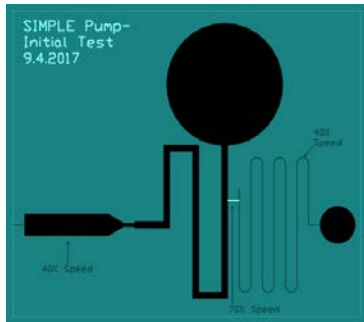
- 40% speed raster
- 40% speed engrave all except 70% speed engrave for passive valve
- 0.11 in acrylic

#### Photos



# Pump 2.0

## AutoCAD File

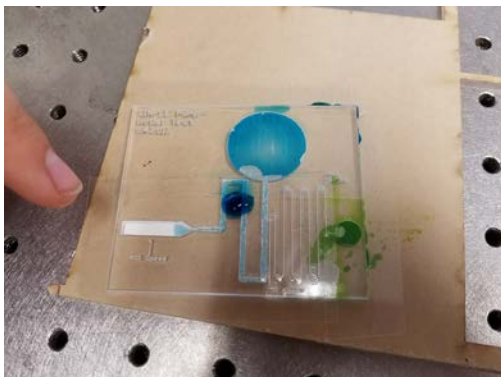
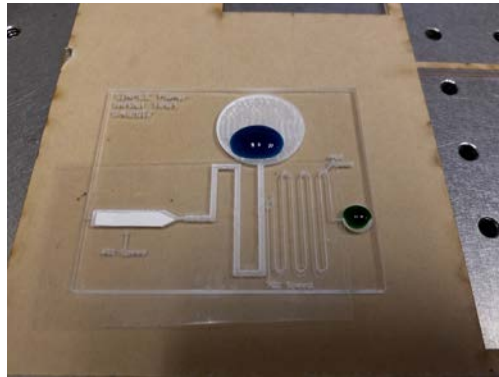
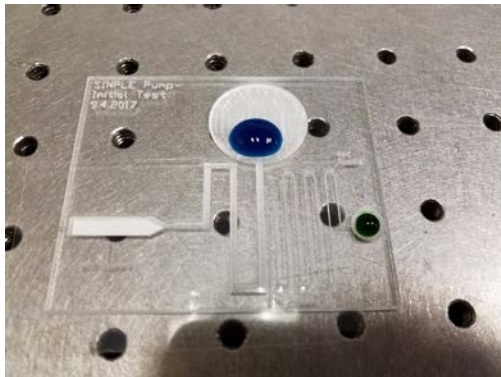


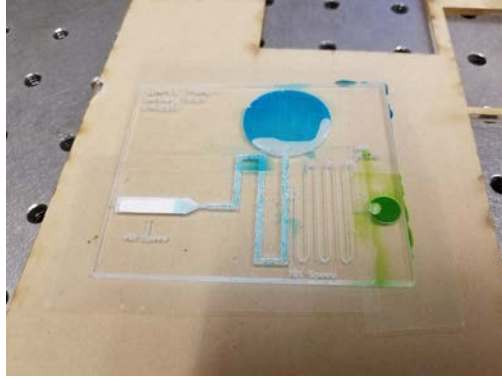
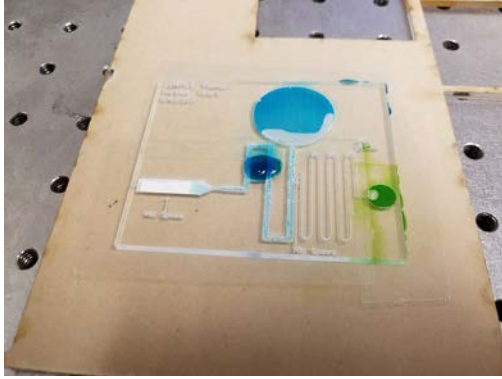
## Settings

- 40% speed raster
- 40% speed engrave all except 70% speed engrave for passive valve
- 0.1 in acrylic

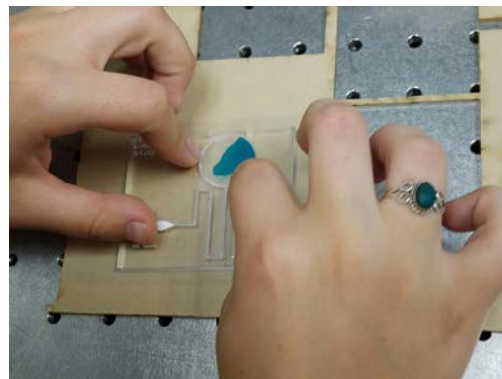
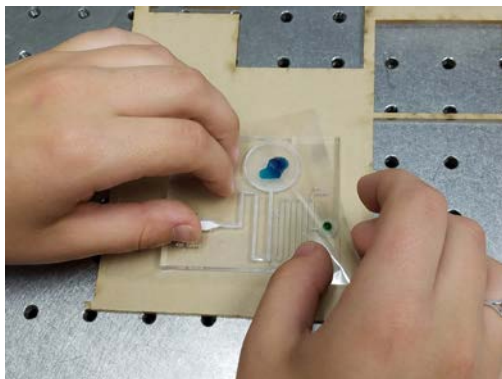
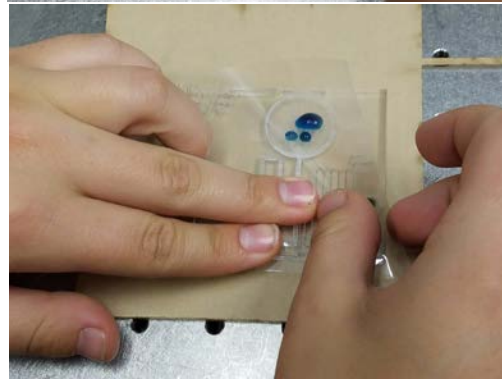
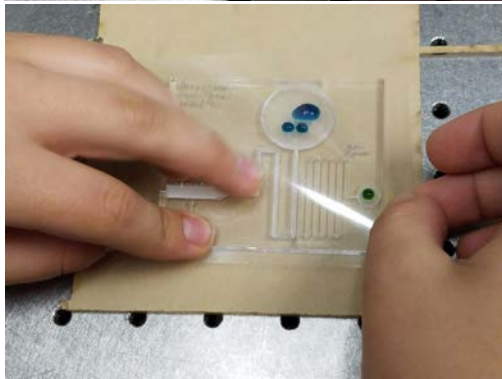
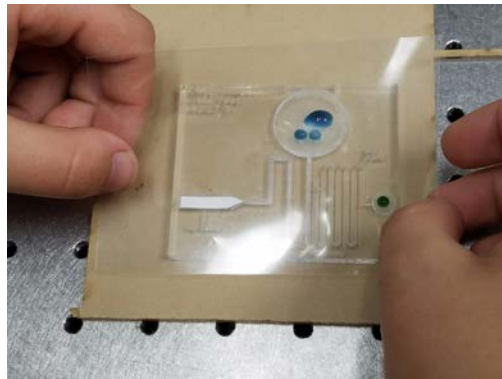
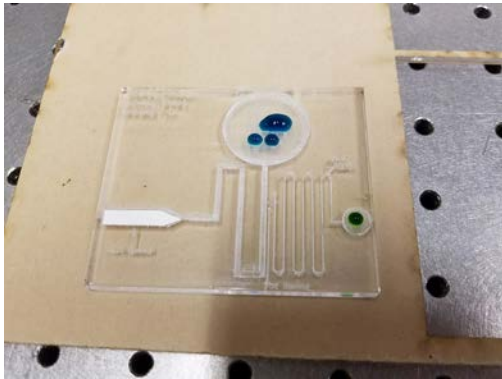
## Photos

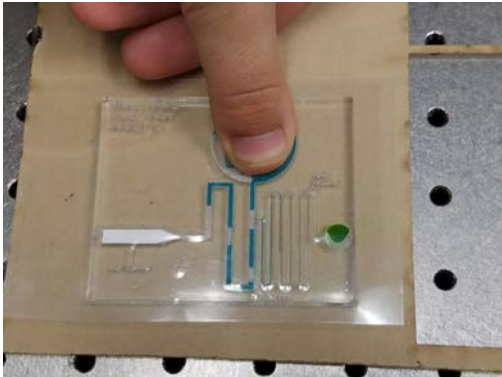
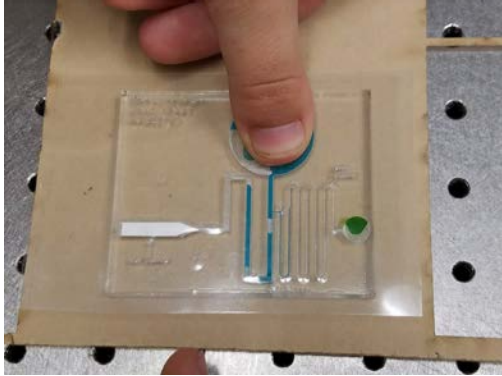
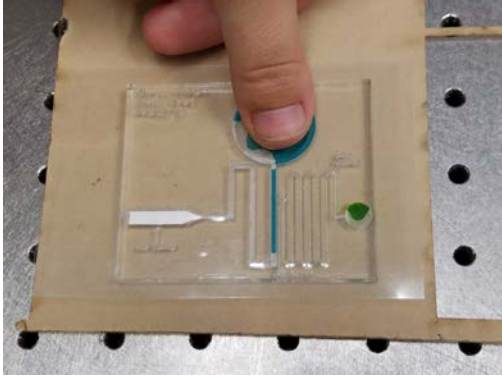
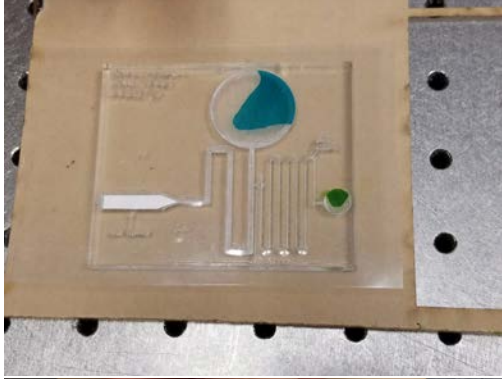
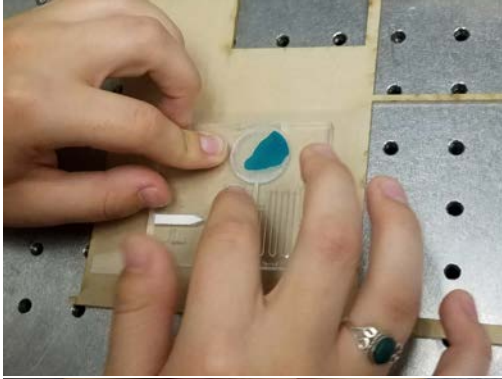
Iteration 1:





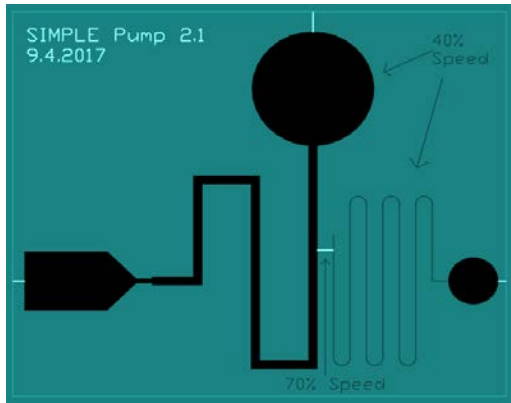
Iteration 2:





## Pump 2.1

### AutoCAD File

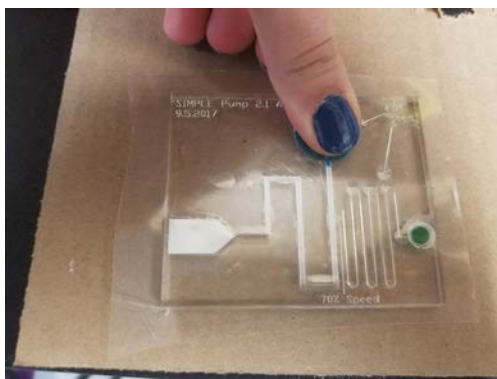
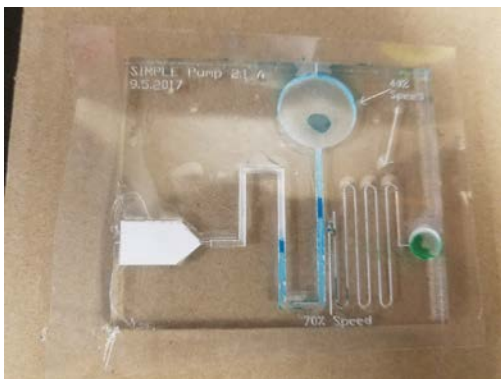
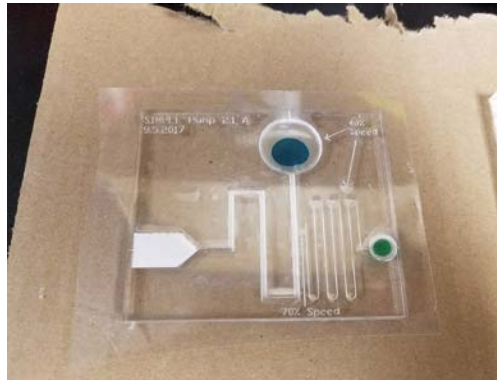
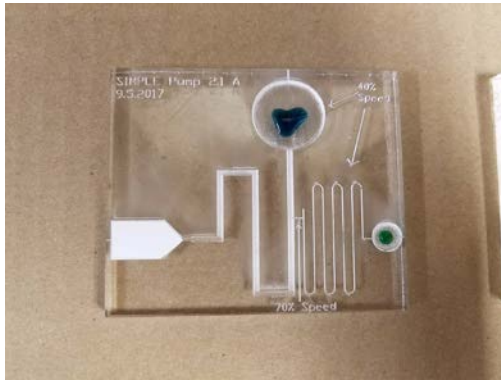


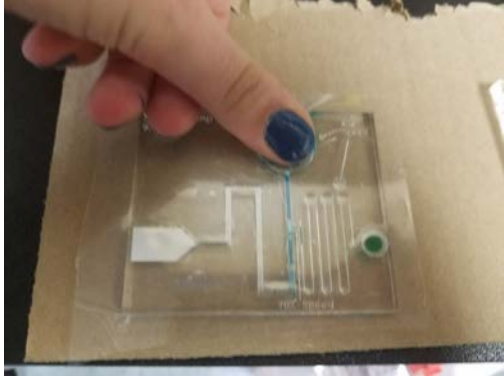
### Settings

- 40% speed raster
- 40% speed engrave all except 70% speed engrave for passive valve
- 0.214" acrylic

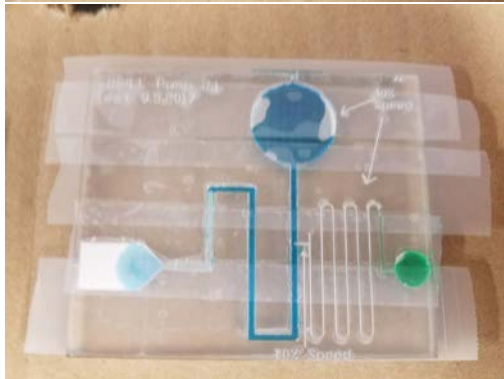
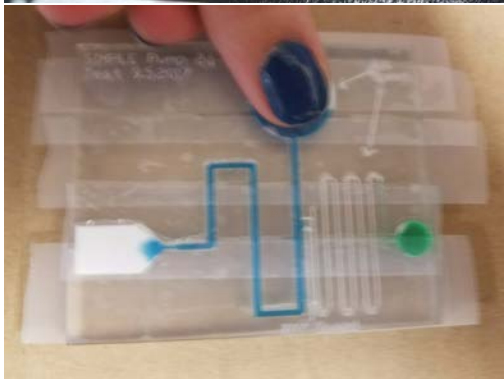
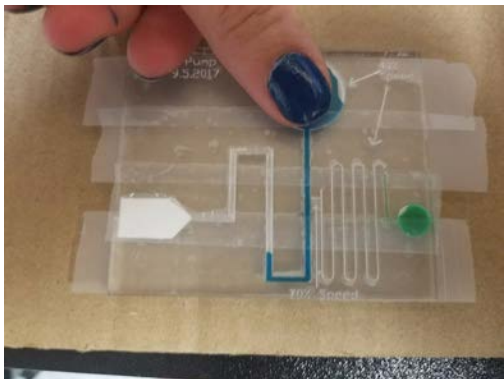
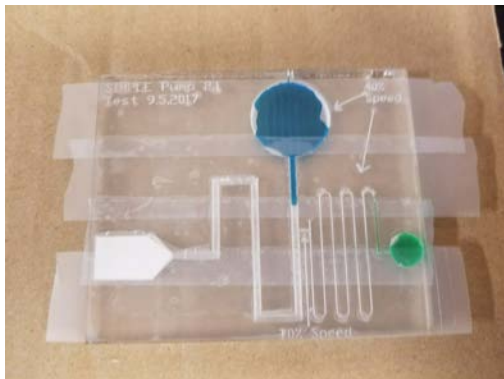
### Photos

#### Iteration 1: Hydrophobic Tape



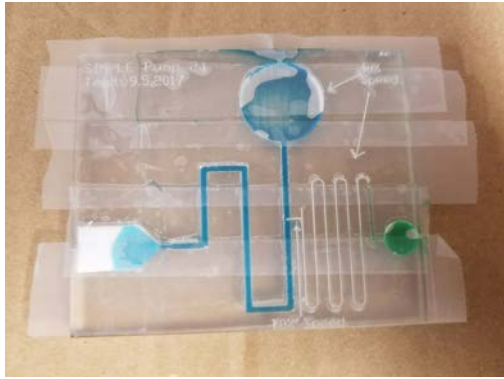


Iteration 2: Scotch Tape



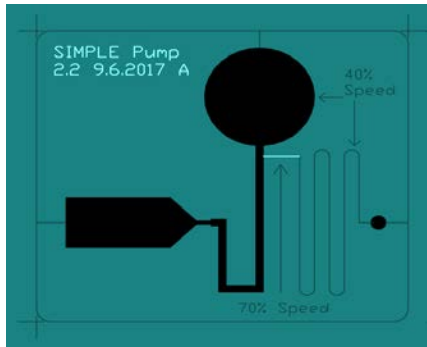


Iteration 3:



## Pump 2.2

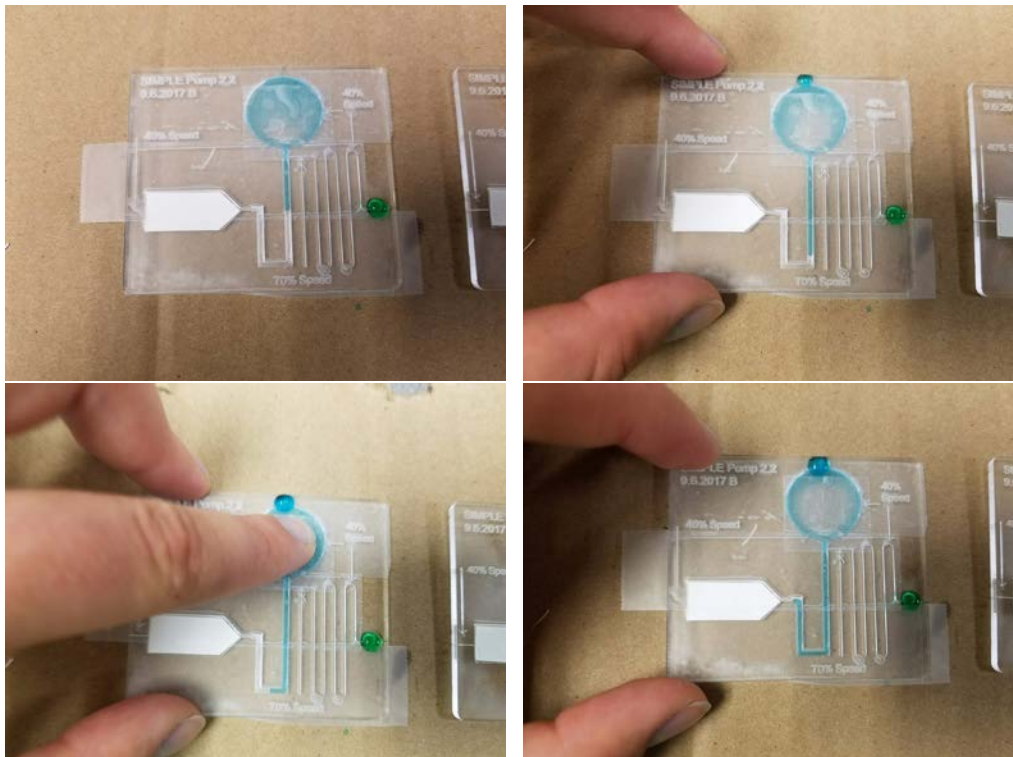
### AutoCAD File

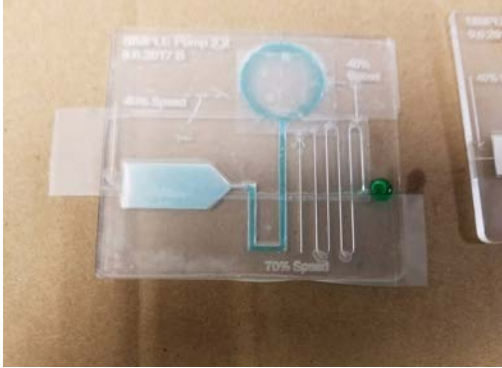
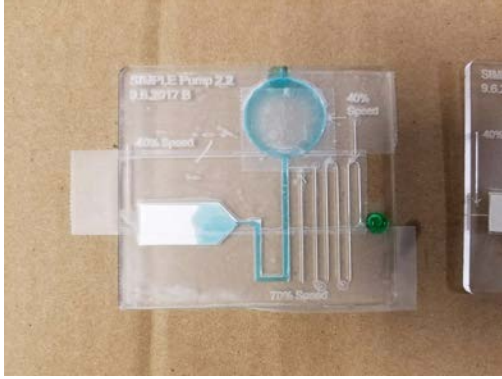
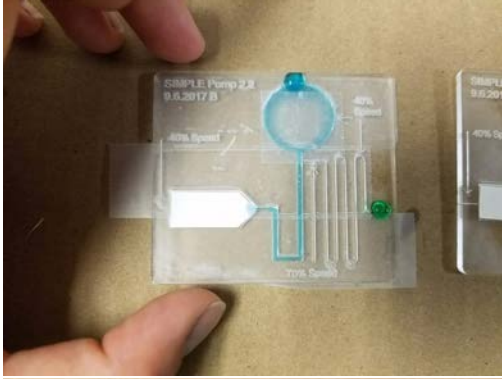


### Settings

- 40% speed raster
- 40% speed engrave all except 70% speed engrave for passive valve
- 0.1in acrylic

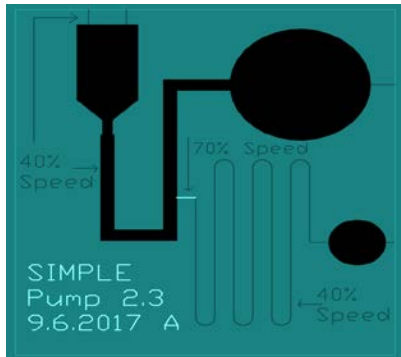
### Photos





## Pump 2.3

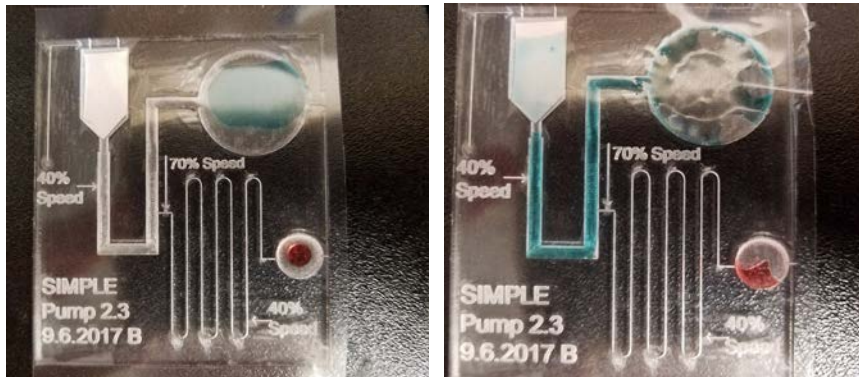
### AutoCAD File



### Settings

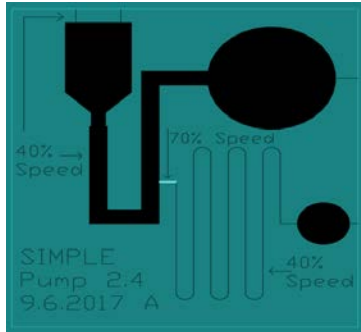
- 40% speed raster
- 40% speed engrave all except 70% speed engrave for passive valve
- 0.1in acrylic

### Photos



## Pump 2.4

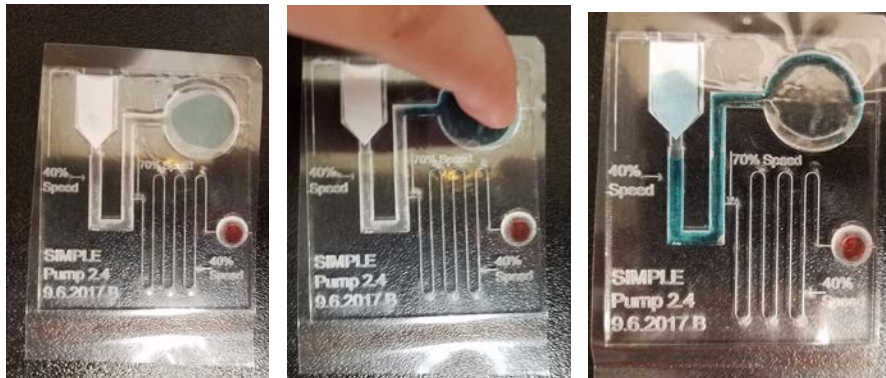
### AutoCAD File



### Settings

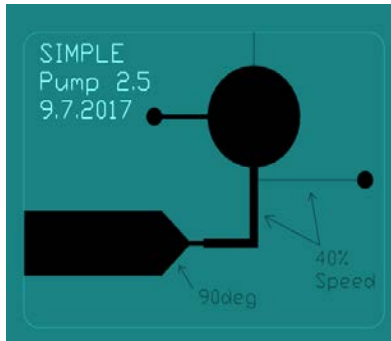
- 40% speed raster
- 40% speed engrave all except 70% speed engrave for passive valve
- 0.1in acrylic

### Photos



## Pump 2.5

### AutoCAD File



### Settings

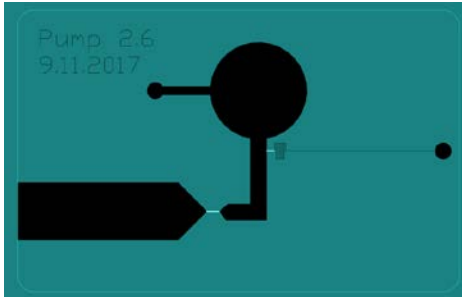
- 40% Vector Engraving
- 40% Raster

### Photos



## Pump 2.6

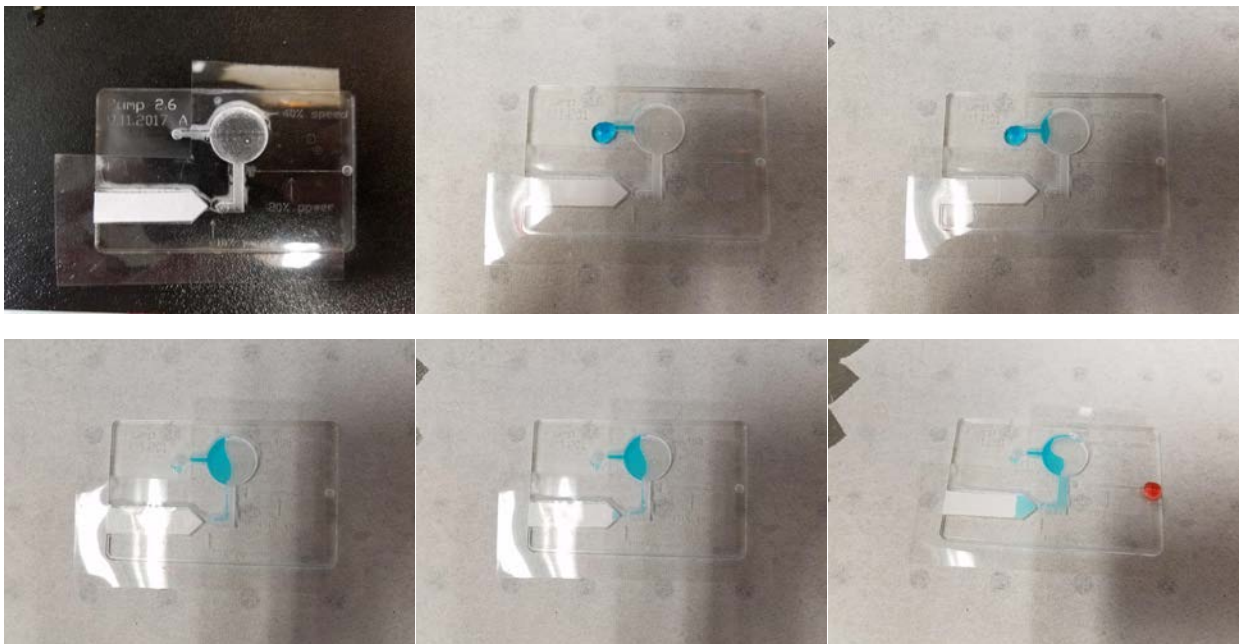
### AutoCAD File

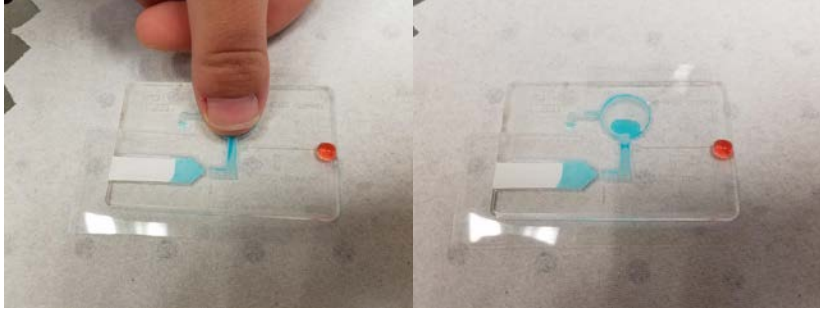


### Settings

- Raster- 40% speed (Estimated- 527um depth based on desire to have the working fluid channel deeper than the vector engraving channel.)
- We could put the paper portion at closer to 90% speed to accommodate the 180um thickness of the paper
- Blue Vector Engraving- 20% power (Desired- 127um depth based on the depth of the channels of the pump group)
- White Vector Engraving- 10% power (Estimated- 57um depth. Based on desire to have these channels shallower than the other channels)

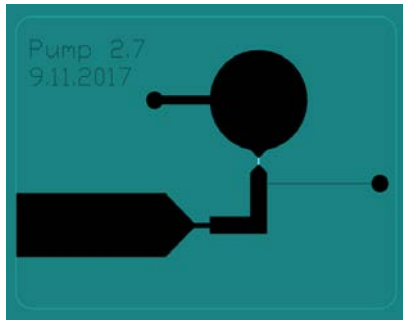
### Photos





## Pump 2.7

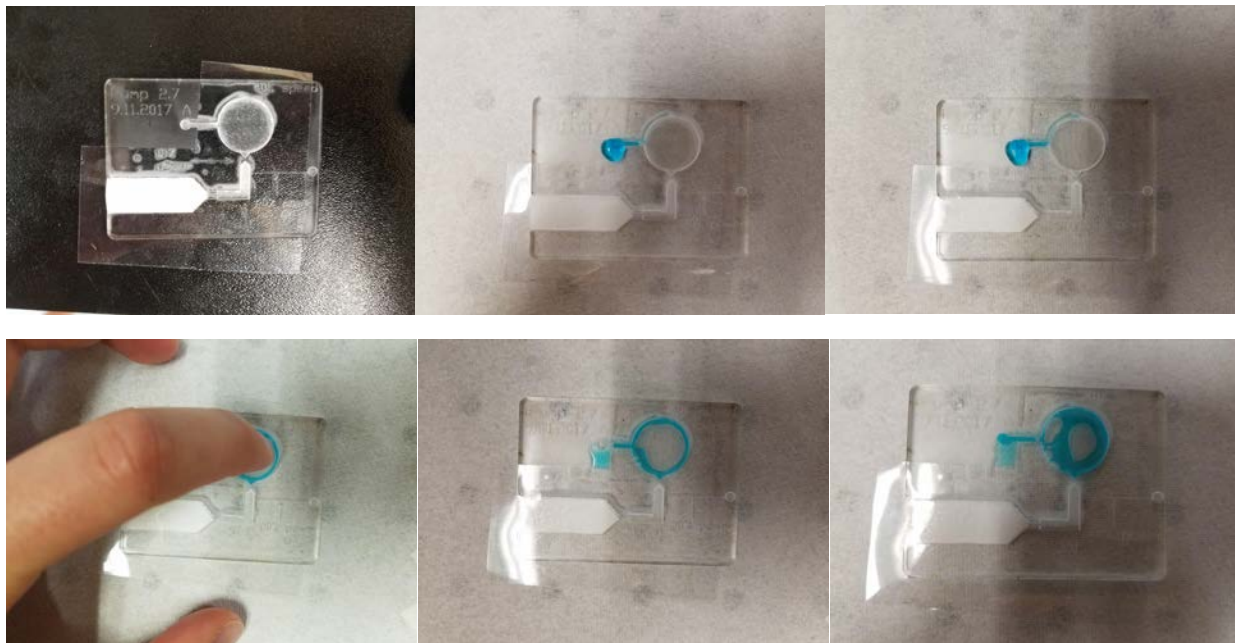
### AutoCAD File



### Settings

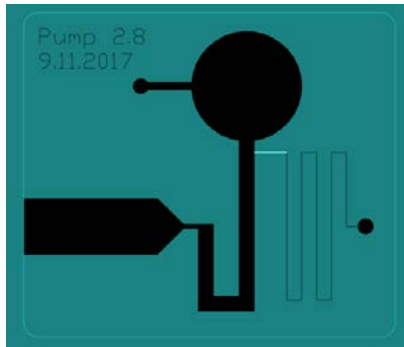
- Raster- 40% speed (Estimated- 527um depth based on desire to have the working fluid channel deeper than the vector engraving channel.)
- We could put the paper portion at closer to 90% speed to accommodate the 180um thickness of the paper
- Blue Vector Engraving- 20% power (Desired- 127um depth based on the depth of the channels of the pump group)
- White Vector Engraving- 10% power (Estimated- 57um depth. Based on desire to have these channels much shallower than the working fluid to keep it from flowing)

### Photos



## Pump 2.8

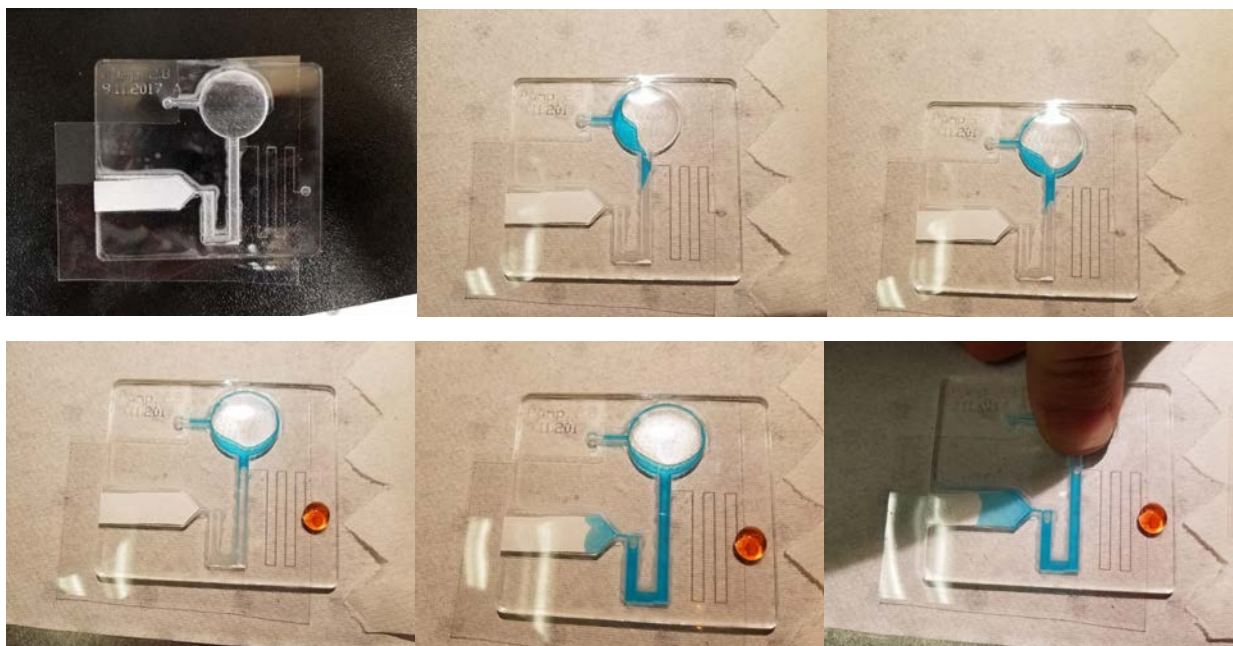
### AutoCAD File



### Settings

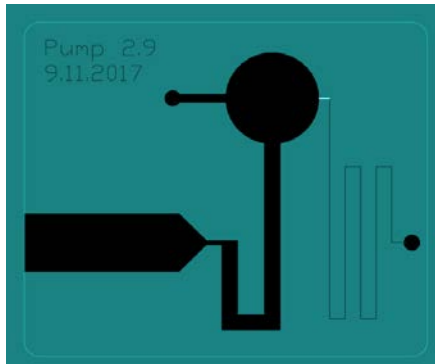
- Raster- 40% speed (Estimated- 527um depth based on desire to have the working fluid channel deeper than the vector engraving channel.)
- We could put the paper portion at closer to 90% speed to accommodate the 180um thickness of the paper
- Blue Vector Engraving- 20% power (Desired- 127um depth based on the depth of the channels of the pump group)
- White Vector Engraving- 10% power (Estimated- 57um depth. Based on desire to have these channels much shallower than the analytic fluid and the working fluid channels to keep the fluid from flowing into those channels)

### Photos



## Pump 2.9

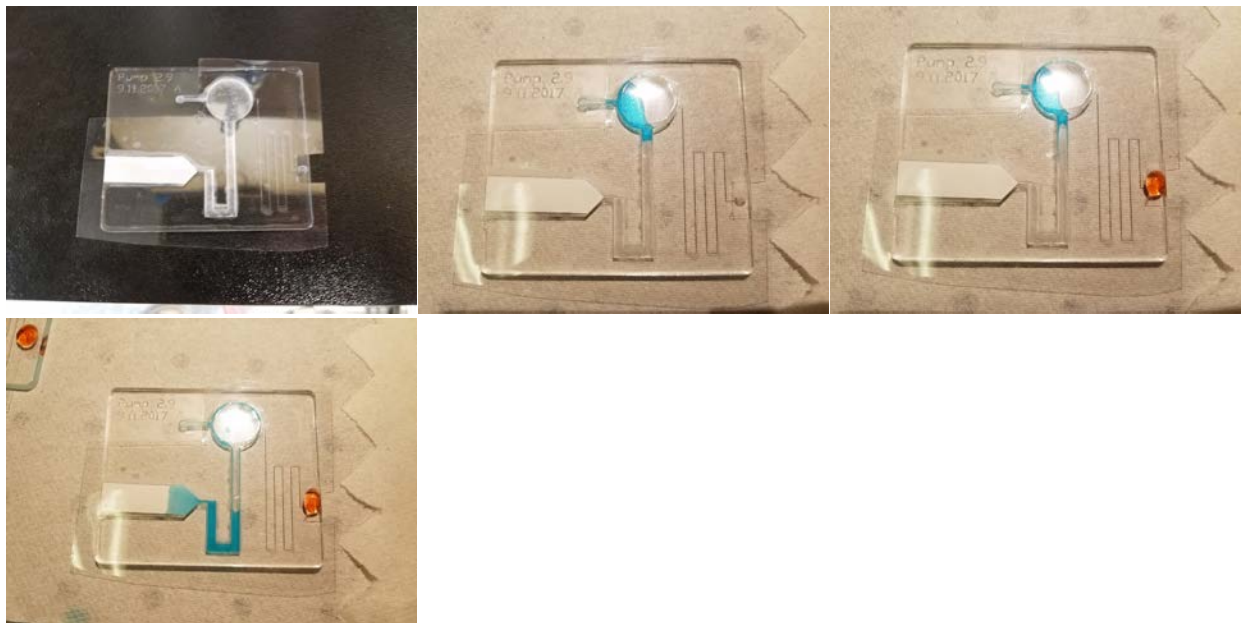
### AutoCAD File



### Settings

- Raster- 40% speed (Estimated- 527um depth based on desire to have the working fluid channel deeper than the vector engraving channel.)
- We could put the paper portion at closer to 90% speed to accommodate the 180um thickness of the paper
- Blue Vector Engraving- 20% power (Desired- 127um depth based on the depth of the channels of the pump group)
- White Vector Engraving- 10% power (Estimated- 57um depth. Based on desire to have these channels much shallower than the analytic fluid and the working fluid channels to keep the fluid from flowing into those channels)

### Photos



## Pump 2.10

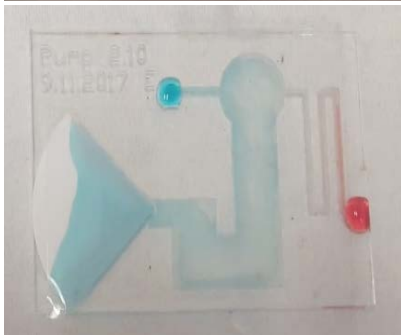
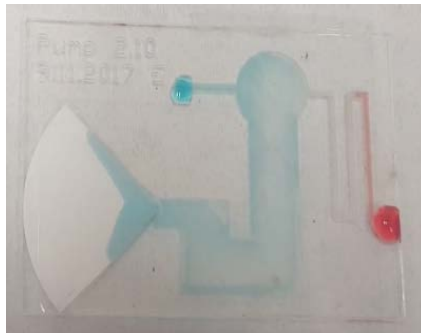
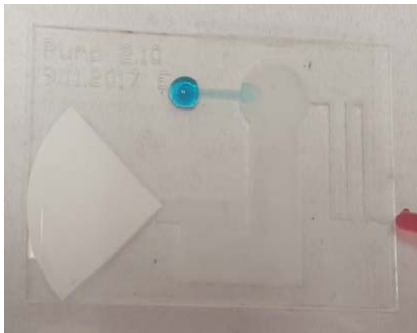
### AutoCAD File



### Settings

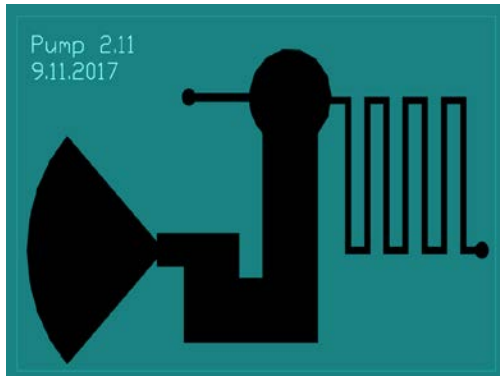
- Raster- 40% speed (Estimated- 527um depth based on desire to have the working fluid channel deeper than the vector engraving channel.)
- Blue Vector Engraving- 20% power (Desired- 127um depth based on the depth of the channels of the pump group)
- White Vector Engraving- 10% power (Estimated- 57um depth. Based on desire to have these channels much shallower than the analytic fluid and the working fluid channels to keep the fluid from flowing into those channels)

### Photos



## Pump 2.11

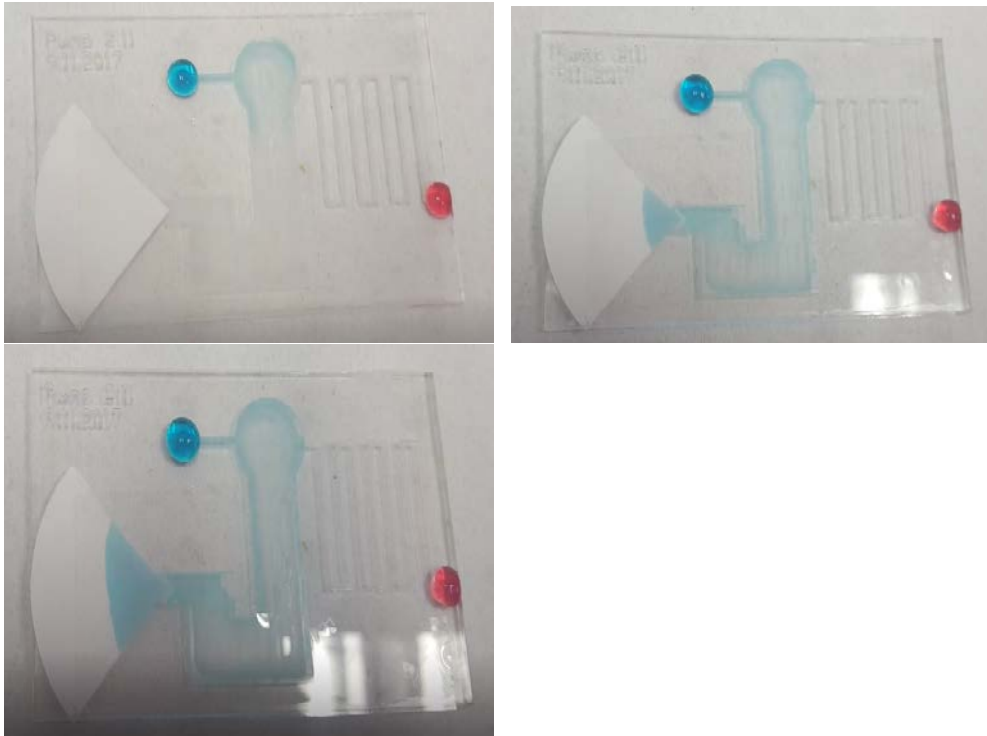
### AutoCAD File



### Settings

- Raster- 40% speed (Estimated- 527um depth based on desire to have the working fluid channel deeper than the vector engraving channel.)
- Blue Vector Engraving- 20% power (Desired- 127um depth based on the depth of the channels of the pump group)
- White Vector Engraving- 10% power (Estimated- 57um depth. Based on desire to have these channels much shallower than the analytic fluid and the working fluid channels to keep the fluid from flowing into those channels)

### Photos



## Pump 2.12

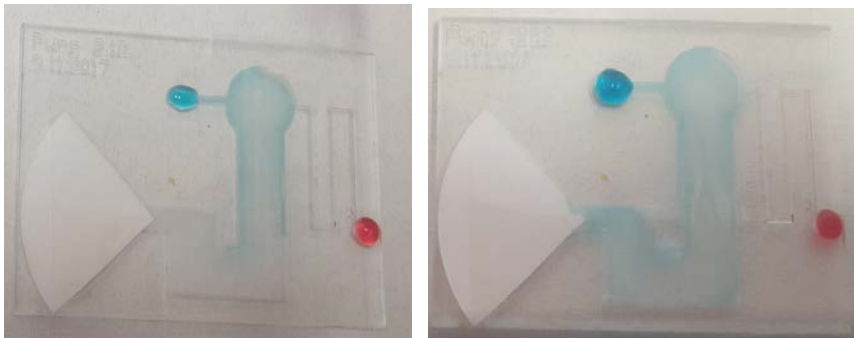
### AutoCAD File



### Settings

- Raster- 40% speed (Estimated- 527um depth based on desire to have the working fluid channel deeper than the vector engraving channel.)
- Blue Vector Engraving- 20% power (Desired- 127um depth based on the depth of the channels of the pump group)
- White Vector Engraving- 10% power (Estimated- 57um depth. Based on desire to have these channels much shallower than the analytic fluid and the working fluid channels to keep the fluid from flowing into those channels)

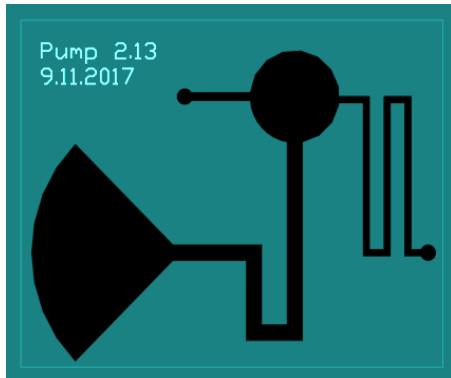
### Photos





## Pump 2.13

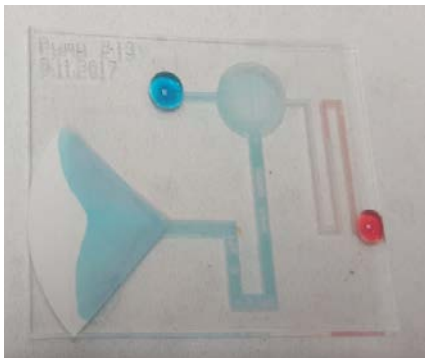
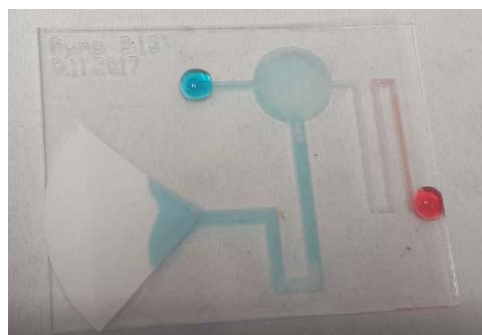
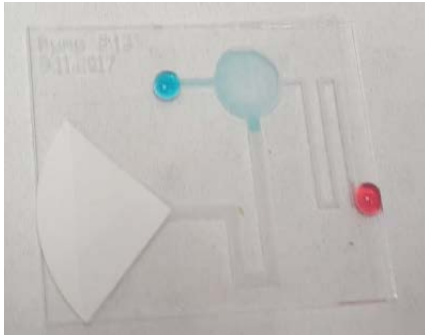
### AutoCAD File



### Settings

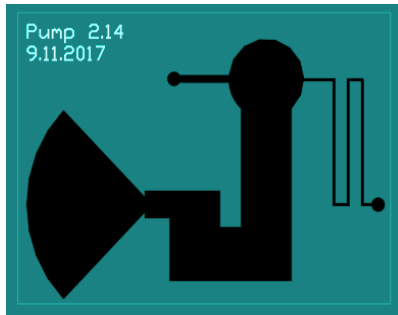
- Raster- 40% speed (Estimated- 527um depth based on desire to have the working fluid channel deeper than the vector engraving channel.)
- Blue Vector Engraving- 20% power (Desired- 127um depth based on the depth of the channels of the pump group)
- White Vector Engraving- 10% power (Estimated- 57um depth. Based on desire to have these channels much shallower than the analytic fluid and the working fluid channels to keep the fluid from flowing into those channels)

### Photos



## Pump 2.14

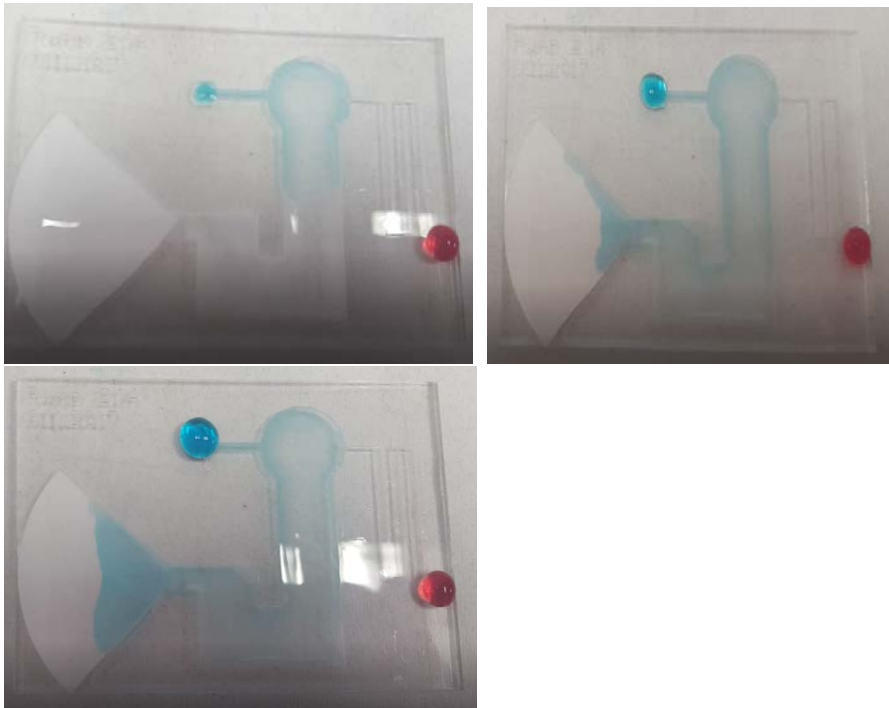
### AutoCAD File



### Settings

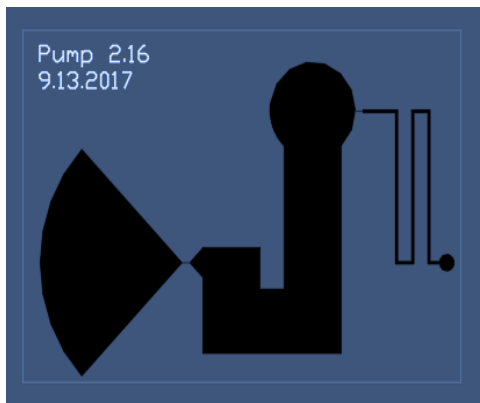
- Raster- 40% speed (Estimated- 527um depth based on desire to have the working fluid channel deeper than the vector engraving channel.)
- Blue Vector Engraving- 20% power (Desired- 127um depth based on the depth of the channels of the pump group)
- White Vector Engraving- 10% power (Estimated- 57um depth. Based on desire to have these channels much shallower than the analytic fluid and the working fluid channels to keep the fluid from flowing into those channels)

### Photos



## Pump 2.16

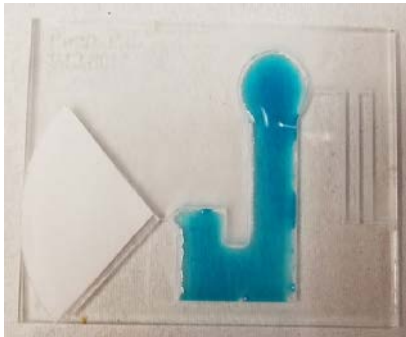
### AutoCAD File



### Settings

- Raster- 40% speed (Estimated- 527um depth based on desire to have the working fluid channel deeper than the vector engraving channel.)
- Blue Vector Engraving- 20% power (Desired- 127um depth based on the depth of the channels of the pump group)
- White Vector Engraving- 10% power (Estimated- 57um depth. Based on desire to have these channels much shallower than the analytic fluid and the working fluid channels to keep the fluid from flowing into those channels)

### Photos



## Pump 2.17

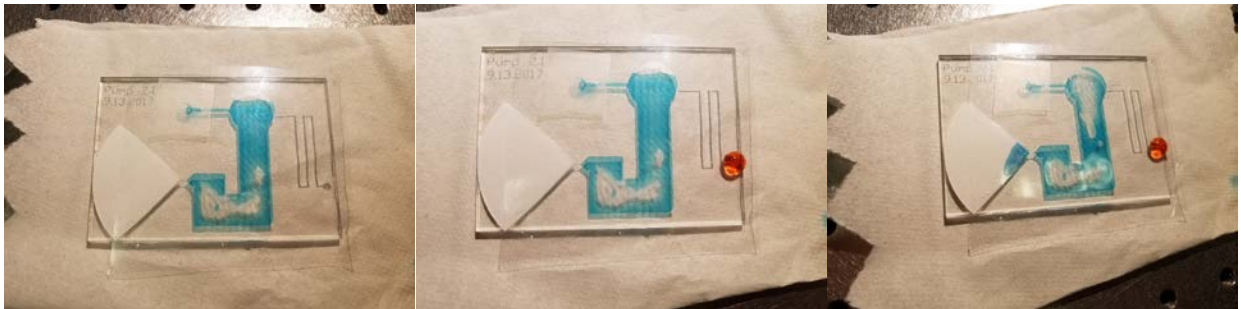
### AutoCAD File



### Settings

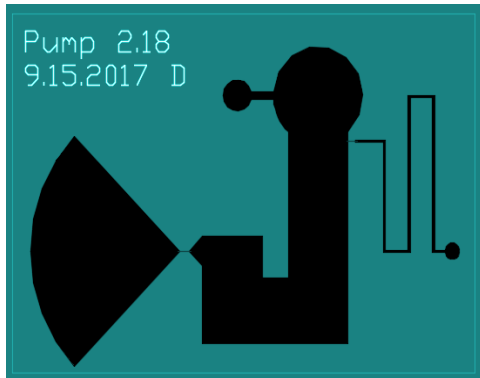
- Raster- 40% speed (Estimated- 527um depth based on desire to have the working fluid channel deeper than the vector engraving channel.)
- Blue Vector Engraving- 20% power (Desired- 127um depth based on the depth of the channels of the pump group)
- White Vector Engraving- 10% power (Estimated- 57um depth. Based on desire to have these channels much shallower than the analytic fluid and the working fluid channels to keep the fluid from flowing into those channels)

### Photos



## Pump 2.18

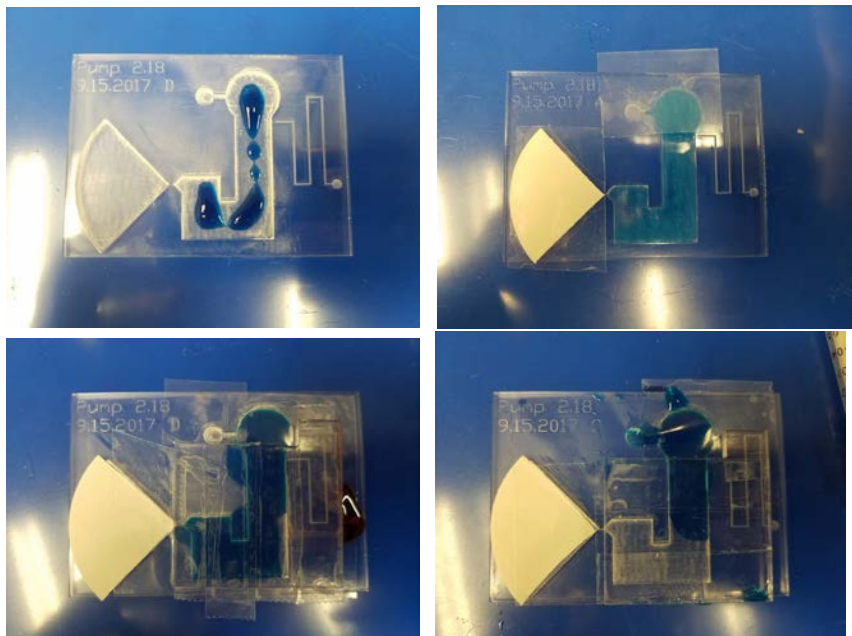
### AutoCAD File



### Settings

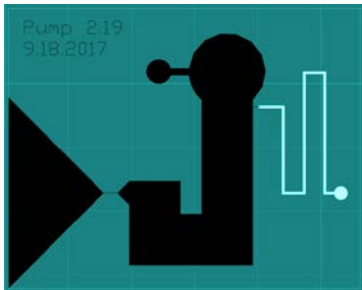
- Raster (Analytic fluid)- 40% power (Estimated- 75.155 um depth based on desire to have the analytic fluid channel to be the same depth and parameters as the droplets team)
- Raster (Working fluid)- 40% speed (Estimated- 527um depth based on desire to have the working fluid channel deeper than the vector engraving channel)
- Blue Vector Engraving- 20% power (Desired- 127um depth based on the depth of the channels of the pump group)

### Photos



## Pump 2.19

### AutoCAD File

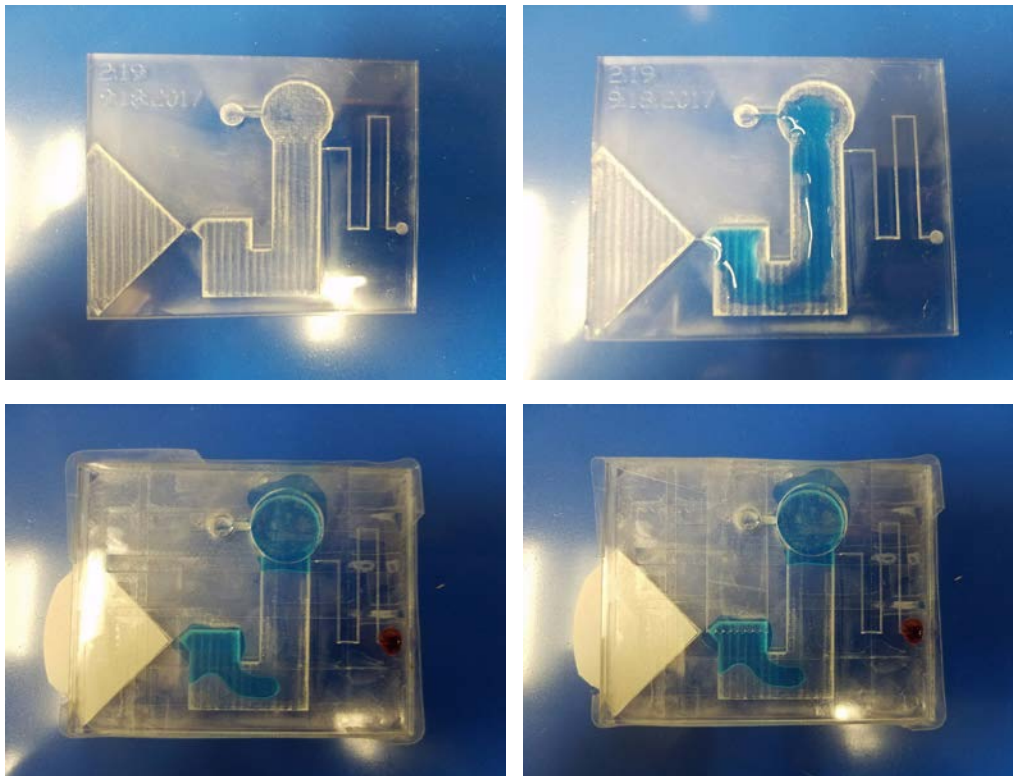


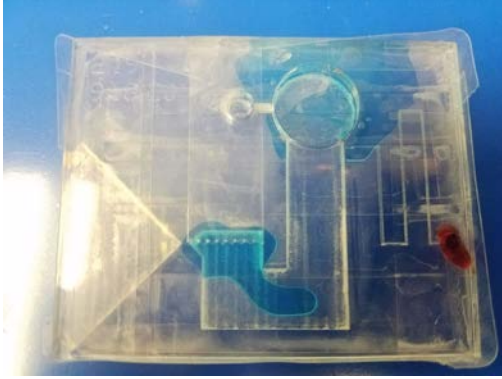
### Settings

- Raster (Analytic fluid)- 40% power (Estimated- 75.155 um depth based on desire to have the analytic fluid channel to be the same depth and parameters as the droplets team)
- Raster (Working fluid)- 40% speed (Estimated- 527um depth based on desire to have the working fluid channel deeper than the vector engraving channel)
- Blue Vector Engraving- 20% power (Desired- 127um depth based on the depth of the channels of the pump group)

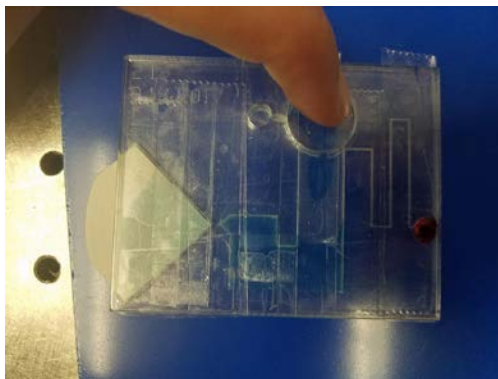
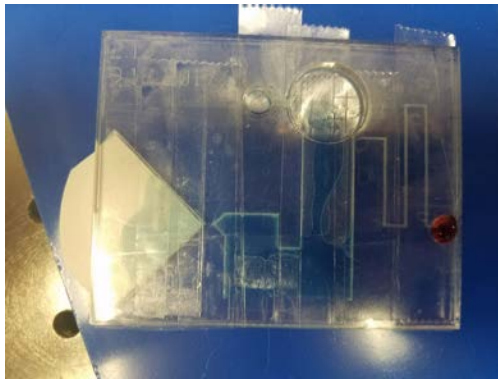
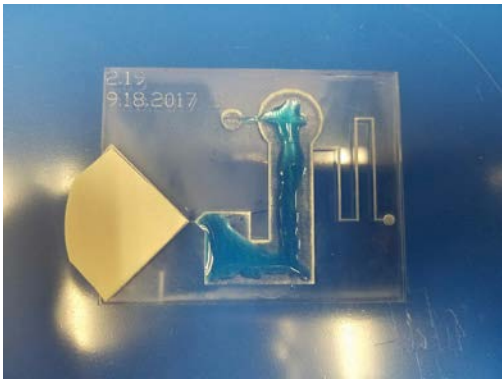
### Photos

Iteration 1:





Iteration 2:



## Pump 2.20

### AutoCAD File

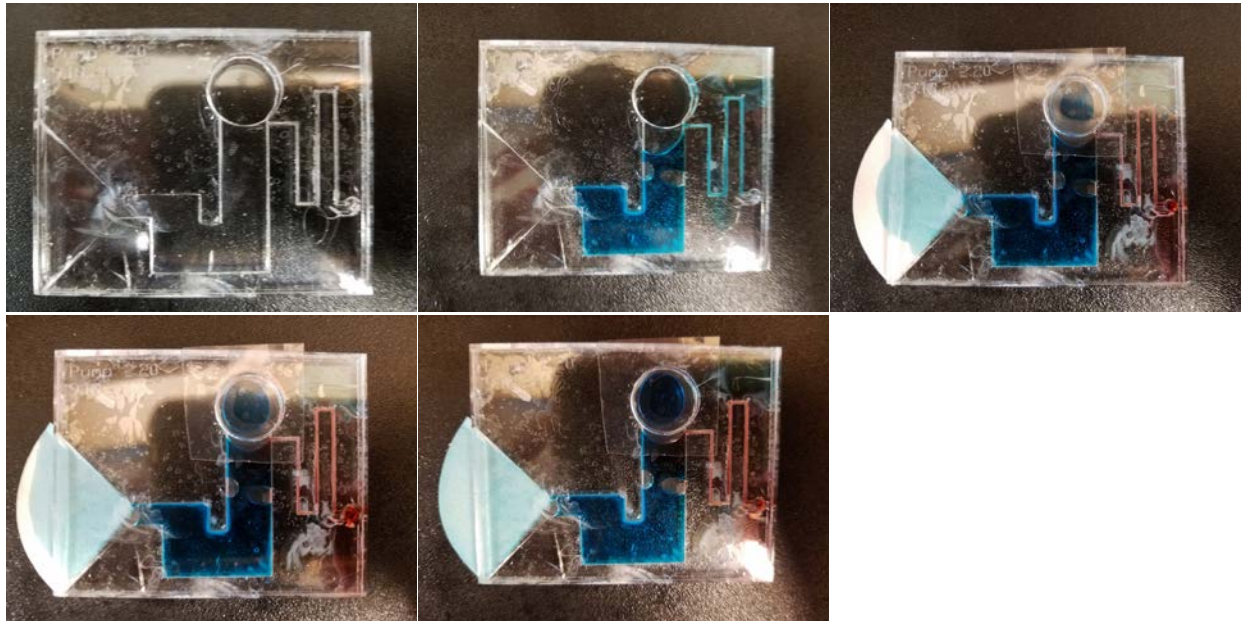


### Settings

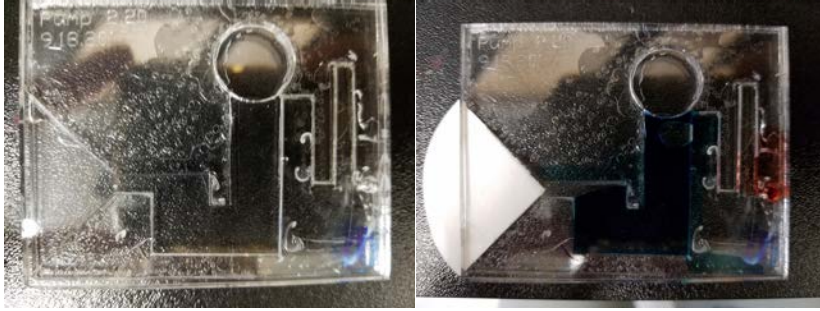
- Raster (Analytic fluid)- 40% power (Estimated- 75.155 um depth based on desire to have the analytic fluid channel to be the same depth and parameters as the droplets team)
- Raster (Working fluid)- 40% speed (Estimated- 527um depth based on desire to have the working fluid channel deeper than the vector engraving channel)
- Blue Vector Engraving- 20% power (Desired- 127um depth based on the depth of the channels of the pump group)

### Photos

Iteration 1:

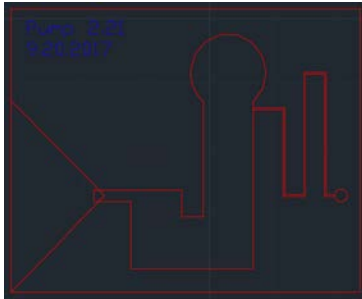


Iteration 2:



## Pump 2.21

### AutoCAD File



### Settings

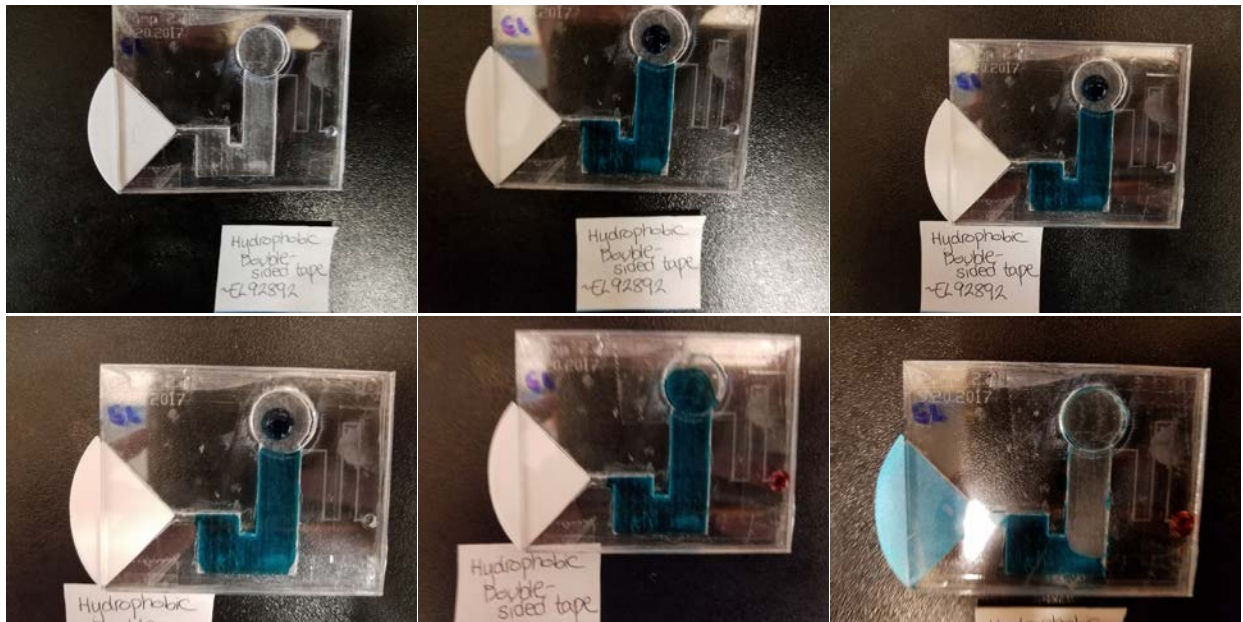
- Raster (Analytic fluid)- 40% power (Estimated- 75.155 um depth based on desire to have the analytic fluid channel to be the same depth and parameters as the droplets team)
- Raster (Working fluid)- 40% speed (Estimated- 527um depth based on desire to have the working fluid channel deeper than the vector engraving channel)
- Blue Vector Engraving- 20% power (Desired- 127um depth based on the depth of the channels of the pump group)

### Photos

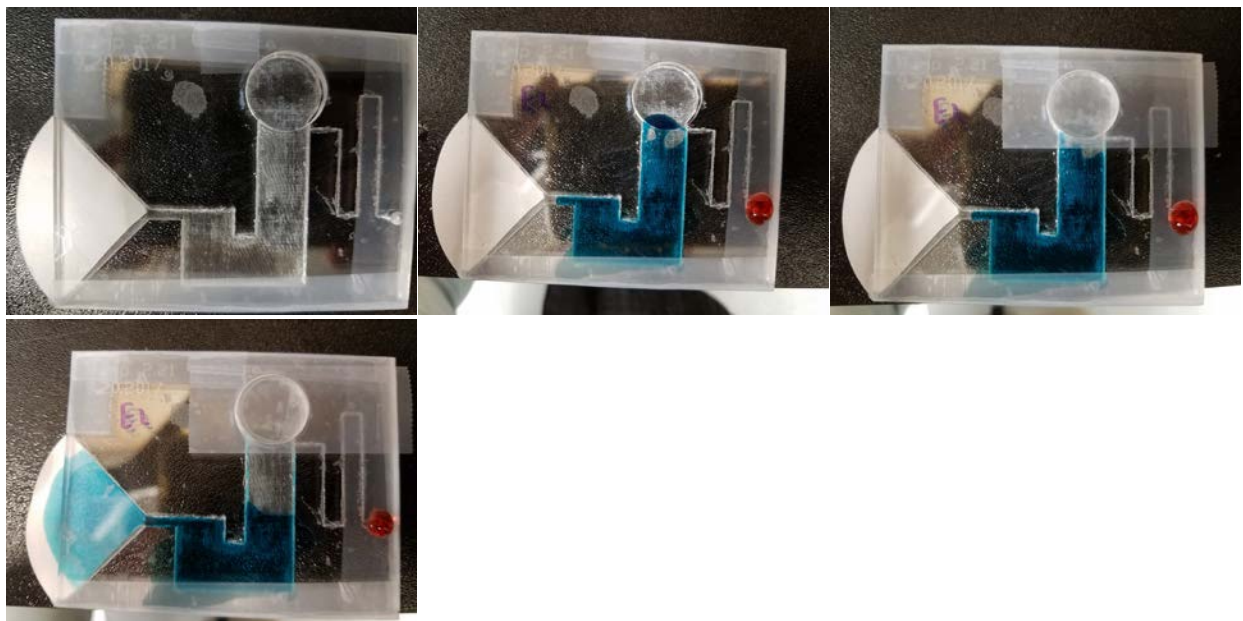
#### Iteration 1:



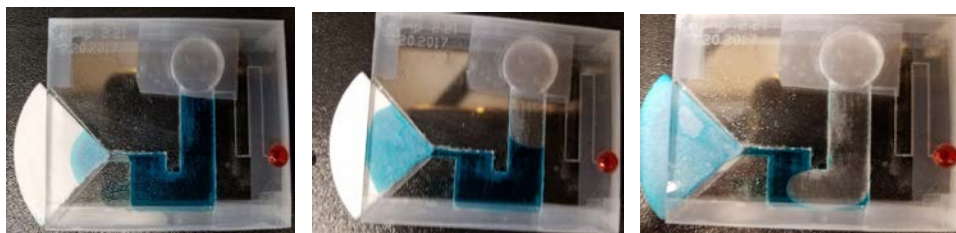
Iteration 2:



Iteration 3:



Iteration 4:

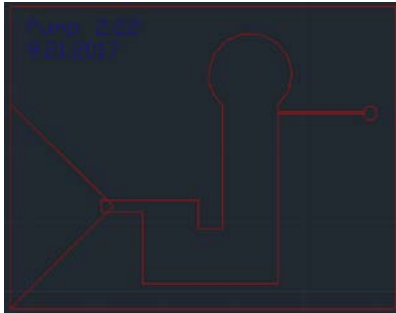


Iteration 5:



## Pump 2.22

### AutoCAD File

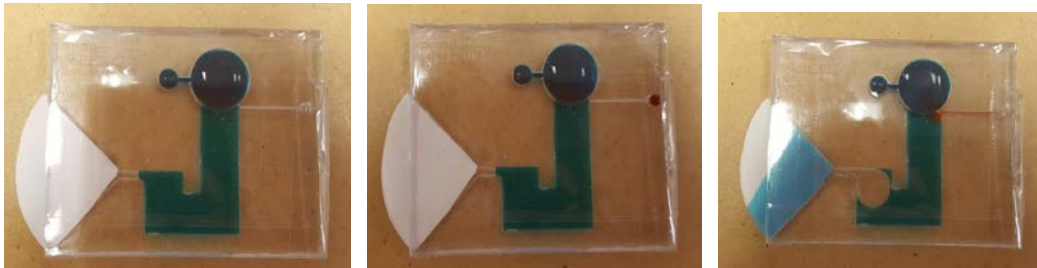


### Settings

- Raster (Analytic fluid)- 40% power (Estimated- 75.155 um depth based on desire to have the analytic fluid channel to be the same depth and parameters as the droplets team)
- Raster (Working fluid)- 40% speed (Estimated- 527um depth based on desire to have the working fluid channel deeper than the vector engraving channel)
- Blue Vector Engraving- 20% power (Desired- 127um depth based on the depth of the channels of the pump group)

### Photos

Iteration 1:

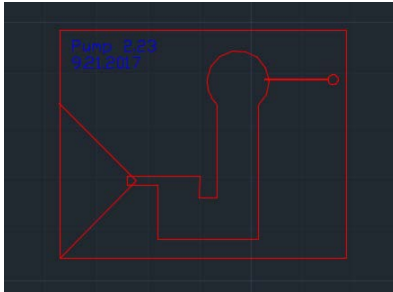


Iteration 2:



## Pump 2.23

### AutoCAD File

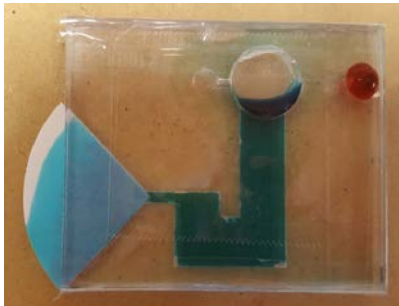


### Settings

- Raster (Analytic fluid)- 40% power (Estimated- 75.155 um depth based on desire to have the analytic fluid channel to be the same depth and parameters as the droplets team)
- Raster (Working fluid)- 40% speed (Estimated- 527um depth based on desire to have the working fluid channel deeper than the vector engraving channel)
- Blue Vector Engraving- 20% power (Desired- 127um depth based on the depth of the channels of the pump group)

### Photos

#### Iteration 1



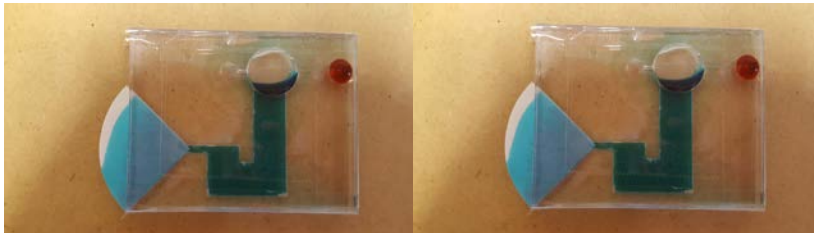
#### Iteration 2:



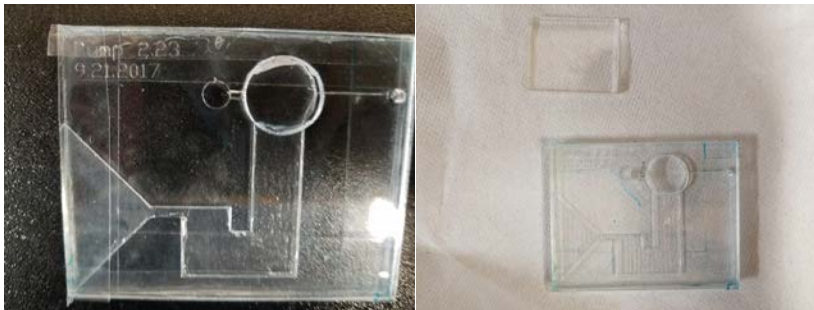
Iteration 3:



Iteration 4:

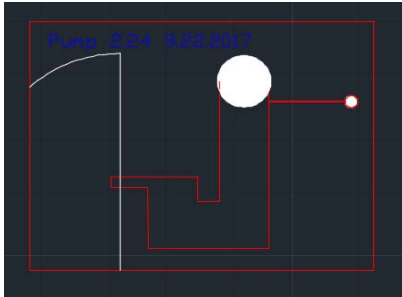


Iteration 5:



## Pump 2.24

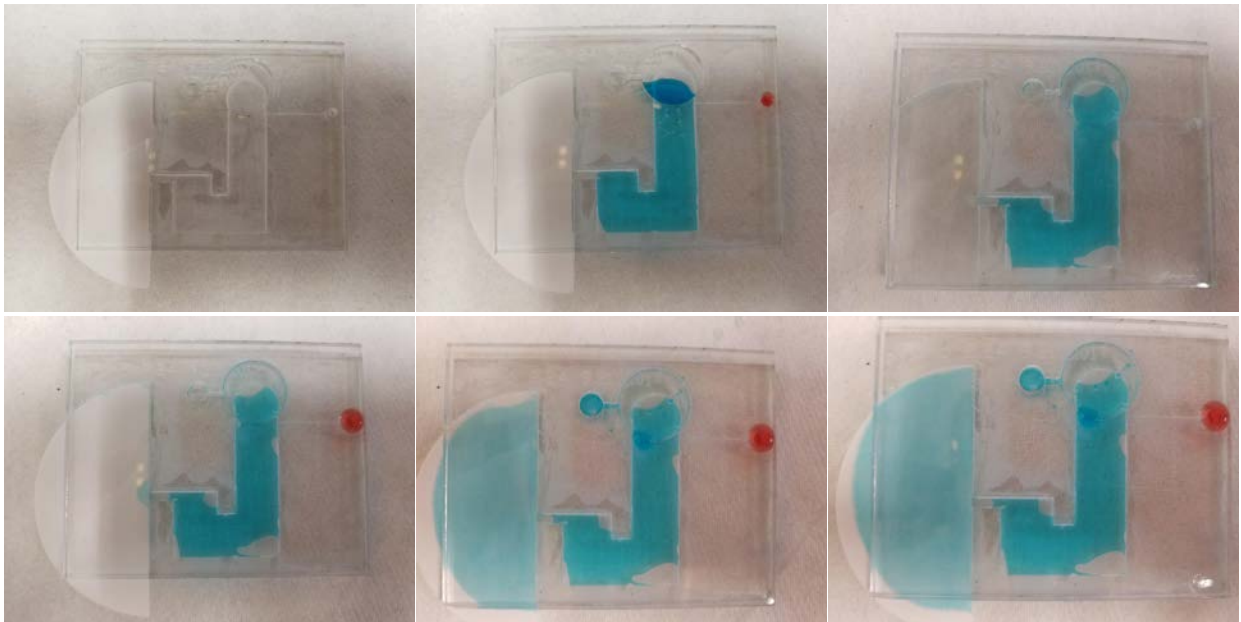
### AutoCAD File



### Settings

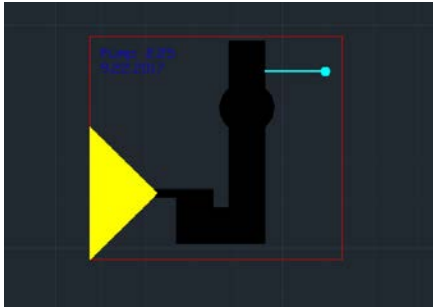
- Raster (Analytic fluid)- 40% power (Estimated- 75.155 um depth based on desire to have the analytic fluid channel to be the same depth and parameters as the droplets team)
- Raster (Working fluid channel)- 40% speed (Estimated- 527um depth based on desire to have the working fluid channel deeper than the vector engraving channel)
- Blue Vector Engraving- 20% power

### Photos



## Pump 2.25

### AutoCAD File

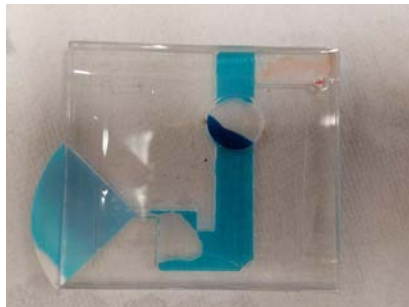


### Settings

- Raster (Analytic fluid)- 40% power (Estimated- 75.155 um depth based on desire to have the analytic fluid channel to be the same depth and parameters as the droplets team)
- Raster (Working fluid channel)- 40% speed (Estimated- 527um depth based on desire to have the working fluid channel deeper than the vector engraving channel)
- Raster (paper chip location)- 30% speed
- Blue Vector Engraving- 20% power

### Photos

Iteration 1:



Iteration 2:

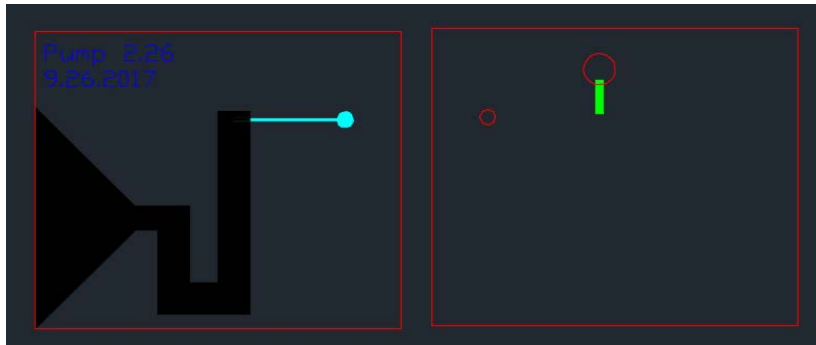


Iteration 3:



## Pump 2.26

### AutoCAD File

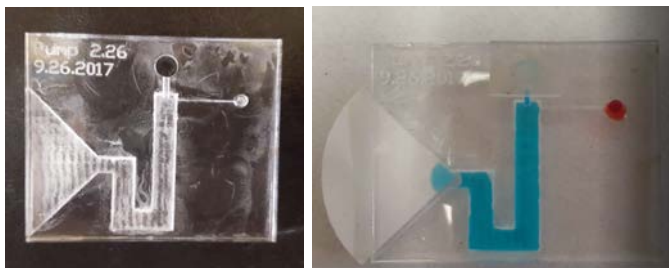


### Settings

- Raster (Analytic fluid)- 40% power (Estimated- 75.155 um depth based on desire to have the analytic fluid channel to be the same depth and parameters as the droplets team)
- Raster (Working fluid channel)- 40% speed (Estimated- 527um depth based on desire to have the working fluid channel deeper than the vector engraving channel)
- Raster (green syringe inlet)- 20%
- Blue Vector Engraving- 20% power
- Replaced finger activation area with syringe input on top chip and reduced width of working fluid channel

### Photos

Iteration 1:

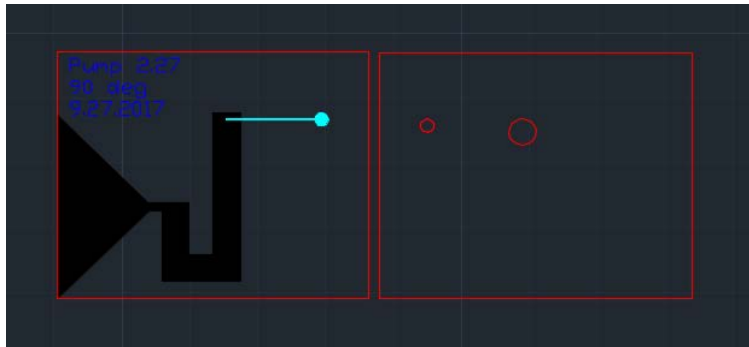


Iteration 2:



## Pump 2.27

### AutoCAD File

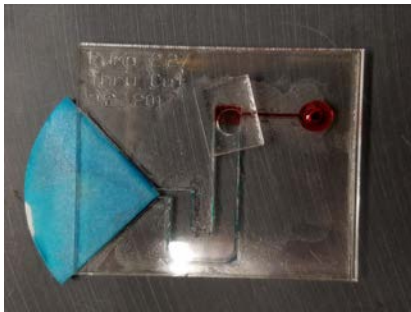


### Settings

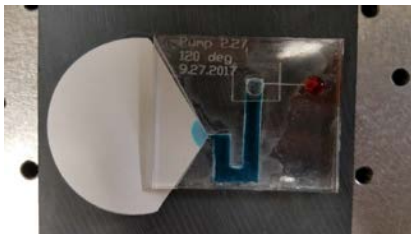
- Raster (Analytic fluid)- 40% power (Estimated- 75.155 um depth based on desire to have the analytic fluid channel to be the same depth and parameters as the droplets team)
- Raster (Working fluid channel)- 40% speed (Estimated- 527um depth based on desire to have the working fluid channel deeper than the vector engraving channel)
- Raster (green syringe inlet)- 20%
- Blue Vector Engraving- 20% power

### Photos

#### Small Acrylic Chip



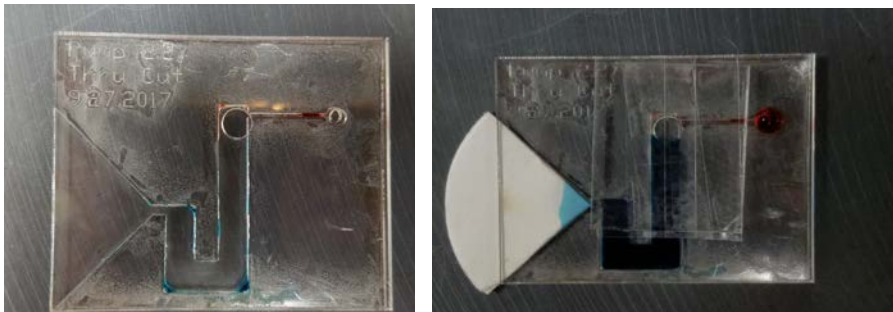
#### 120 Degree Filter Paper



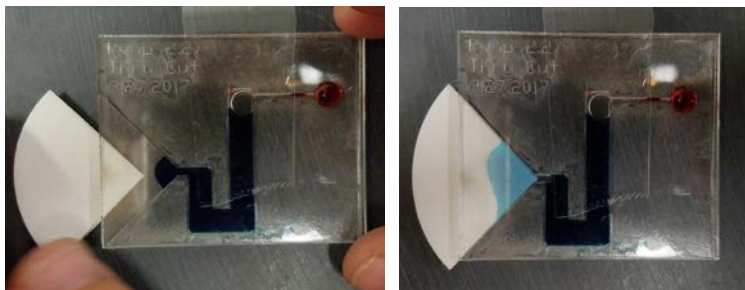
Large Acrylic Cover



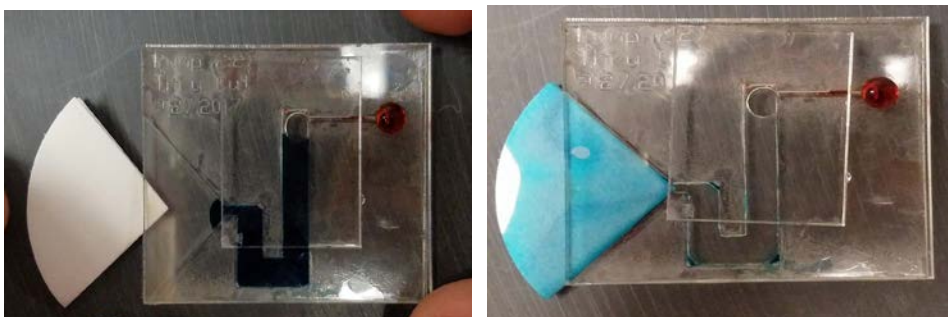
Large Acrylic and Double Stick Tape



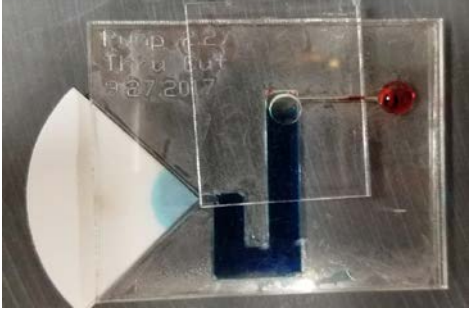
Packing Tape



Water and Large Acrylic Chip

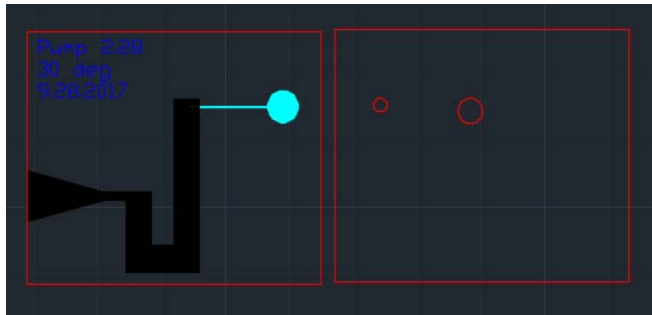


Soap and Large Acrylic Chip



## Pump 2.28

### AutoCAD File



### Settings

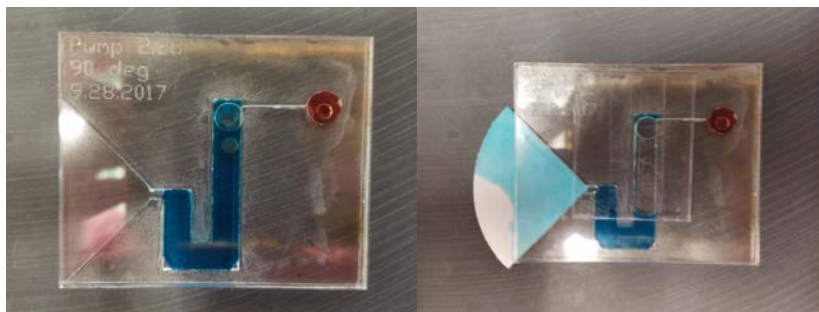
- Raster (Analytic fluid)- 40% power (Estimated- 75.155 um depth based on desire to have the analytic fluid channel to be the same depth and parameters as the droplets team)
- Raster (Working fluid channel)- 40% speed (Estimated- 527um depth based on desire to have the working fluid channel deeper than the vector engraving channel)
- Raster (green syringe inlet)- 20%
- Blue Vector Engraving- 20% power

### Photos

#### Iteration 1



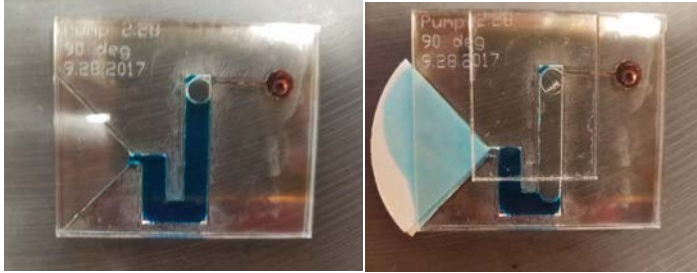
#### Iteration 2



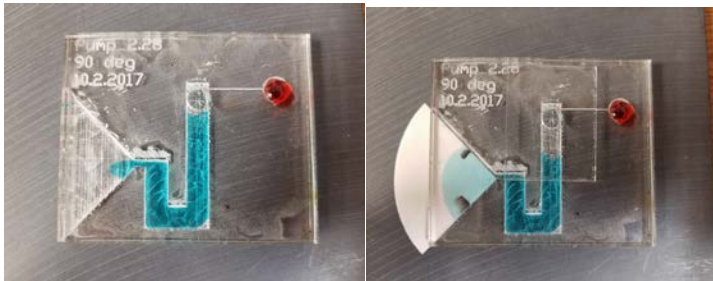
#### Iteration 3



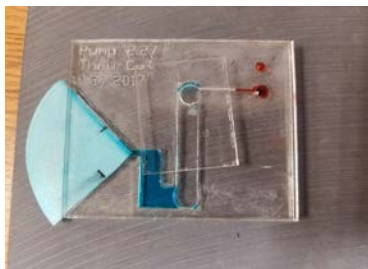
Iteration 4



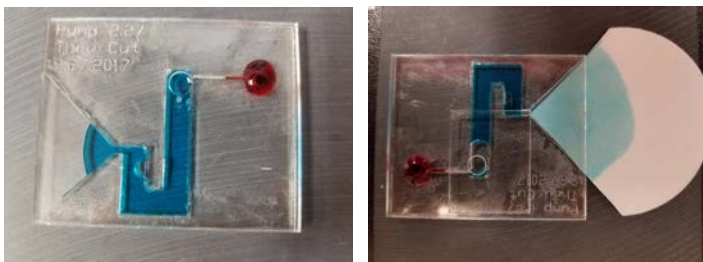
Iteration 5



Iteration 6

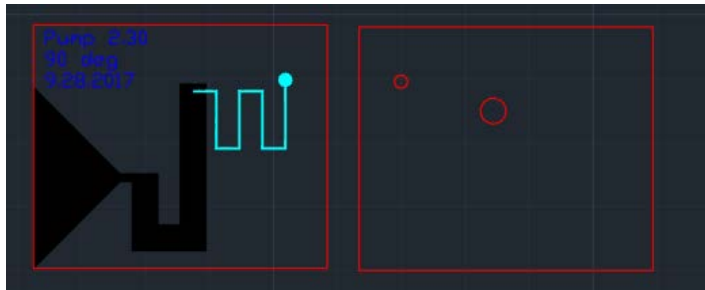


Iteration 7



## Pump 2.30

### AutoCAD File

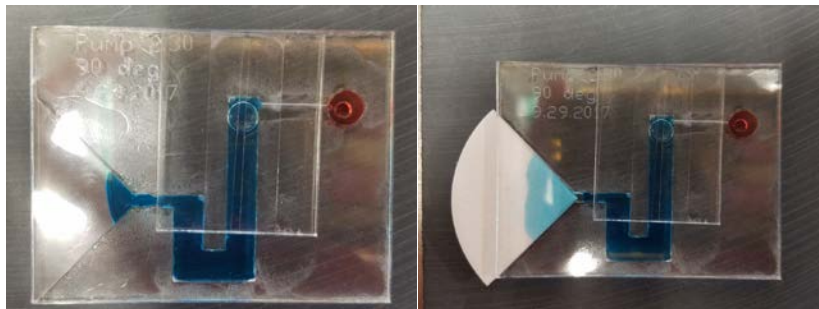


### Settings

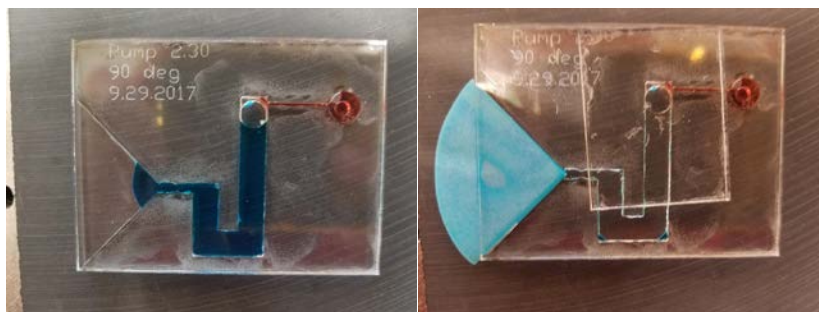
- Raster (Analytic fluid)- 40% power (Estimated- 75.155 um depth based on desire to have the analytic fluid channel to be the same depth and parameters as the droplets team)
- Raster (Working fluid channel)- 40% speed (Estimated- 527um depth based on desire to have the working fluid channel deeper than the vector engraving channel)
- Raster (green syringe inlet)- 20%
- Blue Vector Engraving- 20% power

### Photos

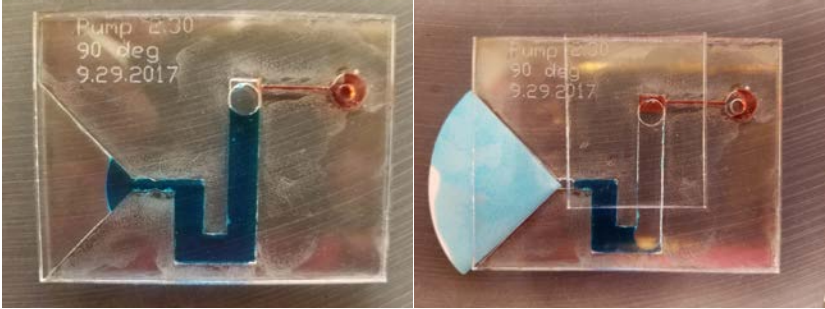
#### Iteration 1



#### Iteration 2



Iteration 3



# ARcare® 92892

## Silicone Transfer Film

### Product Information



#### **PRODUCT DESCRIPTION**

ARcare® 92892 is a 2 mil silicone pressure-sensitive adhesive coated between two fluorosilicone release liners. The product can be coated to optical grade quality.

#### **FEATURES**

- High chemical and thermoxidative resistance
- Optical grade haze, clarity and transmission
- Non-yellowing
- Stable liner release under various conditions
- Broad adhesion properties suitable for use on high surface energy substrates such as glass or metal, as well as non-polar plastic substrates

#### **BENEFITS**

- Optical quality silicone pressure-sensitive adhesive
- Stable liner release over time under various conditions

#### **PRODUCT APPLICATIONS**

Suggested for use in high temperature, high humidity applications and applications that involve chemical exposure. ARcare® 92892 has low haze, high clarity and high transmission to facilitate use in display and other optical applications. Users should assure the product meets the specific needs of their application(s). Adhesives Research can tailor the product to meet the needs of specific applications as requested by customers.

#### **PRODUCT PROFILE AND DIAGRAM**

Liner: 2 mil PET liner  
 Adhesive: 2 mil SR-29 SiPSA  
 Liner: 2 mil PET liner



#### **ADHESIVE PERFORMANCE PROPERTIES – Typical Values\***

1 hour 180° Peel to Glass:	68 oz/in
Static Shear (1000 g, 25°C):	>1300 minutes
Transmission <sup>1</sup> :	99%
Haze <sup>1</sup> :	0.28
Clarity <sup>1</sup> :	98.9
Easy Release (300 ipm):	40 g/2 in
Tight Release (300 ipm):	100 g/2 in
Refractive Index:	1.41

Test Notes: <sup>1</sup>Byk Gardner Haze-Gard Plus

\*All stated values are nominal and should only be used as a guide for selection. They are not specifications.

#### **STORAGE AND SHELF LIFE**

Unconverted product should be stored at 70°F ± 20°F (21°C ± 11°C) and 50% ± 20% relative humidity, out of direct sunlight. The shelf life of the product is not to exceed one year from date of manufacture.

# ARcare® 92734

Moisture Barrier Pressure-Sensitive Transfer Film



## PRODUCT DESCRIPTION

ARcare® 92734 is an optically clear moisture barrier pressure-sensitive adhesive (PSA). It is a hydrophobic adhesive with excellent thermoxidative and UV stability. It is supplied as an unsupported transfer film between release liners.

## FEATURES AND BENEFITS

- 1 mil optically clear transfer film
- good moisture barrier properties, low equilibrium moisture uptake
- high optical transmission, high clarity, low haze, non-yellowing
- high thermoxidative stability and chemical resistance

## PRODUCT APPLICATIONS

Suggested as a moisture barrier adhesive for use in various electronics and optical device applications. It is suitable for use in combination with high barrier films such as inorganically coated plastics. It exhibits good adhesion to a variety of substrates. The adhesive is uncrosslinked, and as such is not recommended for high shear and high temperature applications. Users should assure the product meets the specific needs of their application(s). Adhesives Research can tailor the product to meet the needs of specific applications as requested by customers.

## PRODUCT PROFILE AND DIAGRAM – Typical Values\*

COMPONENT	THICKNESS
Clear PET Easy Release Liner:	2 mils
Barrier PSA:	1 mil
Clear PET Tight Release Liner	2 mils



## ADHESIVE AND PHYSICAL PROPERTIES – Typical Values\*

TEST	TYPICAL VALUE	
<b>180° peel</b> to stainless steel after 1h dwell Ref. Test Method: ART 1005 12" per min. after corresponding dwell time 304 Stainless Steel panel	<u>Peel Force</u> 45 oz./inch	<u>Failure Mode</u> No Transfer
<b>180° peel</b> to glass after 1h dwell Ref. Test Method: ART 1005 12" per min. after corresponding dwell time Sodalime Glass panel	<u>Peel Force</u> 60 oz./inch	<u>Failure Mode</u> No Transfer
<b>500g static shear</b> to stainless steel Ref. Test Method: ART 1011, PSTC -107 500 g weight, room temperature 304 Stainless Steel panel	<u>Time</u> 50 min.	<u>Failure Mode</u> Split Transfer (cohesive)
<b>Transmission:</b> 99.8% <b>Clarity:</b> 87.5% <b>Haze:</b> 0.04% Byk-Garnder haze gard plus		
<b>Moisture Permeability</b> (Mocon PERMATRAN-W Model 3/33, 100% RH, 25°C)	2.2 g-mil/m <sup>2</sup> -day	

\*All stated values are nominal and should only be used as a guide for selection. They are not specifications.

## Appendix F: Gravity Pump Chip Assembly

1. Laser cut an acrylic chip with desired channel design
2. Use hydrophobic tape to create the fourth wall of the microfluidic channels on an acrylic chip; firmly push the tape down to remove any air and ensure a firm seal
3. Punch a hole the size of the outer diameter of the fluid tubing of the in a medicine cup or similar fluid reservoir
4. Insert tube partially into the medicine cup and use UV hardened glue to seal the junction of the tube and medicine cup
5. Rest the medicine cup on an adjustable stand and lower the tube into the microfluidic chip until the tube is below the top surface of the chip, but not touching the bottom surface
6. Use UV hardened glue to seal the connection of the tube and acrylic chip



*Figure 1: Step 4*

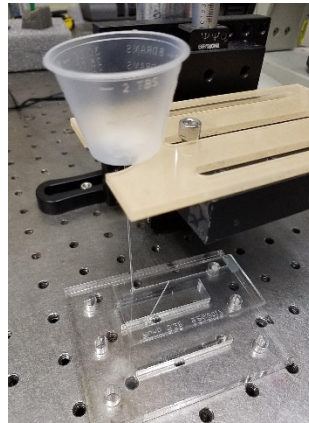


*Figure 2: Step 5*

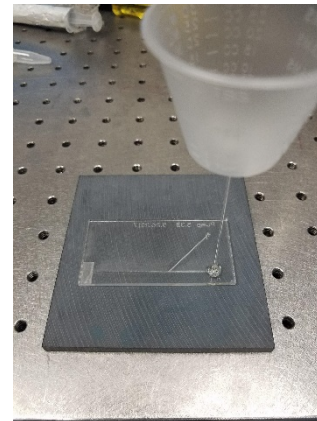


*Figure 3: Fully Assembled Gravity Pump*

## Appendix G: Gravity Pump Calculations

This MathCad file was used to calculate what the required height of a tube would give to achieve a desired flow rate. Please note that some of these numbers will not match exactly what was put in the paper because for each calculation, this same file was used and this appendix only includes the master file, not the files for each various iteration.

### Constant Parameters

1. Diameter of the tube:

$$D_t := 5 \times 10^{-3} \quad \text{m}$$

2. Cross-sectional area of the tube:

$$A_t := \frac{\pi \cdot (D_t)^2}{4} = 1.963 \times 10^{-5} \quad \text{m}^2$$

2. Channel parameters (for channel rastered at 40% speed)

$$h := 127 \times 10^{-6} \quad \text{m}$$

$$w := 350 \cdot 10^{-6} \quad \text{m}$$

3. Cross-sectional area of the channel:

$$A_c := h \cdot w = 4.445 \times 10^{-8} \quad \text{m}^2$$

4. Hydraulic Diameter of the channel:

$$D_H := \frac{4A_c}{2 \cdot (h + w)} = 1.864 \times 10^{-4} \quad \text{m}$$

5. Length of channel:

$$L_{23} := 0.025 \quad \text{m}$$

# Olive Oil Parameters

For Olive Oil,

1. Density

$$\rho_{\text{olive}} := 860 \frac{\text{kg}}{\text{m}^3}$$

2. Dynamic Viscosity

$$\mu_{\text{olive}} := 84 \cdot 10^{-3}$$

2. Kinematic Viscosity

$$\nu_{\text{olive}} := \frac{\mu_{\text{olive}}}{\rho_{\text{olive}}} = 9.767 \times 10^{-5} \frac{\text{m}^2}{\text{s}}$$

3. Flow rate:

$$Q_{\text{olive}} := 2.722 \cdot 10^{-10} \frac{\text{m}^3}{\text{s}}$$

In the vertical tubing:

4. Velocity

$$V_{\text{oil,t}} := \frac{Q_{\text{oil}}}{A_t} = 6.112 \times 10^{-6} \frac{\text{m}}{\text{s}}$$

5. Reynold's Number

$$Re_{\text{oil,t}} := V_{\text{oil,t}} \cdot \frac{D_t}{\nu_{\text{oil}}} = 7.074 \times 10^{-4}$$

In the channel:

6. Velocity

$$V_{\text{oil,c}} := \frac{Q_{\text{oil}}}{A_c} = 2.7 \times 10^{-3} \frac{\text{m}}{\text{s}}$$

7. Reynold's Number

$$Re_{\text{oil,c}} := \frac{V_{\text{oil,c}} \cdot D_H}{\nu_{\text{oil}}} = 0.012$$

Solve for required height of tube:

$$\left[ \rho_{\text{oil}} \cdot 9.81 \cdot (-z_{\text{oil}}) + \left( \frac{64}{Re_{\text{oil,t}}} \right) \cdot \left( \frac{z_{\text{oil}}}{D_t} \right) \cdot \left( \frac{\rho_{\text{oil}} \cdot V_{\text{oil,t}}^2}{2} \right) + \left( \frac{64}{Re_{\text{oil,c}}} \right) \cdot \left( \frac{L_{23}}{D_H} \right) \cdot \left( \frac{\rho_{\text{oil}} \cdot V_{\text{oil,c}}^2}{2} \right) \right] \rightarrow -9122.9857118395436242739 \cdot z_{\text{oil}} + 2498.04006318180000718$$

$$z_{\text{oil}} := \frac{5076.0174}{9122.9857} = 0.556 \text{ m} \quad (\text{This is when we had the channel at } 0.05\text{m})$$

$$z_{\text{oil,2}} := \frac{999.216}{9122.9857} = 0.11 \text{ m} \quad (\text{This is when we shortened the channel to } 0.01\text{m})$$

$$z_{\text{oil,3}} := \frac{2498.04}{9122.9857} = 0.274 \text{ m} \quad (\text{This is when we shortened the channel to } 0.025\text{m})$$

## Water Parameters

For water,

1. Density

$$\rho_w := 1000 \frac{\text{kg}}{\text{m}^3}$$

2. Kinematic Viscosity

$$\nu_w := 0.902 \cdot 10^{-6} \frac{\text{m}^2}{\text{s}}$$

3. Flow rate:

$$Q_w := 4.167 \cdot 10^{-11} \frac{\text{m}^3}{\text{s}}$$

In the vertical tubing:

4. Velocity

$$V_{w,t} := \frac{Q_w}{A_t} = 2.122 \times 10^{-6} \frac{\text{m}}{\text{s}}$$

5. Reynold's Number

$$Re_{w,t} := V_{w,t} \cdot \frac{D_t}{\nu_w} = 0.012$$

In the channel:

6. Velocity

$$V_{w,c} := \frac{Q_w}{A_c} = 9.375 \times 10^{-4} \frac{\text{m}}{\text{s}}$$

7. Reynold's Number

$$Re_{w,c} := \frac{V_{w,c} \cdot D_H}{\nu_w} = 0.194$$

Solve for required height of tube:

$$\left[ \rho_w \cdot 9.81 \cdot (-z_w) + \left( \frac{64}{Re_{w,t}} \right) \cdot \left( \frac{z_w}{D_t} \right) \cdot \left( \frac{\rho_w \cdot V_{w,t}^2}{2} \right) + \left( \frac{64}{Re_{w,c}} \right) \cdot \left( \frac{L_{23}}{D_H} \right) \cdot \left( \frac{\rho_w \cdot V_{w,c}^2}{2} \right) \right] \text{solve, } z_w \rightarrow 0.0019852380793594620333 \text{ m}$$

## Appendix H: Theoretical vs. Analytic Flow Rates for Olive Oil

This appendix has the set up for the calculations to obtain our theoretical flow rate of olive oil in our gravity driven pumps with our new diameters. This appendix only includes the calculations for the tube with an inner diameter of 1.2mm but the method would be the same for the other tubes of 2.7mm and 3mm as well.

### Constant Parameters

2. Channel parameters (for channel rastered at 40% power)

$$h := 127 \times 10^{-6} \quad \text{m}$$

$$w := 350 \cdot 10^{-6} \quad \text{m}$$

3. Cross-sectional area of the channel:

$$A_c := h \cdot w = 4.445 \times 10^{-8} \quad \text{m}^2$$

4. Hydraulic Diameter of the channel:

$$D_H := \frac{4A_c}{2 \cdot (h + w)} = 1.864 \times 10^{-4} \quad \text{m}$$

5. Length of channel:

$$L_{23} := 0.06 \quad \text{m}$$

For Olive Oil,

1. Density

$$\rho_{\text{olive}} := 860 \quad \frac{\text{kg}}{\text{m}^3}$$

2. Kinematic Viscosity

$$\nu_{\text{olive}} := \frac{84 \cdot 10^{-3}}{\rho_{\text{olive}}} = 9.767 \times 10^{-5} \quad \frac{\text{m}^2}{\text{s}}$$

### Olive Oil Test 1 Parameters

1. Diameter of the tube:

$$D_{t1} := 1.2 \cdot 10^{-3} \quad \text{m}$$

2. Cross-sectional area of the tube:

$$A_{t1} := \frac{\pi \cdot (D_{t1})^2}{4} = 1.131 \times 10^{-6} \quad \text{m}^2$$

3. Height of liquid

$$z_{\text{olive}} := .3048 \text{ m}$$

**Calculate the theoretical flow rate from these parameters**

$$\left[ \rho_{\text{olive}} \cdot 9.81 \cdot z_{\text{olive}} + \frac{64 \cdot \nu_{\text{olive}} \cdot z_{\text{olive}} \cdot \rho_{\text{olive}} \cdot Q_{\text{olive1}}}{(2D_{\text{tl}})^2 \cdot A_{\text{tl}}} \right] + \frac{64 \cdot \nu_{\text{olive}} \cdot L_{23} \cdot \rho_{\text{olive}} \cdot Q_{\text{olive1}}}{(2D_{\text{H}})^2 \cdot A_{\text{c}}} \text{ solve, } Q_{\text{olive1}}$$

$$Q_{\text{olive1}} := 4.900 \cdot 10^{-11} \quad \frac{\text{m}^3}{\text{s}}$$

$$Q_{\text{olive.12}} := Q_{\text{olive1}} \cdot 10^9 \cdot 60 = 2.94 \quad \frac{\mu\text{L}}{\text{min}}$$

$$V_{\text{olive.th}} := \frac{Q_{\text{olive1}}}{A_{\text{c}}} = 1.102 \times 10^{-3} \quad \frac{\text{m}}{\text{s}}$$

$$V_{\text{olive.th1}} := V_{\text{olive.th}} \cdot 10^3 = 1.102$$

## Appendix I: Gravity Pump Pressure Equalization Calculations

The calculations in this appendix were used to calculate the necessary height of the water tube in the gravity pump to ensure equal pressure at the junction between the olive oil and the water.

### Constant Parameters

1. Channel parameters (for channel rastered at 40% power)

$$h := 127 \times 10^{-6} \quad \text{m}$$

$$w := 350 \cdot 10^{-6} \quad \text{m}$$

2. Cross-sectional area of the channel:

$$A_c := h \cdot w = 4.445 \times 10^{-8} \quad \text{m}^2$$

3. Hydraulic Diameter of the channel:

$$D_H := \frac{4A_c}{2 \cdot (h + w)} = 1.864 \times 10^{-4} \quad \text{m}$$

### Constant Olive Oil Parameters

1. Diameter of the tube:

$$D_{to} := 3 \times 10^{-3} \quad \text{m}$$

2. Cross-sectional area of the tube:

$$A_{to} := \frac{\pi \cdot (D_{to})^2}{4} = 7.069 \times 10^{-6} \quad \text{m}^2$$

3. Length of channel before junction:

$$L_o := 18.6 \cdot 10^{-3} \quad \text{m}$$

## Olive Oil Properties

### 1. Density

$$\rho_{\text{olive}} := 860 \frac{\text{kg}}{\text{m}^3}$$

### 2. Dynamic Viscosity

$$\mu_{\text{olive}} := 84 \cdot 10^{-3}$$

### 3. Kinematic Viscosity

$$\nu_{\text{olive}} := \frac{\mu_{\text{olive}}}{\rho_{\text{olive}}} = 9.767 \times 10^{-5} \frac{\text{m}^2}{\text{s}}$$

### 4. Oil Height

$$z_o := 0.2064 \text{ m}$$

### 5. Olive Oil Speed in channel

$$V_{\text{oc}} := 9 \cdot 10^{-4} \frac{\text{m}}{\text{s}}$$

### 6. Olive Oil Flow Rate

$$Q_{\text{oc}} := V_{\text{oc}} \cdot A_c = 4.001 \times 10^{-11} \frac{\text{m}^3}{\text{s}}$$

$$Q_{\text{oc}2} := Q_{\text{oc}} \cdot 60 \cdot 10^9 = 2.4 \frac{\mu\text{L}}{\text{min}}$$

### 7. Olive Oil Speed in tube

$$V_{\text{ot}} := \frac{Q_{\text{oc}}}{A_{\text{to}}} = 5.66 \times 10^{-6} \frac{\text{m}}{\text{s}}$$

## Reynolds Number

$$\text{Re}_{\text{olive.c}} := \frac{\rho_{\text{olive}} \cdot V_{\text{oc}} \cdot D_H}{\mu_{\text{olive}}} = 1.717 \times 10^{-3}$$

$$\text{Re}_{\text{olive.t}} := \frac{\rho_{\text{olive}} \cdot V_{\text{ot}} \cdot D_{\text{to}}}{\mu_{\text{olive}}} = 1.738 \times 10^{-4}$$

## Pressure Drop in Oil

$$P_{\text{olive}} := \left[ \rho_{\text{olive}} \cdot 9.81 \cdot (z_o) - \left( \frac{64}{\text{Re}_{\text{olive.t}}} \right) \cdot \left( \frac{z_o}{D_{\text{to}}} \right) \cdot \left( \frac{\rho_{\text{olive}} \cdot V_{\text{ot}}^2}{2} \right) \right] - \left( \frac{64}{\text{Re}_{\text{olive.c}}} \right) \cdot \left( \frac{L_o}{D_H} \right) \cdot \left( \frac{\rho_{\text{olive}} \cdot V_{\text{oc}}^2}{2} \right) = 445.523 \text{ Pa}$$

## Constant Water Parameters

1. Diameter of the tube:

$$D_{tw} := 0.5 \times 10^{-3} \text{ m}$$

2. Cross-sectional area of the tube:

$$A_{tw} := \frac{\pi \cdot (D_{tw})^2}{4} = 1.963 \times 10^{-7} \text{ m}^2$$

3. Length of total channel:

$$L_{wt} := 63 \cdot 10^{-3} \text{ m}$$

4. Length of channel before junction

$$L_w := 25.2 \cdot 10^{-3} \text{ m}$$

## Water Properties

1. Density

$$\rho_w := 1000 \frac{\text{kg}}{\text{m}^3}$$

2. Kinematic Viscosity

$$\nu_w := 0.902 \cdot 10^{-6} \frac{\text{m}^2}{\text{s}}$$

3. Velocity of Tube

$$V_{tw}(z_w) := \frac{Q_w(z_w)}{A_{tw}} \frac{\text{m}}{\text{s}}$$

$$\text{Re}_{tw}(z_w) := \frac{Q_w(z_w) \cdot D_{tw}}{A_{tw} \cdot \nu_w}$$

4. Velocity of Channel

$$V_{cw}(z_w) := \frac{Q_w(z_w)}{A_c} \frac{\text{m}}{\text{s}}$$

$$\text{Re}_{cw}(z_w) := \frac{Q_w(z_w) \cdot D_H}{A_c \cdot \nu_w}$$

## Pressure Drop in Water

$$P_w(z_w) := \rho_w \cdot 9.81 \cdot (-z_w) + \left( \frac{64}{\text{Re}_{tw}(z_w)} \right) \cdot \left( \frac{z_w}{D_{tw}} \right) \cdot \left( \frac{\rho_w \cdot V_{tw}(z_w)^2}{2} \right) + \left( \frac{64}{\text{Re}_{cw}(z_w)} \right) \cdot \left( \frac{L_w}{D_H} \right) \cdot \left( \frac{\rho_w \cdot V_{cw}(z_w)^2}{2} \right)$$

$$z_w := (P_w(z_w) - P_{olive}) \text{ solve, } z_w \rightarrow \begin{pmatrix} -0.15209034441477424435 \\ -2.0029583520031810305 \\ 0.59809724574516767252 \end{pmatrix}$$

**Therefore,  $z_w$  is 0.598m**

## Flow Rate as a function of height

$$Q_w(z_w) := \left[ \rho_w \cdot 9.81 \cdot (-z_w) + \left[ \frac{64 \cdot \nu_w \cdot z_w \cdot \rho_w \cdot Q_w}{(2D_{tw})^2 \cdot A_{tw}} \right] + \frac{64 \cdot \nu_w \cdot L_{wt} \cdot \rho_w \cdot Q_w}{(2D_H)^2 \cdot A_c} \right] \text{ solve, } Q_w \rightarrow \frac{9810.0 \cdot z_w}{2.9400628975388591224e11 \cdot z_w + 5.8888235360401305532e11}$$

## Appendix J: Weight Driven Pumps Calculations

This appendix has the MathCAD file we used to calculate the weight that was required to be added to a syringe to produce a specific, desired flow rate. Although this Appendix only includes the oil calculations, the same calculations were performed for water. This file included the new determined friction force and accounts for this friction force by also not counting head loss in the syringe and needle as those were accounted for in the friction force experiment.

### Oil Calculations:

#### Fluid Properties

$$\rho_{\text{olive}} := 860 \frac{\text{kg}}{\text{m}^3}$$

$$\mu_{\text{olive}} := 84 \cdot 10^{-3}$$

$$\nu_{\text{olive}} := \frac{\mu_{\text{olive}}}{\rho_{\text{olive}}} = 9.767 \times 10^{-5} \frac{\text{m}^2}{\text{s}}$$

#### Design Variables:

1. Flow rate:

$$Q_{\text{olive}} := 16.9 \frac{\mu\text{L}}{\text{min}}$$

$$Q_{\text{olive.2}} := Q_{\text{olive}} \cdot \frac{10^{-9}}{60} = 2.817 \times 10^{-10}$$

2. Syringe:

$$D_s := 4.78 \cdot 10^{-3} \text{ m}$$

$$A_s := \frac{\pi \cdot D_s^2}{4} = 1.795 \times 10^{-5}$$

$$L_s := 0.05$$

3. Tube:

$$D_t := 0.5 \cdot 10^{-3} \text{ m}$$

$$A_t := \frac{\pi \cdot D_t^2}{4} = 1.963 \times 10^{-7} \text{ m}^2$$

$$L_t := 0.0508 \text{ m}$$

4. Channel:

$$h := 127 \cdot 10^{-6} \text{ m}$$

$$w := 350 \cdot 10^{-6} \text{ m}$$

$$A_c := h \cdot w = 4.445 \times 10^{-8} \text{ m}^2$$

$$D_H := \frac{4A_c}{2 \cdot (h + w)} = 1.864 \times 10^{-4} \text{ m}$$

$$L_c := 0.06 \text{ m}$$

5. Needle:

$$D_n := 0.325 \cdot 10^{-3} \text{ m}$$

$$A_n := \frac{\pi \cdot D_n^2}{4} = 8.296 \times 10^{-8} \text{ m}^2$$

$$L_n := 6.35 \cdot 10^{-3} \text{ m}$$

## Calculating Velocities in sections given flow rate

### 1. Syringe

$$V_s := \frac{Q_{\text{olive.2}}}{A_s} = 1.57 \times 10^{-5} \quad \frac{\text{m}}{\text{s}}$$

$$Re_s := \frac{V_s \cdot D_s}{\nu_{\text{olive}}} = 7.681 \times 10^{-4}$$

### 2. Tube

$$V_t := \frac{Q_{\text{olive.2}}}{A_t} = 1.435 \times 10^{-3} \quad \frac{\text{m}}{\text{s}}$$

$$Re_t := \frac{V_t \cdot D_t}{\nu_{\text{olive}}} = 7.343 \times 10^{-3}$$

### 3. Channel

$$V_c := \frac{Q_{\text{olive.2}}}{A_c} = 6.337 \times 10^{-3} \quad \frac{\text{m}}{\text{s}}$$

$$Re_c := \frac{V_c \cdot D_H}{\nu_{\text{olive}}} = 0.012$$

### 4. Needle

$$V_n := \frac{Q_{\text{olive.2}}}{A_c} = 6.337 \times 10^{-3} \quad \frac{\text{m}}{\text{s}}$$

$$Re_n := \frac{V_n \cdot D_n}{\nu_{\text{olive}}} = 0.021$$

## Calculating the pressure drop in the section:

### 2. Tube

$$\Delta P_t := \left( \frac{64}{Re_t} \right) \cdot \left( \frac{L_t}{D_t} \right) \cdot \left( \frac{\rho_{\text{olive}} \cdot V_t^2}{2} \right) = 783.535 \quad \text{Pa}$$

### 3. Channel

$$\Delta P_c := \left( \frac{64}{Re_c} \right) \cdot \left( \frac{L_c}{D_H} \right) \cdot \left( \frac{\rho_{\text{olive}} \cdot V_c^2}{2} \right) = 2.942 \times 10^4$$

## Solve Bernoulli's Equation

$$h_1 := L_s + L_t + L_n = 0.107$$

$$h_L := \Delta P_t + \Delta P_c = 3.021 \times 10^4$$

$$P_1 := \left( P_1 + \frac{1}{2} \cdot \rho_{\text{olive}} \cdot V_s^2 + \rho_{\text{olive}} \cdot 9.81 \cdot h_1 - \frac{1}{2} \cdot \rho_{\text{olive}} \cdot V_c^2 - h_L \right) \text{ solve, } P_1 \rightarrow 29301.926395809495913$$

$$F_1 := P_1 \cdot A_s = 0.526 \quad \text{N}$$

### Calculate Friction Force

$$F_{fo} := 2.16 \text{ N}$$

$$F_t := F_1 + F_{fo} = 2.686 \text{ N}$$

### Calculate required weight

$$m_m := \frac{F_t}{9.81} = 0.274 \text{ kg}$$

$$m_i := \frac{m_m}{0.454} = 0.603 \text{ lb}$$

## Appendix K: Weight Driven Pump Flow Rate Calculations

This appendix shows the calculations used to determine theoretical flow rate for the weight driven pump given a specified added weight.

### Oil Calculations:

#### Fluid Properties

$$\rho_{\text{olive}} := 860 \frac{\text{kg}}{\text{m}^3}$$

$$\mu_{\text{olive}} := 84 \cdot 10^{-3}$$

$$\nu_{\text{olive}} := \frac{\mu_{\text{olive}}}{\rho_{\text{olive}}} = 9.767 \times 10^{-5} \frac{\text{m}^2}{\text{s}}$$

#### 2. Syringe:

$$D_s := 4.78 \cdot 10^{-3} \text{ m}$$

$$A_s := \frac{\pi \cdot D_s^2}{4} = 1.795 \times 10^{-5} \text{ m}^2$$

$$L_s := 0.05$$

#### 4. Channel:

$$h := 127 \cdot 10^{-6} \text{ m}$$

$$w := 350 \cdot 10^{-6} \text{ m}$$

$$A_c := h \cdot w = 4.445 \times 10^{-8} \text{ m}^2$$

$$D_H := \frac{4A_c}{2 \cdot (h + w)} = 1.864 \times 10^{-4} \text{ m}$$

$$L_c := 0.06 \text{ m}$$

#### 3. Tube:

$$D_t := 0.5 \cdot 10^{-3} \text{ m}$$

$$A_t := \frac{\pi \cdot D_t^2}{4} = 1.963 \times 10^{-7} \text{ m}^2$$

$$L_t := 0.0508 \text{ m}$$

#### 5. Needle:

$$D_n := 0.325 \cdot 10^{-3} \text{ m}$$

$$A_n := \frac{\pi \cdot D_n^2}{4} = 8.296 \times 10^{-8} \text{ m}^2$$

$$L_n := 6.35 \cdot 10^{-3} \text{ m}$$

## Calculating the pressure drop in the section:

### 1. Syringe

$$\Delta P_s(Q_{olive}) := \left( \frac{64}{Re_s(Q_{olive})} \right) \cdot \left( \frac{L_s}{D_s} \right) \cdot \left( \frac{\rho_{olive} \cdot V_s(Q_{olive})^2}{2} \right) \quad \text{Pa}$$

### 2. Tube

$$\Delta P_t(Q_{olive}) := \left( \frac{64}{Re_t(Q_{olive})} \right) \cdot \left( \frac{L_t}{D_t} \right) \cdot \left( \frac{\rho_{olive} \cdot V_t(Q_{olive})^2}{2} \right)$$

### 3. Channel

$$\Delta P_c(Q_{olive}) := \left( \frac{64}{Re_c(Q_{olive})} \right) \cdot \left( \frac{L_c}{D_H} \right) \cdot \frac{\rho_{olive} \cdot V_c(Q_{olive})^2}{2}$$

### 4. Needle

$$\Delta P_n(Q_{olive}) := \left( \frac{64}{Re_n(Q_{olive})} \right) \cdot \left( \frac{L_n}{D_n} \right) \cdot \left( \frac{\rho_{olive} \cdot V_n(Q_{olive})^2}{2} \right)$$

### 5. End Tubing

$$\Delta P_{et}(Q_{olive}) := \left( \frac{64}{Re_t(Q_{olive})} \right) \cdot \left( \frac{L_n}{D_n} \right) \cdot \left( \frac{\rho_{olive} \cdot V_t(Q_{olive})^2}{2} \right)$$

## Calculating Velocities in sections given flow rate

### 1. Syringe

$$V_s(Q_{olive}) := \frac{Q_{olive}}{A_s} \quad \frac{\text{m}}{\text{s}}$$

$$Re_s(Q_{olive}) := \frac{Q_{olive} \cdot D_s}{A_s \cdot \nu_{olive}}$$

### 2. Tube

$$V_t(Q_{olive}) := \frac{Q_{olive}}{A_t} \quad \frac{\text{m}}{\text{s}}$$

$$Re_t(Q_{olive}) := \frac{Q_{olive} \cdot D_t}{A_t \cdot \nu_{olive}}$$

### 3. Channel

$$V_c(Q_{olive}) := \frac{Q_{olive}}{A_c} \quad \frac{\text{m}}{\text{s}}$$

$$Re_c(Q_{olive}) := \frac{Q_{olive} \cdot D_H}{A_c \cdot \nu_{olive}}$$

### 4. Needle

$$V_n(Q_{olive}) := \frac{Q_{olive}}{A_c} \quad \frac{\text{m}}{\text{s}}$$

$$Re_n(Q_{olive}) := \frac{Q_{olive} \cdot D_n}{A_c \cdot \nu_{olive}}$$

## Solve Bernoulli's Equation

$$h_1 := L_s + L_t + L_n = 0.107$$

$$h_L(Q_{olive}) := \Delta P_s(Q_{olive}) + \Delta P_t(Q_{olive}) + \Delta P_c(Q_{olive}) + \Delta P_n(Q_{olive}) + \Delta P_{et}(Q_{olive})$$

$$P_1(Q_{olive}) := \left[ \left( \frac{-1}{2} \cdot \rho_{olive} \cdot V_s(Q_{olive})^2 - \rho_{olive} \cdot 9.81 \cdot h_1 \right) + \frac{1}{2} \rho_{olive} \cdot V_c(Q_{olive})^2 \right] + h_L(Q_{olive})$$

## Calculate Forces

$$F_1(Q_{olive}) := P_1(Q_{olive}) \cdot A_s \quad \text{N}$$

$$F_{fo} := 2.16 \quad \text{N}$$

$$F_t(Q_{olive}) := F_1(Q_{olive}) + F_{fo} \quad \text{N}$$

## Total Weight

$$m_m := .450$$

## Solve for Flow Rate:

$$Q_{olive} := (F_t(Q_{olive}) - m_m \cdot 9.81) \text{ solve, } Q_{olive} \rightarrow \begin{pmatrix} -0.00051192385072706717197 \\ 1.1357707378850519171e-9 \end{pmatrix}$$

$$Q_{olive2} := Q_{olive} \cdot 60 \cdot 10^9 = \begin{pmatrix} -3.072 \times 10^7 \\ 68.146 \end{pmatrix} \frac{\mu\text{L}}{\text{min}}$$